

**OPTIMIZATION AND FAILURE ANALYSIS OF A  
CABLE BASED PARALLEL MANIPULATOR  
FOR SUBSEA APPLICATIONS**

BY  
**ASIM GHAFFAR**

A Thesis Presented to the  
DEANSHIP OF GRADUATE STUDIES  
**KING FAHD UNIVERSITY OF PETROLEUM & MINERALS**  
DHAHRAN, SAUDI ARABIA

In Partial Fulfillment of the  
Requirements for the Degree of

**MASTER OF SCIENCE**  
In

**MECHANICAL ENGINEERING**

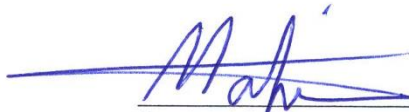
APRIL, 2014

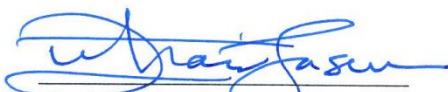
KING FAHD UNIVERSITY OF PETROLEUM & MINERALS


DHAHRAN- 31261, SAUDI ARABIA


**DEANSHIP OF GRADUATE STUDIES**


This thesis, written by **Asim Ghaffar** under the direction his thesis advisor and approved by his thesis committee, has been presented and accepted by the Dean of Graduate Studies, in partial fulfillment of the requirements for the degree of **MASTER OF SCIENCE IN MECHANICAL ENGINEERING**.

  
Dr. Mahir Hassan  
(Advisor)

  
Dr. Zuhair Mattoug Gasem  
(Department Chairman)

  
Dr. Muhammad Hawwa  
(Member)

  
Dr. Salam A. Zummo  
(Dean of Graduate Studies)

  
Dr. Mehmet Sunar  
(Member)

Date: 8/5/14



©ASIM GHAFAR

2014

Dedicated to my Parents

## **ACKNOWLEDGMENTS**

All praise and thanks to Almighty, the Creator of all worlds for giving me the courage to accomplish this work sincerely and successfully. May the peace and blessings of Allah be upon His holy prophet (PBUH), his family and his companions.

I would like to wish my appreciation to Mechanical Engineering Department of King Fahd University of Petroleum and Minerals, for providing me an opportunity to continue my studies. I am also grateful to all the faculty members, staff members and technicians of the department for their support.

I would like to express my sincere gratitude to my thesis advisor Dr. Mahir Hassan for his unlimited guidance, assistance and encouragement throughout the work. Special thanks to my committee members Dr. Muhammad Hawwa and Dr. Mehmet Sunar for their useful suggestions, reviews and comments.

I would also like to acknowledge the support provided by King Abdulaziz City for Science and Technology (KACST) as part of the National Science, Technology and Innovation Plan (NSTIP) through the Science and Technology Unit at King Fahd University of Petroleum and Minerals (KFUPM) for funding this research through project # 11-ELE1623-04.

I thank all my colleagues, students and friends of Mechanical Engineering department for giving me remarkable company, especially Tausiff Firaque, Waqas Aslam and Ateeq ur Rehman for making my stay memorable. I would also like to thank Mamoun Haroub and Najam ul Qadir for guiding me throughout my work.

Finally, special thanks to my Parents, brothers and all family members for their encouragement, moral support and continuous prayers.

# TABLE OF CONTENTS

ACKNOWLEDGMENTS .....	V
TABLE OF CONTENTS .....	VI
LIST OF TABLES .....	IX
LIST OF FIGURES .....	X
LIST OF ABBREVIATIONS .....	XIII
ABSTRACT (ENGLISH).....	XIV
ABSTRACT (ARABIC).....	XVI
CHAPTER 1 INTRODUCTION.....	1
1.1 Parallel manipulators .....	1
1.2 Cable based parallel manipulators.....	2
1.3 Literature Review .....	3
1.4 Research objective .....	10
1.5 Research outline .....	10
CHAPTER 2 FORCES ACTING ON SUBMERGED BODIES.....	12
2.1 Introduction.....	12
2.2 Forces exerted by the flowing fluid .....	12
2.3 Expressions for Drag and Lift Forces .....	13
2.4 Pressure Drag and Friction Drag .....	14

<b>2.5 Boundary layer Friction Drag .....</b>	<b>15</b>
<b>2.6 Hydrostatic Forces .....</b>	<b>17</b>
 <b>CHAPTER 3 SHIP POSITION OPTIMIZATION FOR NON-REDUNDANT CABLES.....</b>	
<b>3.1 Theoretical Background.....</b>	<b>19</b>
3.1.1 Position Analysis .....	21
3.1.2 Velocity Analysis .....	27
3.1.3 Force Analysis .....	28
<b>3.2 Layout Optimization.....</b>	<b>30</b>
3.2.1 Fundamentals on Workspace evaluation .....	30
3.2.2 Singularity Analysis.....	31
3.2.3 Maximizing Workspace .....	33
3.2.4 Maximizing Stiffness in the Workspace .....	46
<b>3.3 Results and Discussions .....</b>	<b>53</b>
 <b>CHAPTER 4 SHIP POSITION OPTIMIZATION FOR REDUNDANT CABLES 55</b>	
<b>4.1 Introduction.....</b>	<b>55</b>
<b>4.2 Inverse Kinematic Analysis.....</b>	<b>57</b>
<b>4.3 Static Analysis: Bounded Cable tensions.....</b>	<b>60</b>
<b>4.4 Dykstra's Projection Algorithm .....</b>	<b>64</b>
<b>4.5 Optimizing Cable tensions using Dykstra's algorithm.....</b>	<b>67</b>
<b>4.6 Layout Optimization.....</b>	<b>69</b>
4.6.1 Maximizing workspace volume .....	69
4.6.2 Maximizing Stiffness in the workspace .....	83
<b>4.7 Results and Discussions .....</b>	<b>92</b>
 <b>CHAPTER 5 FAILURE ANALYSIS.....</b>	
<b>5.1 Theoretical background .....</b>	<b>95</b>
5.1.1 Effect of Cable Breakage on Manipulator Velocity .....	96

5.1.2 Effect of Cable Breakage on Manipulator Force .....	97
<b>5.2 Post failure trajectory .....</b>	<b>98</b>
5.2.1 Simulation of cable 2 failure.....	101
5.2.2 Simulation of cable 6 failure.....	104
<b>5.3 Post failure tension in the cables.....</b>	<b>109</b>
5.3.1 Post failure tensions in CPM with six cables.....	109
5.3.2 Post failure tensions in CPM with eight cables .....	115
5.3.3 Post failure tensions in CPM with ten cables.....	117
<b>5.4 Layout Optimization.....</b>	<b>119</b>
5.4.1 Minimizing post failure tension in the cables .....	119
5.4.2 Optimized fault tolerance ship positions.....	131
<b>5.5 Comparison of optimized ship positions .....</b>	<b>139</b>
<b>5.6 Layout Optimization using a combined criterion .....</b>	<b>142</b>
5.6.1 Ship position optimization for CPM having six cables .....	146
5.6.2 Ship position optimization for CPM having eight cables .....	148
5.6.3 Ship position optimization for CPM having ten cables .....	151
<b>5.7 Results and discussions.....</b>	<b>154</b>
<b>CHAPTER 6 CONCLUSIONS.....</b>	<b>157</b>
<b>REFERENCES.....</b>	<b>160</b>
<b>VITAE.....</b>	<b>166</b>



## LIST OF TABLES

Table 3.1: Computed Workspace for CPM with six cables.....	36
Table 3.2: Computed minimum natural frequency for CPM with six cables .....	51
Table 4.1: Computed Workspace for CPM with eight cables. ....	73
Table 4.2: Computed Workspace for CPM with ten cables.....	81
Table 4.3: Computed minimum natural frequency for CPM with eight cables.....	87
Table 4.4: Computed minimum natural frequency for CPM with ten cables.....	90
Table 4.5: Comparison of different CPM layouts.....	93
Table 5.1: Post Failure Tension values in the cables. ....	116
Table 5.2: Post Failure Tension values in the cables. ....	118
Table 5.3: Computed $\Delta\tau_{max}$ for CPM with six cables .....	123
Table 5.4: Computed $\Delta\tau_{max}$ for CPM with eight cables.....	126
Table 5.5: Computed $\Delta\tau_{max}$ for CPM with ten cables. ....	129
Table 5.6: Computed $\Delta\tau_{max}$ for fault tolerance design for CPM with eight cables.....	134
Table 5.7: Computed $\Delta\tau_{max}$ for fault tolerance design for CPM with ten cables.....	137
Table 5.8: Comparison of optimized ship positions of CPM with six cables.....	140
Table 5.9: Comparison of optimized ship positions of CPM with eight cables. ....	141
Table 5.10: Comparison of optimized ship positions of CPM with ten cables.....	141
Table 5.11: Optimized ship positions for CPM with six cables. ....	146
Table 5.12: Optimized ship positions for CPM with eight cables. ....	149
Table 5.13: Optimized ship positions for CPM with ten cables. ....	152

## LIST OF FIGURES

Figure 2.1: Vector Representation of forces .....	13
Figure 2.2: Plate held parallel. ....	15
Figure 2.3: Plate held perpendicular .....	15
Figure 2.4: Boundary layer. ....	16
Figure 3.1: Schematic Diagram of the cable driven manipulator layout. ....	20
Figure 3.2: Vector notation representation of the platform. ....	21
Figure 3.3: Algorithm flowchart for workspace optimum ship positions.....	34
Figure 3.4: Optimum ship positions for CPM with maximum workspace .....	37
Figure 3.5: Manipulators planer workspace x-y by varying $\theta x$ and fixing $\theta y = \theta z = 0$ ...	39
Figure 3.6: Manipulators planer workspace x-y by varying $\theta y$ and fixing $\theta x = \theta z = 0$ ..	41
Figure 3.7: Manipulators planer workspace x-y by varying $\theta z$ and fixing $\theta y = \theta z = 0$ ..	43
Figure 3.8: Manipulators workspace for position 1 in figure 3.4(a).....	45
Figure 3.9: Algorithm flowchart for stiffness optimum ship positions .....	49
Figure 3.10: Optimum ship positions for CPM with maximum stiffness.....	52
Figure 4.1: Schematic Diagram of the CPM layout with eight cables.....	56
Figure 4.2: Schematic Diagram of the CPM layout with ten cables.....	56
Figure 4.3: Planer translational CPM layout with two cases .....	63
Figure 4.4: Flow chart for Dykstra's Algorithm. ....	66
Figure 4.5: Algorithm flowchart for workspace optimum ship positions.....	71
Figure 4.6: Optimum ship positions for maximum workspace with eight cables CPM...	74
Figure 4.7: Manipulators planer workspace x-y by varying $\theta x$ and fixing $\theta y = \theta z = 0$ ..	77
Figure 4.8: Manipulators planer workspace x-y by varying $\theta y$ and fixing $\theta x = \theta z = 0$ ...	78

Figure 4.9: Manipulators planer workspace x-y by varying $\theta_z$ and fixing $\theta_x = \theta_y = 0$ ..	79
Figure 4.10: Optimum ship positions for maximum workspace with ten cables CPM ....	82
Figure 4.11: Algorithm flowchart for stiffness optimum ship positions .....	85
Figure 4.12: Optimum ship positions for maximum stiffness with eight cables CPM.....	88
Figure 4.13: Optimum ship positions for maximum stiffness with ten cables CPM.....	91
Figure 4.14: Graph comparing CPM layouts for workspace and stiffness .....	93
Figure 5.1: Algorithm flowchart for post failure trajectory of the manipulator .....	100
Figure 5.2: Trajectories of the manipulator in case of cable no. 2 breakage. ....	103
Figure 5.3: Trajectories of the manipulator in case of cable no. 6 breakage. ....	107
Figure 5.4: Cable tension along the trajectory in case of cable no. 2 breakage.....	111
Figure 5.5: Cable tension along the trajectory in case of cable no. 6 breakage.....	114
Figure 5.6: Algorithm flowchart for minimum post failure tensions ship positions .....	121
Figure 5.7: Optimum ship positions for min. post failure tensions with six cables.....	124
Figure 5.8: Optimum ship positions for min. post failure tensions with eight cables ....	127
Figure 5.9: Optimum ship positions for min. post failure tensions with ten cables .....	130
Figure 5.10: Algorithm flowchart for fault tolerance design.....	132
Figure 5.11: Optimized fault tolerance positions of the ships with eight cables CPM...	135
Figure 5.12: Optimized fault tolerance positions of the ships with ten cables CPM.....	138
Figure 5.13: Algorithm flowchart for optimized ship positions using Eq. (5.16). ....	145
Figure 5.14: Optimum ship positions using figure 5.13 for CPM with six cables .....	147
Figure 5.15: Optimum ship positions using figure 5.13 for CPM with eight cables .....	150
Figure 5.16: Optimum ship positions using figure 5.13 for CPM with ten cables .....	153
Figure 5.17: Comparison of CPM layouts in case of a failure.....	155

Figure 5.18: Comparison of CPM layouts for a combined criterion value.....	156
--	-----

## LIST OF ABBREVIATIONS

CPM	Cable based parallel manipulator
CSP	Column space
DOF	Degree of freedom
$f_{min}$	Minimum natural frequency
J	Jacobian matrix
K	Stiffness matrix
M	Inertia matrix
NSP	Null space
P	Position vector
Q	Rotation matrix
$Val_{opt}$	Optimum value
W	Wrench vector
$x$ - $y$ - $z$	Global coordinate frame
$x_p y_p z_p$	Moving coordinate frame
$\rho$	Fluid density
$\tau$	Cable tensions
$\phi$ - $\theta$ - $\varphi$	Roll-pitch-yaw angles

## **ABSTRACT**

Full Name : Asim Ghaffar

Thesis Title : Optimization and failure analysis of a cable driven parallel manipulator for subsea applications

Major Field : Mechanical Engineering

Date of Degree : April 2014

The current research involves the optimization and failure analysis of a cable driven parallel manipulator (CPM) for subsea applications. In CPM, cables are used instead of rigid links to manipulate the moving platform. The CPM consists of a rectangular platform having six degree-of-freedom (DOF) moving inside sea connected to ships on sea surface via cables. The position and velocity analysis of CPM was conducted using inverse kinematics. Principle of virtual work was applied for the static analysis. In order to calculate the workspace of the manipulator, the wrench feasible workspace was defined as the set of all poses where the manipulator can apply the required set of wrenches without losing cable tensions. The stiffness and natural frequencies of the moving platform were discussed and the ship position optimization of CPM was conducted by maximizing the workspace as well as the stiffness of the moving platform. The study presents the optimization and failure analysis for redundant as well as non-redundant CPM. For the case of redundant cables, Dykstra's projection algorithm was utilized to calculate the minimum-2-norm solution for the cable tensions. Failure analysis was performed to analyze the effect of cable failure on the performance of the manipulator. The effect of having different number of cables on the workspace, stiffness and fault tolerance of the manipulator was studied on CPM with six, eight and ten cables

and it was observed that the performance of the CPM was improved by using higher number of cables. In the event of a failure, the post failure trajectory and post failure tensions were calculated and ship position optimization was performed in order to minimize the post failure tensions. A combined criterion of optimization was also established to maximize the workspace and stiffness of the manipulator and simultaneously minimize the effect of a cable failure.

## ملخص الرسالة

الاسم الكامل: عاصم غفار

عنوان الرسالة: تحليل الأعطال وتحسينها للمعالج المشغل بواسطة كوابل متوازية لتطبيقات ما تحت البحار

التخصص: قسم الهندسة الميكانيكية

تاريخ الدرجة العلمية: ابريل 2014

البحث الحالي يشارك في تحليل العطل وتحسينه للمعالج المشغل بواسطة حبال متوازية لتطبيقات ما تحت البحار. في هذا المعالج , الحبال تستخدم بدلا من السلاسل الصلبة لمعالجة المنصة المتحركة. ويتكون هذا النظام من منصة مستطيلة والتي تملك حرية للحركة في ستة اتجاهات وتتحرك في وسط البحر ومتصلة بالسفن من على سطح البحر بواسطة الحبال. بيانات الموقع والسرعة أجريت بواسطة الحركات العكسية, وللحصول على البيانات الثابتة طبق مايسمى بمبدأ العمل الافتراضي, ولحساب مساحة العمل للمعالج تم تعريف مساحة الحركة الممكنة كمجموعة من كل المواقع التي ممكن للمعالج أن يحدث فيها مجموعة محددة من الحركة دون أن يخسر قوة الشد للحبال. وتم التحدث عن الصلابة والترددات الطبيعية للمنصة المتحركة وكذلك تحسين مكان العمل لهذا النظام تم إجراؤه بتكبير مساحة العمل وكذلك الصلابة للمنصة المتحركة. الدراسة تعرض تحسين وتحليل للعطل للنظم التي تعمل والتي وضعت كاحتياط أيضا لحالة الحبال الاحتياطية استخدمت الاسقاط اللوغاريتمي لدايكسترا وذلك للحصول على أقل قوة شد في الحبال. بيانات الأعطال تم إجراؤها لتحليل تأثير عطل الحبل على مستوى أداء المعالج. التأثير الناتج من استخدام عدد مختلف من الحبال على مساحة العمل والصلابة وكذلك المدى المسموح للعطل على المعالج أجريت على النظام مع ستة ، ثمانية وعشرة حبال وتم ملاحظة زيادة مستوى الأداء على النظام كلما قمنا باستخدام عدد أكبر من الحبال. في حدوث العطل, مسار ما بعد العطل وقوة الشد بعد العطل أوجدت والدراسة لتحسين منطقة الشحن أجريت لتقليل قوة الشد بعد العطل. المعيار المثالي المدموج كذلك أوجد لزيادة مساحة العمل وكذلك الصلابة للمعالج وفي نفس الوقت تقليل تأثير عطل الحبل.



# **CHAPTER 1**

## **INTRODUCTION**

### **1.1 Parallel manipulators**

A parallel manipulator is a robotic system in which two or more serial chain robots support an end-effector. It consists of a base and an end-effector with  $n$ -degrees of freedom that are linked together by several linkages. A manipulator is a parallel manipulator when the end effector is connected to the base using separate and independent kinematic chains.

The definition of parallel manipulator includes redundant mechanisms with more actuators than the number of controlled degrees of freedom of the end effector. In parallel manipulators, each link is usually short, simple and rigid against unwanted motion, thus making the overall structure simple.

Parallel manipulators possess different characteristics as compared to serial manipulators. In parallel manipulators, the load is distributed among different chains or cables thus each chain supports only a fraction of total load. Therefore, they have a greater payload/weight ratio. Actuators can be mounted on the base of the manipulator which reduces the weight of the moving parts of the structure. This gives good inertial properties to the parallel manipulator and can be used for high speed applications. Moreover, they have high flexibility, high stiffness and high accuracy.

As a drawback, they have a reduced size of the workspace as compared to serial manipulators of the same size. In order to increase the workspace area the whole structure needs to be changed. Parallel manipulators may have different types of singularities in which the control of the robot is lost and in worst case the structure can be damaged due to very large forces that are generated in the vicinity of singular poses.

## **1.2 Cable based parallel manipulators**

Cable based parallel manipulators (CPM) are a type of parallel manipulators that has recently gain interest in large workspace manipulation tasks. Instead of rigid links, cables are used in order to manipulate the moving platform. It has a relatively simple form, with multiple cables attached to the moving platform or the end effector. The manipulator is controlled by cables attached to motors that can extend or retract the cables. These motors may be fixed in a specific location or mounted to moving bases.

The mechanical structure of a cable based parallel manipulator consists of a moving platform and a fixed or mobile base. These two elements are connected through multiple cables that can extend or retract. CPM's are structurally similar to conventional parallel robots but they have several advantages when compared to them. They have a large workspace area for their size, limited mostly by cable lengths and interference with the surroundings. They have few moving parts which give good inertial properties to the manipulators. These properties make them suitable for used in applications which require high velocity and acceleration. Some other characteristics include high payload to weight ratio, transportability and economical construction. It is also possible to reconfigure them by simply relocating the motors and update the control system accordingly.

The first disadvantage of CPM is the possible interference of cables with each other, with the load or with the environment. This is an important problem in spatial redundant systems, although efficient interference detection algorithms are available. Moreover, cables can only pull but cannot push and therefore they must be maintained in tension at all times during manipulator operation. This issue is much important and a definition of this tensionability is available as a property for cable based manipulators, to indicate that all cables must remain in tension during operation at any load. In the last decade cable based manipulators have been used in several applications.

Cable based manipulators are well suited for many applications such as manipulation of heavy payloads, haptic, cleanup of disaster areas, access to remote sites and interaction with hazardous environments. It can also be used for aerial transport of payloads which is very common in industrial and military applications. In recent years, it has been used for undersea towing applications to transport objects to environments that are inaccessible by other means. Conventional oceanographic data collection is largely dependent on towed systems. Towing can be established via single cable but that will give only a limited controllability of the payload.

### **1.3 Literature Review**

A wide variety of cable based parallel manipulators have been developed. Because of the physical characteristics of the cables, workspace design and analysis are different from those of conventional parallel manipulators. There have been a number of CPM designs presented in the literature such as NIST Robocrane [1], Falcon-7 [2], WARP [3], WiRo [4], DeltaBot [5], and the hybrid cable-actuated robot developed by Mroz et al. [6]. The kinematic analysis of a cable driven parallel manipulator (CPM)

having symmetric layout of eight cables with the planer translational motion of the manipulator was studied by Hassan et al. [7]. He also optimized the manipulator cables layout based on maximizing the manipulator stiffness and its lowest natural frequency in the workspace. As cables can only apply force in one direction, CPM needs to be redundantly actuated in order to keep all cables in tension at all times during its operation. Verhoeven et al. [8] pointed out that for obtaining  $n$  degrees of freedom for the end-effector, it is necessary to use  $n + 1$  cables. This is in order to make sure that negative tensions are avoided. At the same time, this condition increases the possibility of cables interference making the control more difficult [9]. Cable based manipulators can be classified as fully constrained and under constrained based on the number of cables and degrees of freedom of the manipulator. In the fully constrained manipulators the pose of the end-effector can be determined as a function of the cables lengths only. In case of under constrained manipulators the pose is not completely determined by cable lengths and the gravity has to be considered as another constrained for solving the problem.

In Frantiza et al. [10], optimization of tension distribution was studied. Using a method based on the analysis of the workspace condition, tension constraints and limiting torque constraints on the actuators, he found an analytical solution for optimal tension distribution and used it to compute the force in each cable for compensation of dynamic errors. The method was based on minimization of the sum of the cable tensions at each pose. Their method however was only applicable to CPMs having one redundant cable. Carvalho et al. [42] studied the optimization using genetic algorithm, in such a way that the cables have a minimum tension on it. Hassan et al. [11] presented a projection method to calculate the optimal solutions for the actuators force distribution in CPMs. The

optimization was formulated as a projection on an intersection of convex sets and the Dykstra's projection method was used to obtain the solutions. The method was demonstrated by applying it to 3 DOF CPM. Robert et al. [12] used the null space of the Jacobian matrix to analyze the static force equilibrium in CPMs at a certain configuration. Because of actuation redundancy in CPMs, there exist infinite solutions for balancing a given external load. It is important to minimize the cable forces in CPM to avoid excessive cable forces during operation as well as to minimize the size of the actuators during design. Mikelsons et al. [13] presented an algorithm for the real time calculation of force distribution in tendon based parallel manipulators. Agrawal et al. [14] proposed a control approach to maintain tension in cable suspended redundant robots that use linear and quadratic programming techniques.

The workspace of the CPM has been studied by many researchers. Several definitions of workspace characterization can be found in the literature. According to [25], the term controllable workspace was used to denote the set of all postures where the manipulator can be controlled with positive tensions in the cables. Agrawal et al. [15] defined the statically reachable workspace as the set of all poses that can be reached with static ensured conditions. In Bosscher et al. [16] the term wrench feasible workspace defines the set of all poses where the manipulator can apply the required set of wrenches.

Otherwise, the workspace can be defined by considering only the geometry of the mechanism. In this case the workspace is a property of the mechanism itself and is related to its design only. For example, in Gouttefarde et al. [17], the wrench closure workspace of CPM contains the set of all poses where the manipulator can balance any external wrench, and it depends only on the geometry of the mechanism. Other classifications of

the workspace are given in Merlet et al. [18]. A constant orientation workspace or translational workspace is defined as the set of all poses of the end effector that can be reached with a fixed orientation. An orientation workspace is defined as the set of all possible orientation that the end effector can assume in a fixed position. A maximal workspace is defined as the set of all positions of the end effector that can be reached with at least one orientation. An inclusive orientation workspace is defined as the set of all positions of the end effector that can be reached with at least one orientation inclusive laying in a given range. A total orientation includes the set of all positions of the end effector that can be reached with all orientations defined by a given range. A dexterous workspace is defined as the set of positions of the end effector that can be reached with any orientation.

For cable based manipulators the workspace definition involves both geometrical and static parameters. By considering a fully constrained CPM it is possible to define a force closure workspace as a set of poses of the end effector where the force closure condition can be satisfied [19]. It depends only on geometrical parameters of the manipulator and its end effector pose. Zarif et al. [46] formulated the force feasible workspace for redundant cable driven parallel manipulators in terms of linear matrix inequality. A feasible wrench workspace can be defined as a set of poses of the end effector that satisfies also static requirements. It depends not only on the geometrical configuration but also on the forces acting on the system. Tensions in cables and the external wrench have to be considered for the workspace definition.

The evaluation of different kinds of workspace can be obtained with several techniques (geometrical, analytical and numerical) and the analysis depends on the

application requests. The workspace bounds possible applications of the manipulator. Indices can be used in order to characterize and optimize the workspace description. One of the important characteristic of the workspace is its dimension determined by an area, for a planer manipulator, or a volume, for a spatial manipulator. For example, it is possible to consider a volume index defined by the ratio between the workspace volume and the volume of the robot Merlet [20].

Apart from its quantification, indices can be used to describe some quality of the workspace. Specifically, tensions are fundamental parameters for the evaluation of the workspace of CPM. In [19], a tension factor is proposed as a performance index with the aim to evaluate the quality of force closure at a specific configuration. It is defined as the ratio between the minimum and maximum tension on cables. A performance index can be used in order to monitor the closeness to singular configuration. Aref et al. [43] investigated a cable driven redundant parallel manipulator for high speed and large workspace applications. A collision free workspace was derived by applying fast geometrical intersection detection method.

A stiffness model for cable based manipulators was developed by Behzadipur et al. [5] and he also discussed the stability taking into account the effect of tension in the cables. According to Tsai et al. [21], end effector displacements depend not only on the applied wrench but also on the stiffness of the structure. Stiffness strongly affects the accuracy of the end effector pose. According to Ceccarelli [22] physical and geometrical characteristics of links are the most important parameters that influence the stiffness behavior of the manipulator. The stiffness matrix of a CPM depends on tensions acting in

cables and on the manipulator configuration Merlet [20]. Therefore, the manipulator would be stable if stiffness matrix is positive definite.

Pashkevich et al. [44] developed a stiffness modelling method based on a multi-dimensional lumped parameter model that replaces the link flexibility by localized 6-dof virtual springs that describe both translational/rotational compliance and the coupling between them. Ahmad et al. [45] obtained a stiffness model and provided an additional index to use for multi-objective structural optimization to obtain an optimal compromise between a light weight design and the stiffness performance for high precision motion within a larger workspace.

The problem of controlling multiple robots manipulating and transporting a payload in three dimensions via cables are considered by Nathan et al. [23]. Different configurations of the robot were developed that ensure static equilibrium of the payload at a desired pose while keeping constraints on the tension and provided the analysis of payload stability for these configurations. It was demonstrated by a team of aerial robots via simulation and experimentation. The forward and inverse kinematics of payload has been developed. Equations of motion have been derived that maps the motion of the payload and the motion of the robots in the presence of dry friction and tension constraints. Controlling of multiple robots has been achieved so that they can cooperatively tow an object that is subjected to gravity and other forces from an initial configuration to any desired position. Position analysis for this model was simply achieved by using the standard inverse kinematics for parallel platforms. In order to obtain the velocity analysis, quasi-static model was developed.



The effect of failure on the mobility and static force of cable based parallel manipulators is also investigated by many researchers. Manipulator failure is the inability of the manipulator to perform its required function. Failure in CPM may occur due to several failure modes such as cable breakage, cable jam or undesired flexibility of cable, sensor failure, actuator failure and transmission failure. These failures could result in the loss of DOF, loss of actuation and loss of motion constraint. Failure analysis of serial manipulators has captured more attention as compared to parallel manipulators. Ting et al. [26] investigated the post failure recovery from the full or partial loss of actuator torque in the closed loop manipulators. The failure mode and effect analysis was performed by Notash et al. [27] to study the failure modes of parallel manipulators with their effects on the DOF, actuation and constraint. For fault tolerant designs, redundancy types, such as redundant DOF, redundant sensing, redundant actuation and redundant legs/branches, have been suggested. Notash et al. [28,29] studied the effect of redundancy in joint displacement sensing for parallel manipulators to reduce the number of forward displacement solutions/assembly modes, to allow the fixtureless calibration of manipulators [30]; and to facilitate the joint sensor fault detection, isolation and recovery [31]. It has been proposed that the redundancy in actuation can reduce the singularity configurations in parallel manipulators [32, 33]. Chen et al. [34] partitioned the task space into major and secondary tasks in order to complete the major task and optimize a secondary goal such as actuator fault tolerance. The reduced motion of parallel manipulators due to active joint jam and the design modification to compensate for the accuracy degradation were investigated in [35, 36]. Roberts et al. [37] studied the effect of losing a wire on the null space of the Jacobian matrix of a planer wire actuated

manipulator. Methodologies for the fault tolerance of wire-actuated parallel manipulators are required to compensate for their performance degradation after failure. Notash [38] studied the kinematics and static modelling of planar wire actuated manipulators and reported simulation results for the loss of wire force.

## **1.4 Research objective**

The ultimate goal of this research is to analyze and optimize the kinematic layout of a cable based parallel manipulator (CPM) for Subsea applications. Failure analysis is also performed in order to analyze the effect of cable failure on the performance of the manipulator. Following are the specific objectives of current research work:

- Conduct velocity and force analysis of a cable driven parallel manipulator (CPM) for Subsea applications. This is performed prior to optimization using inverse kinematics.
- Perform ship position optimization of CPM to maximum the workspace and stiffness of the manipulator.
- Optimize the cable tensions for the case of redundancy in order to improve the manipulator workspace.
- Perform failure analysis to analyze the effect of a cable failure on the performance of the manipulator and to minimize cable tensions after failure through ship position optimization.

## **1.5 Research outline**

In chapter 2, forces acting on submerged bodies are going to be investigated. The expressions for the lift and drag forces will be calculated based on impulse momentum

principle. The hydrostatic forces are also studied. These expressions for the forces acting on submerged bodies will be useful since the CPM is designed to work inside sea.

In chapter 3, a CPM design is proposed for non-redundant cables and the ship position optimization is performed based on maximizing workspace and stiffness of the manipulator. The workspace of the manipulator has been evaluated by considering geometrical constraints and force analysis. Results have been plotted and discussed. Two algorithms have been proposed to calculate the optimum ship positions.

Chapter 4 illustrates the ship position optimization of CPM for the case of redundant cables. Dykstra's algorithm is used to find the minimum-2-norm solution to the cable tensions and to increase the manipulator's workspace. The optimization is demonstrated for eight and ten cables.

In chapter 5, the effect of failure on the position and force capability of CPM is investigated. One of the important failures in CPM which is due to cable breakage is considered. The trajectory of the manipulator and the tension in the remaining cables is determined when one of the cables is broken. Ship position optimization is performed such that the maximum tension after failure is minimized. A combined optimization criterion is also presented that incorporates the three parameters i.e. workspace, stiffness and post failure tensions in the cables. The optimization is conducted for six, eight and ten cable manipulators.

In chapter 6, the conclusions have been drawn for the current research work.

## CHAPTER 2

### FORCES ACTING ON SUBMERGED BODIES

#### 2.1 Introduction

In engineering applications, there are many problems that involve bodies submerged in a fluid. In such problems either the body is moving in a fluid or the fluid is flowing around the submerged body. Examples of which may include motion of small particles in water, motion of large bodies such as ships or submarines through water or structures such as bridges which are submerged in water.

#### 2.2 Forces exerted by the flowing fluid

Whenever there is a relative motion between the fluid and the submerged body there is always a force exerted by the flowing fluid to the body and the body exerts an equal and opposite force on the fluid. There are usually four kinds of forces associated between a moving fluid and the body.

- **Drag Force and thrust force:** The force that is directed in the opposite direction of the moving body is known as drag force. The thrust force is in the direction of the moving body.
- **Lift Force (Buoyancy) and weight:** Buoyancy is the upward force exerted by the fluid on the body. It is directed upward while the weight acts downward.

When the symmetrical body is moving through an ideal fluid, the pressure distribution around the body is uniform and therefore the resultant force acting on the body is zero. However real fluids have viscosity and if the body is moved through real

fluid such as air or water at a uniform velocity, the body experiences a resistance to motion.

When the symmetrical body such as sphere is facing a symmetrical flow, lift force will be zero. For the production of lift force, there must be asymmetrical flow of fluid. But drag force is always present. It may be possible to create drag without lift but impossible the other way round.

The flow of the fluid around a body is dependent on fluid viscosity. At low Reynold's number, the fluid is deformed in a very wide zone around the body causing pressure and friction forces. With increase of Reynold's number, viscous effects are confined to the boundary layer causing the dominant effect of friction forces around the body.

## 2.3 Expressions for Drag and Lift Forces

Consider a body  $dA$  held stationary in a fluid moving with velocity  $U$ . Here  $\theta$  is the angle of inclination of the tangent to the element as shown in figure 1.

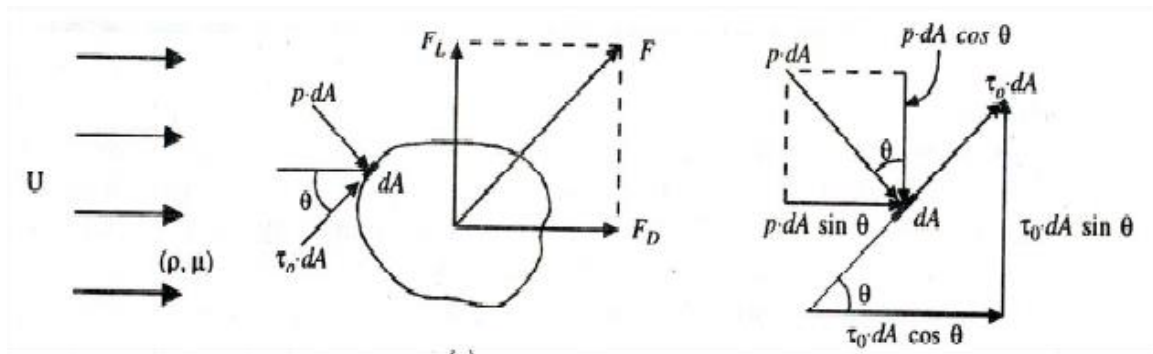


**Figure 2.1 Vector Representation of forces [39].**

As shown in figure 2.1, the force acting on the small element  $dA$  has two components one along tangent called the shear force and one is acting normal called the pressure force.

The summation of the forces acting on the entire region of  $dA$  are the drag force acting in the x-direction and the lift force acting along y-direction. These forces are given by Eq. (2.1) as:

$$\begin{aligned} F_D &= \int P dA \sin\theta + \int \tau dA \cos\theta \\ F_L &= \int \tau dA \sin\theta - \int P dA \cos\theta \end{aligned} \quad (2.1)$$

The component  $\int P dA \sin\theta$  is the pressure drag and  $\int \tau dA \cos\theta$  is the shear drag. The role of shear stresses to the lift is small and can be neglected.

When the body is moving through a fluid density  $\rho$  with a uniform velocity  $U$ , the expressions for drag and lift forces are given by:

$$\begin{aligned} F_D &= C_D A \\ F_L &= C_L A \end{aligned} \quad (2.2)$$

Where  $C_D$  and  $C_L$  are the coefficients of drag and lift forces respectively.

## 2.4 Pressure Drag and Friction Drag

Pressure drag and friction drag depends on the following parameters.

- Shape of the body
- Characteristics of fluid

- Orientation of the body immersed in the fluid

Two cases are observed. When the body such as a thin plate is held parallel to the direction of the fluid flow, there will be friction drag only and the pressure drag will be zero.

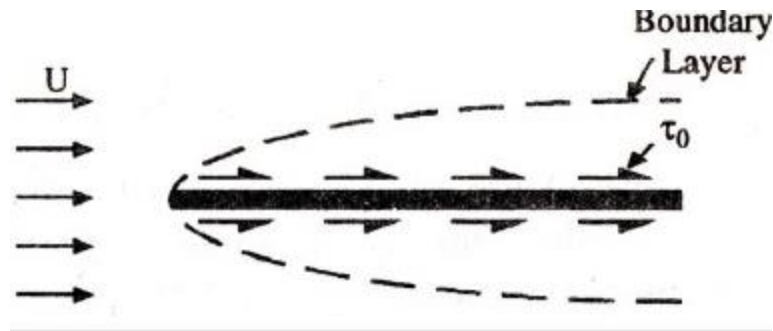


**Figure 2.2 Plate held parallel [39].**

Similarly, when the thin plate is held perpendicular to the moving fluid, in this case friction drag will be zero and the total drag is only due to pressure force.

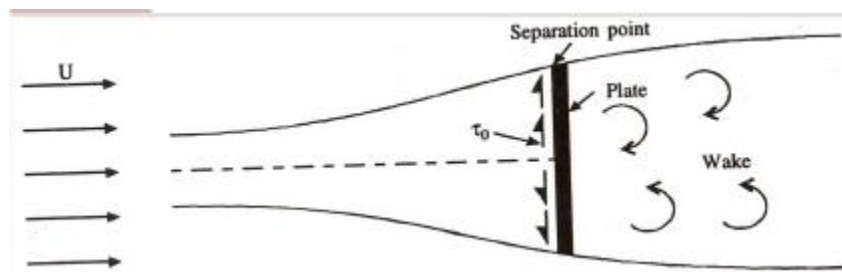


**Figure 2.3 Plate held perpendicular [39].**

## 2.5 Boundary layer Friction Drag

When a fluid comes in contact with the body, a portion of the fluid near the boundary cannot slip away from the boundary layer and it has the same velocity as that of the boundary. Therefore, there is no relative motion between fluid and the body at the

boundary surface. This condition is known as no slip condition. If the body is stationary, the fluid velocity at the boundary layer is zero.

Thus, at the boundary surface, the fluid undergoes retardation. This layer of fluid affects the adjacent layers of fluid as well. Therefore, the velocity of the fluid gradually increases from zero at the boundary surface to the velocity of the main stream. This region is known as boundary layer. This is shown in the figure 2.4. So in the boundary layer there is a resistance due to viscosity.

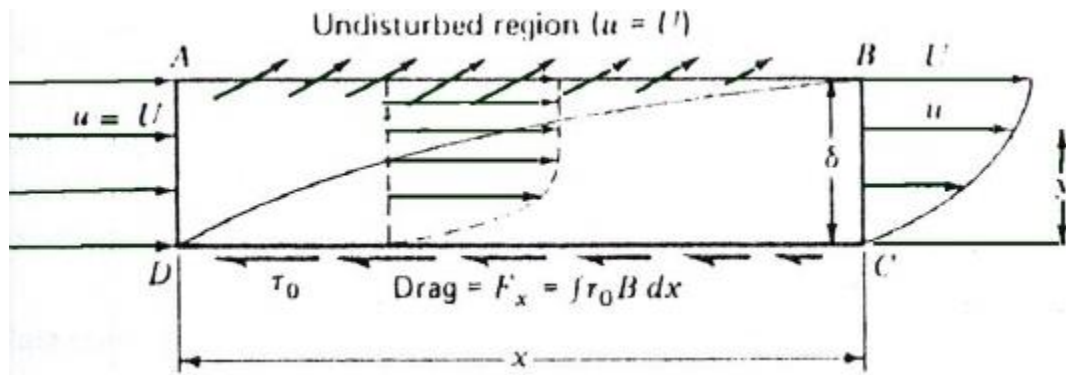


**Figure 2.4 Boundary layer [39].**

Consider the thickness of the boundary layer BC in which the fluid has reached 99% of the velocity of the main stream. The control volume is separated at a distance of  $x$  along the plate.

According to impulse momentum principle,

$F_x = \text{Drag force} = \text{rate of momentum of the fluid leaving through BC and AB} - \text{rate of momentum of the fluid in entering through DA}.$



Therefore, the flow rate and rate of momentum in  $x$ -direction across DA, BC and AB is given by:

- Flow rate along DA =  $Ub\delta$  and momentum =  $\rho(Ub\delta)U$
- Flow rate along BC =  $b \int u dy$  and momentum =  $\rho b \int u dy u$
- Flow rate along AB =  $Ub\delta - b \int u dy$  and momentum =  $\rho(Ub\delta - b \int u dy)U$

Therefore the above equation becomes after substituting these values:

$$\text{Drag force} = \rho b \int u(U - u) dy \quad (2.3)$$

Eq. (2.3) is the expression for the drag force acting on a body in the  $x$ -direction. This is valid only when the flow is laminar and there is no pressure gradient acting along the surface.

## 2.6 Hydrostatic Forces

Pressure in a fluid does not only vary in the horizontal direction but also varies in the vertical direction. This is due to the fact that more fluid rests on deeper layers and the effect of this extra weight on deeper layers is balanced by the increase in pressure.

Pressure in a fluid increases linearly with depth. The pressure difference between two points in a constant density fluid is proportional to the vertical distance between the points and the density of the fluid.

To obtain the equation for the hydrostatic force, consider an element of arbitrary shape submerged in a fluid. The absolute pressure at any point on a plate submerged in a fluid of constant density is given by Eq. (2.4):

$$P = P_o + \rho gh = P_o + \rho gy \sin\theta \quad (2.4)$$

Where  $h$  is the vertical distance of the point from the free surface and  $y$  is the distance of the point from the  $x$ -axis. The resultant force acting on the surface is determined by integrating the force  $P dA$  acting on a differential area  $dA$  over the entire surface area,

$$F_R = \int P dA = \int (P_{atm} + \rho gy \sin\theta) dA = P_o A + \rho g \sin\theta \int y dA \quad (2.5)$$

Here the first moment of area is related to the  $y$ -coordinate of the centroid by:

$$Y_c = 1/A \int y dA \quad (2.6)$$

Therefore, substituting the value to obtain the expression:

$$F_R = (P_o + \rho gy_c \sin\theta) A = (P_o + \rho gh_c) A = P_c A \quad (2.7)$$

Therefore it is concluded that the magnitude of the resultant hydrostatic force acting on a surface completely submerged in a fluid is equal to the product of the pressure at the centroid of the surface and the area of the surface.

This chapter summarizes the forces acting on a submerged body. Since the manipulator will be working inside deep sea, therefore, the forces discussed above will be acting on it but only the weight and lift buoyancy force will be considered in this work. This is because it is assumed that the manipulator will be moving at a very low velocity such that the dynamic forces can be neglected.

# CHAPTER 3

## SHIP POSITION OPTIMIZATION FOR NON- REDUNDANT CABLES

### 3.1 Theoretical Background

The subsea cable based parallel manipulator (CPM) considered in this study consists of a rectangular platform under the sea surface and attached to the moving ships at the sea surface via cables. There are six cables with lengths  $l_1, l_2, \dots, l_6$  attached to the manipulator at one end at points  $B_1, B_2, \dots, B_6$ , and to the individual ships on the sea surface at points  $A_1, A_2, \dots, A_6$  as shown in figure 3.1. The global coordinate frame  $x$ - $y$ - $z$  is fixed at the center of the cylindrical workspace with its axis aligned with the sides of the moving platform. The moving coordinate frame  $x_p$ - $y_p$ - $z_p$  is attached at the center  $P$  of the manipulator with its axes aligned with platform dimensions  $m$ ,  $n$  and  $o$ . The platform dimensions are given as  $m = 4m$ ,  $n = 5m$  and  $o = 0.3m$ . The moving platform can translate as well as rotate by extending or retracting the cables or by moving the ships along  $x$ - $y$ - $z$  axis. Each ship can move in a circular trajectory of radius 50m. The positions of the ships will be optimized in section 3.2 such that the manipulator can have the maximum workspace.

The moving platform will be equipped with grippers to perform pick and place operations and to carry out transportation of objects from one place to another under the sea surface. The moving platform is able to translate as well as rotate along all three axis  $x$ - $y$ - $z$ .

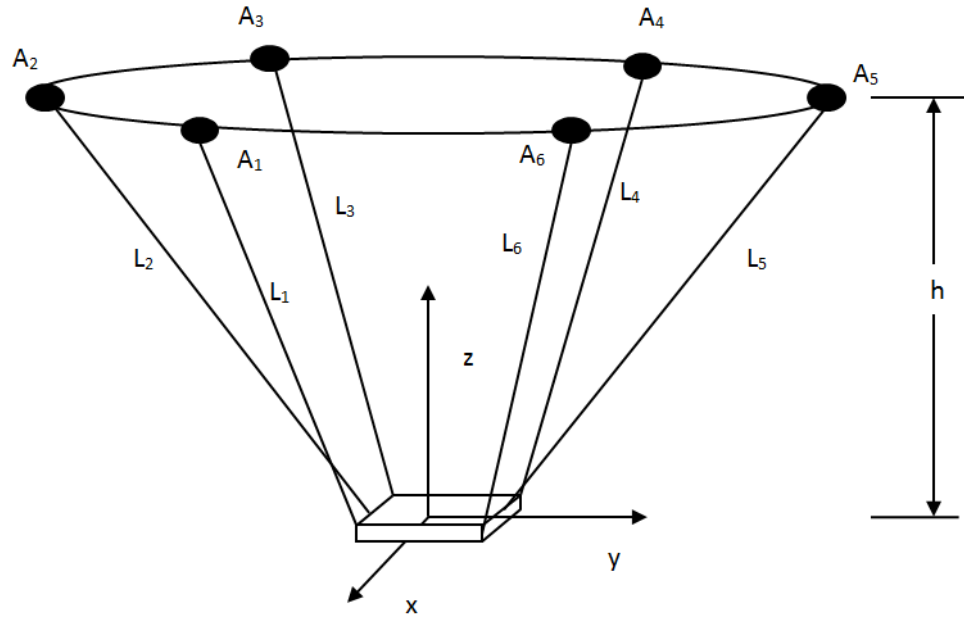


**Figure 3.1 Schematic Diagram of the cable driven manipulator layout.**

In this section, position, velocity and force analyses for the cable based manipulator shown in figure 3.1 are performed. Section 3.2 is devoted to the optimization of ship positions in order to maximize the workspace and stiffness of the moving platform.

### 3.1.1 Position Analysis

In this section, the position analysis of the parallel manipulator is developed using inverse kinematics. The moving platform with its vector notations is shown in figure 3.2.

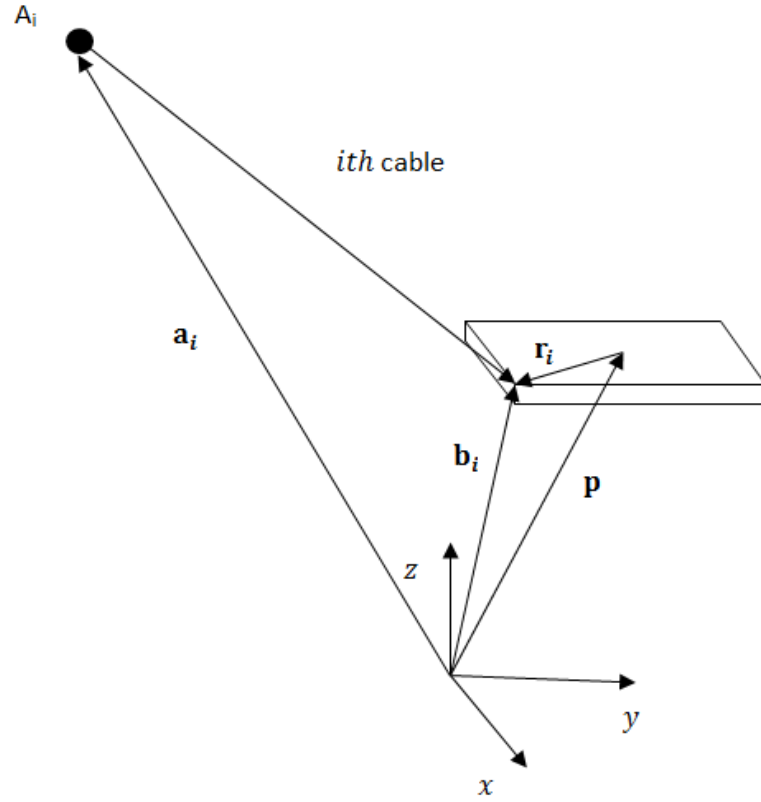


**Figure 3.2 Vector notation representation of the platform.**

As shown in figure 3.2, the length of the *ith* cable from point A to point B can be expressed as:

$$\mathbf{l}_i = \mathbf{b}_i - \mathbf{a}_i \quad (3.1)$$

where  $\mathbf{l}_i$  is the length of the cable connecting ship to the moving platform,  $\mathbf{b}_i$  is the position vector of point  $B_i$ , and  $\mathbf{a}_i$  is the position vector of point  $A_i$ . All vectors are expressed in global coordinate system.

Vector  $\mathbf{b}_i$  can be expressed as:

$$\mathbf{b}_i = \mathbf{p} + \mathbf{r}_i \quad (3.2)$$

where  $\mathbf{p}$  is the position vector of point  $P$  which is the center of the moving platform,  $\mathbf{r}_i$  is a vector from point  $P$  to point  $B_i$  in the global fixed frame expressed as:

$$\mathbf{r}_i = \mathbf{Q}\mathbf{r}_{mi} \quad (3.3)$$

$\mathbf{r}_{mi}$  represents a vector from point  $P$  to  $B_i$  in the moving frame.  $\mathbf{Q}$  is the rotation vector that represents the orientation of the moving platform with respect to the fixed frame and is given as:

$$\mathbf{Q} = \begin{bmatrix} \cos \emptyset \cos \theta \cos \psi \sin \theta \sin \psi - \sin \emptyset \cos \psi \cos \emptyset \sin \theta \cos \psi + \sin \emptyset \sin \psi \\ \sin \emptyset \cos \theta \sin \emptyset \sin \theta \sin \psi + \cos \emptyset \cos \psi \sin \emptyset \sin \theta \cos \psi - \cos \emptyset \sin \psi \\ -\sin \theta & \cos \theta \sin \psi & \cos \theta \cos \psi \end{bmatrix} \quad (3.4)$$

where  $\emptyset$  is the rotation angle about z-axis,  $\theta$  about y-axis and  $\psi$  about x-axis.

These are known as Roll-Pitch-Yaw angles.

The terms  $\mathbf{r}_{mi}$  ( $i = 1$  to 6) can be expressed as:

$$\mathbf{r}_{m1} = \left( \frac{m}{2}, -\frac{n}{2}, \frac{o}{2} \right)^T$$

$$\mathbf{r}_{m2} = \left( 0, -\frac{n}{2}, \frac{o}{2} \right)^T$$

$$\mathbf{r}_{m3} = \left( -\frac{m}{2}, -\frac{n}{2}, \frac{o}{2} \right)^T$$

$$\mathbf{r}_{m4} = \left( \frac{m}{2}, \frac{n}{2}, \frac{o}{2} \right)^T$$

$$\mathbf{r}_{m5} = \left(0, \frac{n}{2}, \frac{o}{2}\right)^T$$

$$\mathbf{r}_{m6} = \left(-\frac{m}{2}, \frac{n}{2}, \frac{o}{2}\right)^T \quad (3.5)$$

Multiplying the terms of  $\mathbf{r}_{mi}$  with rotation matrix  $\mathbf{Q}$  gives the terms of  $r_i$  as:

$\mathbf{r}_1$

$$= \begin{pmatrix} (\cos \emptyset \cos \theta) \frac{m}{2} - (\cos \emptyset \sin \theta \sin \psi - \sin \emptyset \cos \psi) \frac{n}{2} + (\cos \emptyset \sin \theta \cos \psi + \sin \emptyset \sin \psi) \frac{o}{2}, \\ (\sin \emptyset \cos \theta) \frac{m}{2} - (\sin \emptyset \sin \theta \sin \psi + \cos \emptyset \cos \psi) \frac{n}{2} + (\sin \emptyset \sin \theta \cos \psi - \cos \emptyset \sin \psi) \frac{o}{2}, \\ (-\sin \theta) \frac{m}{2} - (\cos \theta \sin \psi) \frac{n}{2} + (\cos \theta \cos \psi) \frac{o}{2} \end{pmatrix}$$

$$\mathbf{r}_2 = \begin{pmatrix} -(\cos \emptyset \sin \theta \sin \psi - \sin \emptyset \cos \psi) \frac{n}{2} + (\cos \emptyset \sin \theta \cos \psi + \sin \emptyset \sin \psi) \frac{o}{2}, \\ -(\sin \emptyset \sin \theta \sin \psi + \cos \emptyset \cos \psi) \frac{n}{2} + (\sin \emptyset \sin \theta \cos \psi - \cos \emptyset \sin \psi) \frac{o}{2}, \\ -(\cos \theta \sin \psi) \frac{n}{2} + (\cos \theta \cos \psi) \frac{o}{2} \end{pmatrix}$$

$\mathbf{r}_3$

$$= \begin{pmatrix} -(\cos \emptyset \cos \theta) \frac{m}{2} - (\cos \emptyset \sin \theta \sin \psi - \sin \emptyset \cos \psi) \frac{n}{2} + (\cos \emptyset \sin \theta \cos \psi + \sin \emptyset \sin \psi) \frac{o}{2}, \\ -(\sin \emptyset \cos \theta) \frac{m}{2} - (\sin \emptyset \sin \theta \sin \psi + \cos \emptyset \cos \psi) \frac{n}{2} + (\sin \emptyset \sin \theta \cos \psi - \cos \emptyset \sin \psi) \frac{o}{2}, \\ (\sin \theta) \frac{m}{2} - (\cos \theta \sin \psi) \frac{n}{2} + (\cos \theta \cos \psi) \frac{o}{2} \end{pmatrix}$$

$\mathbf{r}_4$

$$= \begin{pmatrix} (\cos \emptyset \cos \theta) \frac{m}{2} + (\cos \emptyset \sin \theta \sin \psi - \sin \emptyset \cos \psi) \frac{n}{2} + (\cos \emptyset \sin \theta \cos \psi + \sin \emptyset \sin \psi) \frac{o}{2}, \\ (\sin \emptyset \cos \theta) \frac{m}{2} + (\sin \emptyset \sin \theta \sin \psi + \cos \emptyset \cos \psi) \frac{n}{2} + (\sin \emptyset \sin \theta \cos \psi - \cos \emptyset \sin \psi) \frac{o}{2}, \\ (-\sin \theta) \frac{m}{2} + (\cos \theta \sin \psi) \frac{n}{2} + (\cos \theta \cos \psi) \frac{o}{2} \end{pmatrix}$$

$$\mathbf{r}_5 = \begin{pmatrix} (\cos\emptyset\sin\theta\sin\psi - \sin\emptyset\cos\psi)\frac{n}{2} + (\cos\emptyset\sin\theta\cos\psi + \sin\emptyset\sin\psi)\frac{o}{2}, \\ (\sin\emptyset\sin\theta\sin\psi + \cos\emptyset\cos\psi)\frac{n}{2} + (\sin\emptyset\sin\theta\cos\psi - \cos\emptyset\sin\psi)\frac{o}{2}, \\ (\cos\theta\sin\psi)\frac{n}{2} + (\cos\theta\cos\psi)\frac{o}{2} \end{pmatrix}$$

$\mathbf{r}_6 =$

$$\begin{pmatrix} -(\cos\emptyset\cos\theta)\frac{m}{2} + (\cos\emptyset\sin\theta\sin\psi - \sin\emptyset\cos\psi)\frac{n}{2} + (\cos\emptyset\sin\theta\cos\psi + \sin\emptyset\sin\psi)\frac{o}{2}, \\ -(\sin\emptyset\cos\theta)\frac{m}{2} + (\sin\emptyset\sin\theta\sin\psi + \cos\emptyset\cos\psi)\frac{n}{2} + (\sin\emptyset\sin\theta\cos\psi - \cos\emptyset\sin\psi)\frac{o}{2}, \\ (\sin\theta)\frac{m}{2} + (\cos\theta\sin\psi)\frac{n}{2} + (\cos\theta\cos\psi)\frac{o}{2} \end{pmatrix}$$

(3.6)

Similarly, the terms  $\mathbf{a}_i$  ( $i = 1$  to 6) can be expressed as:

$$\begin{aligned}\mathbf{a}_1 &= (g_1, s_1, h)^T \\ \mathbf{a}_2 &= (g_2, s_2, h)^T \\ \mathbf{a}_3 &= (g_3, s_3, h)^T \\ \mathbf{a}_4 &= (g_4, s_4, h)^T \\ \mathbf{a}_5 &= (g_5, s_5, h)^T \\ \mathbf{a}_6 &= (g_6, s_6, h)^T\end{aligned}$$

(3.7)

where  $g_i$  and  $s_i$  and  $h$  are the coordinates of the ships expressed in the fixed coordinate system. Substituting Eq. (3.2) in Eq. (3.1) results in

$$\mathbf{l}_i = \mathbf{p} + \mathbf{r}_i - \mathbf{a}_i \quad (3.8)$$

The square length of the  $i$ th cable can be obtained from Eq. (3.9) as



$$l_i^2 = (\mathbf{p} + \mathbf{r}_i - \mathbf{a}_i)^T (\mathbf{p} + \mathbf{r}_i - \mathbf{a}_i) \quad (3.9)$$

Position vector  $\mathbf{p}$  is given as:

$$\mathbf{p} = \begin{bmatrix} p_x \\ p_y \\ p_z \end{bmatrix} \quad (3.10)$$

where  $p_x$ ,  $p_y$  and  $p_z$  are the  $x$   $y$  and  $z$  coordinates, respectively, of the position vector  $\mathbf{p}$ .

Therefore, substituting Eq. (3.6) and Eq. (3.7) into Eq. (3.9) gives the square of the length of the cables required to position the moving platform at any given position and orientation.

$$\begin{aligned} l_1^2 = & \left( p_x + (\cos \emptyset \cos \theta) \frac{m}{2} - (\cos \emptyset \sin \theta \sin \psi - \sin \emptyset \cos \psi) \frac{n}{2} \right. \\ & \left. + (\cos \emptyset \sin \theta \cos \psi + \sin \emptyset \sin \psi) \frac{o}{2} - g_1 \right)^2 \\ & + \left( p_y + (\sin \emptyset \cos \theta) \frac{m}{2} - (\sin \emptyset \sin \theta \sin \psi + \cos \emptyset \cos \psi) \frac{n}{2} \right. \\ & \left. + (\sin \emptyset \sin \theta \cos \psi - \cos \emptyset \sin \psi) \frac{o}{2} - s_1 \right)^2 \\ & + \left( p_z + (-\sin \theta) \frac{m}{2} - (\cos \theta \sin \psi) \frac{n}{2} + (\cos \theta \cos \psi) \frac{o}{2} - h_1 \right)^2 \end{aligned}$$

$$\begin{aligned}
l_2^2 = & \left( p_x - (\cos\emptyset \sin\theta \sin\psi - \sin\emptyset \cos\psi) \frac{n}{2} + (\cos\emptyset \sin\theta \cos\psi + \sin\emptyset \sin\psi) \frac{o}{2} - g_2 \right)^2 \\
& + \left( p_y - (\sin\emptyset \sin\theta \sin\psi + \cos\emptyset \cos\psi) \frac{n}{2} \right. \\
& \left. + (\sin\emptyset \sin\theta \cos\psi - \cos\emptyset \sin\psi) \frac{o}{2} - s_2 \right)^2 \\
& + \left( p_z - (\cos\theta \sin\psi) \frac{n}{2} + (\cos\theta \cos\psi) \frac{o}{2} - h_2 \right)^2
\end{aligned}$$

$$\begin{aligned}
l_3^2 = & \left( p_x - (\cos\emptyset \cos\theta) \frac{m}{2} - (\cos\emptyset \sin\theta \sin\psi - \sin\emptyset \cos\psi) \frac{n}{2} \right. \\
& \left. + (\cos\emptyset \sin\theta \cos\psi + \sin\emptyset \sin\psi) \frac{o}{2} - g_3 \right)^2 \\
& + \left( p_y - (\sin\emptyset \cos\theta) \frac{m}{2} - (\sin\emptyset \sin\theta \sin\psi + \cos\emptyset \cos\psi) \frac{n}{2} \right. \\
& \left. + (\sin\emptyset \sin\theta \cos\psi - \cos\emptyset \sin\psi) \frac{o}{2} - s_3 \right)^2 \\
& + \left( p_z + (\sin\theta) \frac{m}{2} - (\cos\theta \sin\psi) \frac{n}{2} + (\cos\theta \cos\psi) \frac{o}{2} - h_3 \right)^2
\end{aligned}$$

$$\begin{aligned}
l_4^2 = & \left( p_x + (\cos\emptyset \cos\theta) \frac{m}{2} + (\cos\emptyset \sin\theta \sin\psi - \sin\emptyset \cos\psi) \frac{n}{2} \right. \\
& \left. + (\cos\emptyset \sin\theta \cos\psi + \sin\emptyset \sin\psi) \frac{o}{2} - g_4 \right)^2 \\
& + \left( p_y + (\sin\emptyset \cos\theta) \frac{m}{2} + (\sin\emptyset \sin\theta \sin\psi + \cos\emptyset \cos\psi) \frac{n}{2} \right. \\
& \left. + (\sin\emptyset \sin\theta \cos\psi - \cos\emptyset \sin\psi) \frac{o}{2} - s_4 \right)^2 \\
& + \left( p_z + (-\sin\theta) \frac{m}{2} + (\cos\theta \sin\psi) \frac{n}{2} + (\cos\theta \cos\psi) \frac{o}{2} - h_4 \right)^2
\end{aligned}$$

$$\begin{aligned}
l_5^2 = & \left( p_x + (\cos\phi\sin\theta\sin\psi - \sin\phi\cos\psi) \frac{n}{2} + (\cos\phi\sin\theta\cos\psi + \sin\phi\sin\psi) \frac{o}{2} - g_5 \right)^2 \\
& + \left( p_y + (\sin\phi\sin\theta\sin\psi + \cos\phi\cos\psi) \frac{n}{2} \right. \\
& \left. + (\sin\phi\sin\theta\cos\psi - \cos\phi\sin\psi) \frac{o}{2} - s_5 \right)^2 \\
& + \left( p_z + (\cos\theta\sin\psi) \frac{n}{2} + (\cos\theta\cos\psi) \frac{o}{2} - h_5 \right)^2 \\
l_6^2 = & \left( p_x - (\cos\phi\cos\theta) \frac{m}{2} + (\cos\phi\sin\theta\sin\psi - \sin\phi\cos\psi) \frac{n}{2} + (\cos\phi\sin\theta\cos\psi + \right. \\
& \left. \sin\phi\sin\psi) \frac{o}{2} - g_6 \right)^2 + \left( p_y - (\sin\phi\cos\theta) \frac{m}{2} + (\sin\phi\sin\theta\sin\psi + \cos\phi\cos\psi) \frac{n}{2} + \right. \\
& \left. (\sin\phi\sin\theta\cos\psi - \cos\phi\sin\psi) \frac{o}{2} - s_6 \right)^2 + \left( p_z + (\sin\theta) \frac{m}{2} + (\cos\theta\sin\psi) \frac{n}{2} + \right. \\
& \left. (\cos\theta\cos\psi) \frac{o}{2} - h_6 \right)^2
\end{aligned} \tag{3.11}$$

The square root of the above equations is the lengths of the cables required to move the platform to any desired position and orientation.

### 3.1.2 Velocity Analysis

The velocity of the moving platform is directly related to the cable length change rates. This section is devoted to the Jacobian analysis of the parallel manipulator. Jacobian matrix maps the velocity of the moving platform to the velocities of the cables.

Differentiating Eq. (3.8) with respect to time gives:

$$\dot{l}_i \hat{\mathbf{l}}_i + \boldsymbol{\omega}_i \times \mathbf{l}_i = \mathbf{v} + \boldsymbol{\omega} \times \mathbf{r}_i \tag{3.12}$$

Where  $\dot{l}_i$  is the cable length rate of the  $i$ th cable,  $\hat{\mathbf{l}}_i = [\hat{l}_{ix} \hat{l}_{iy} \hat{l}_{iz}]$  is the unit vector in the direction of vector  $\mathbf{l}_i$ ;  $\boldsymbol{\omega}_i$  is the angular velocity vector of the  $i$ th cable with respect

to the fixed frame. Vector  $\mathbf{V}$  is the velocity of point  $P$  with respect to fixed frame and  $\boldsymbol{\omega}$  is the angular velocity vector of the moving platform with respect to the fixed frame.

Dot multiplying Eq. (3.12) by  $\hat{\mathbf{I}}_i$  gives,

$$\dot{l}_i = \hat{\mathbf{I}}_i \cdot \mathbf{v} + (\mathbf{r}_i \times \hat{\mathbf{I}}_i) \cdot \boldsymbol{\omega} \quad (3.13)$$

Writing Eq. (3.13) for all six cables results in

$$\begin{bmatrix} \dot{l}_1 \\ \dot{l}_2 \\ \dot{l}_3 \\ \dot{l}_4 \\ \dot{l}_5 \\ \dot{l}_6 \end{bmatrix} = \begin{bmatrix} \hat{\mathbf{I}}_1^T (\mathbf{r}_1 \times \hat{\mathbf{I}}_1)^T \\ \hat{\mathbf{I}}_2^T (\mathbf{r}_2 \times \hat{\mathbf{I}}_2)^T \\ \hat{\mathbf{I}}_3^T (\mathbf{r}_3 \times \hat{\mathbf{I}}_3)^T \\ \hat{\mathbf{I}}_4^T (\mathbf{r}_4 \times \hat{\mathbf{I}}_4)^T \\ \hat{\mathbf{I}}_5^T (\mathbf{r}_5 \times \hat{\mathbf{I}}_5)^T \\ \hat{\mathbf{I}}_6^T (\mathbf{r}_6 \times \hat{\mathbf{I}}_6)^T \end{bmatrix} \begin{bmatrix} \mathbf{v} \\ \boldsymbol{\omega} \end{bmatrix} \quad (3.14)$$

Eq. (3.14) can be written as:

$$\begin{bmatrix} \dot{l}_1 \\ \dot{l}_2 \\ \dot{l}_3 \\ \dot{l}_4 \\ \dot{l}_5 \\ \dot{l}_6 \end{bmatrix} = \begin{bmatrix} \hat{l}_{1x} \hat{l}_{1y} \hat{l}_{1z} (r_{1x} \times \hat{l}_{1x}) (r_{1y} \times \hat{l}_{1y}) (r_{1z} \times \hat{l}_{1z}) \\ \hat{l}_{1x} \hat{l}_{1y} \hat{l}_{1z} (r_{2x} \times \hat{l}_{2x}) (r_{2y} \times \hat{l}_{2y}) (r_{2z} \times \hat{l}_{2z}) \\ \hat{l}_{1x} \hat{l}_{1y} \hat{l}_{1z} (r_{3x} \times \hat{l}_{3x}) (r_{3y} \times \hat{l}_{3y}) (r_{3z} \times \hat{l}_{3z}) \\ \hat{l}_{1x} \hat{l}_{1y} \hat{l}_{1z} (r_{4x} \times \hat{l}_{4x}) (r_{4y} \times \hat{l}_{4y}) (r_{4z} \times \hat{l}_{4z}) \\ \hat{l}_{1x} \hat{l}_{1y} \hat{l}_{1z} (r_{5x} \times \hat{l}_{5x}) (r_{5y} \times \hat{l}_{5y}) (r_{5z} \times \hat{l}_{5z}) \\ \hat{l}_{1x} \hat{l}_{1y} \hat{l}_{1z} (r_{6x} \times \hat{l}_{6x}) (r_{6y} \times \hat{l}_{6y}) (r_{6z} \times \hat{l}_{6z}) \end{bmatrix} \begin{bmatrix} v_x \\ v_y \\ v_z \\ \omega_x \\ \omega_y \\ \omega_z \end{bmatrix} \quad (3.15)$$

Substituting the values in Eq. (3.15) gives the cable length rates given the linear and angular velocities of the moving platform.

### 3.1.3 Force Analysis

When a task is performed by the manipulator, the end effector exerts force and moment on the external environment. In order to indicate both force and moment, the

term wrench is used. Wrenches are generated due to the actuation system. In parallel manipulators, these wrenches are transmitted from the actuators to the end-effector through several closed loop kinematic chains. In cable based parallel manipulators, these wrenches are transmitted by extending and retracting cables and by ensuring the conditions of positive tensions.

Static force analysis will be performed in order to determine the feasible workspace of the manipulator.

In parallel manipulators the actuator input wrenches are related to the end-effector output wrench by the transpose of the manipulator Jacobian matrix [21].

Therefore, the equation can be formulated as:

$$\mathbf{W} = \mathbf{J}^T \boldsymbol{\tau} \quad (3.16)$$

Where  $\mathbf{W}$  is the wrench applied to the manipulator and  $\boldsymbol{\tau}$  is the tension of the cables. Eq. (3.16) can be written for all six cables as:

$$\begin{bmatrix} F_x \\ F_y \\ F_z \\ M_x \\ M_y \\ M_z \end{bmatrix} = \begin{bmatrix} \hat{l}_{1x} \hat{l}_{1y} \hat{l}_{1z} (r_{1x} \times \hat{l}_{1x}) (r_{1y} \times \hat{l}_{1y}) (r_{1z} \times \hat{l}_{1z}) \\ \hat{l}_{1x} \hat{l}_{1y} \hat{l}_{1z} (r_{2x} \times \hat{l}_{2x}) (r_{2y} \times \hat{l}_{2y}) (r_{2z} \times \hat{l}_{2z}) \\ \hat{l}_{1x} \hat{l}_{1y} \hat{l}_{1z} (r_{3x} \times \hat{l}_{3x}) (r_{3y} \times \hat{l}_{3y}) (r_{3z} \times \hat{l}_{3z}) \\ \hat{l}_{1x} \hat{l}_{1y} \hat{l}_{1z} (r_{4x} \times \hat{l}_{4x}) (r_{4y} \times \hat{l}_{4y}) (r_{4z} \times \hat{l}_{4z}) \\ \hat{l}_{1x} \hat{l}_{1y} \hat{l}_{1z} (r_{5x} \times \hat{l}_{5x}) (r_{5y} \times \hat{l}_{5y}) (r_{5z} \times \hat{l}_{5z}) \\ \hat{l}_{1x} \hat{l}_{1y} \hat{l}_{1z} (r_{6x} \times \hat{l}_{6x}) (r_{6y} \times \hat{l}_{6y}) (r_{6z} \times \hat{l}_{6z}) \end{bmatrix}^T \begin{bmatrix} \tau_1 \\ \tau_2 \\ \tau_3 \\ \tau_4 \\ \tau_5 \\ \tau_6 \end{bmatrix} \quad (3.17)$$

In order to calculate the tensions in the cables, Eq. (3.17) becomes:

$$\begin{bmatrix} \tau_1 \\ \tau_2 \\ \tau_3 \\ \tau_4 \\ \tau_5 \\ \tau_6 \end{bmatrix} = \left( \begin{bmatrix} \hat{l}_{1x} \hat{l}_{1y} \hat{l}_{1z} (r_{1x} \times \hat{l}_{1x}) (r_{1y} \times \hat{l}_{1y}) (r_{1z} \times \hat{l}_{1z}) \\ \hat{l}_{1x} \hat{l}_{1y} \hat{l}_{1z} (r_{2x} \times \hat{l}_{2x}) (r_{2y} \times \hat{l}_{2y}) (r_{2z} \times \hat{l}_{2z}) \\ \hat{l}_{1x} \hat{l}_{1y} \hat{l}_{1z} (r_{3x} \times \hat{l}_{3x}) (r_{3y} \times \hat{l}_{3y}) (r_{3z} \times \hat{l}_{3z}) \\ \hat{l}_{1x} \hat{l}_{1y} \hat{l}_{1z} (r_{4x} \times \hat{l}_{4x}) (r_{4y} \times \hat{l}_{4y}) (r_{4z} \times \hat{l}_{4z}) \\ \hat{l}_{1x} \hat{l}_{1y} \hat{l}_{1z} (r_{5x} \times \hat{l}_{5x}) (r_{5y} \times \hat{l}_{5y}) (r_{5z} \times \hat{l}_{5z}) \\ \hat{l}_{1x} \hat{l}_{1y} \hat{l}_{1z} (r_{6x} \times \hat{l}_{6x}) (r_{6y} \times \hat{l}_{6y}) (r_{6z} \times \hat{l}_{6z}) \end{bmatrix}^T \right)^{-1} \begin{bmatrix} F_x \\ F_y \\ F_z \\ M_x \\ M_y \\ M_z \end{bmatrix} \quad (3.18)$$

Eq. (3.18) gives the cable tensions in terms of end effector wrench. The wrench can be found from the external forces and moments applied on the moving platform explained in Chapter 2.

### 3.2 Layout Optimization

In this section, optimum positions of the ships are determined to maximize the workspace of the manipulator. Another optimization scheme presented in this section focuses on maximizing the stiffness of the manipulator in the workspace by calculating the smallest natural frequency.

#### 3.2.1 Fundamentals on Workspace evaluation

Workspace is one of the important characteristics of the manipulator. The workspace of a cable-driven manipulator includes the set of all poses a manipulator can reach such that:

- The tensions in the cables are positive i.e.  $\tau_i > 0 \forall i$
- The end-effector should avoid any singular condition i.e.  $Rank(\mathbf{J}) = n$

Several definitions of workspace are available in the literature. For instance, the term controllable workspace is used to denote the set of all poses where the end-effector can be reached with positive tensions in the cables [25]. In [15], the statically reachable

workspace gives the poses where the end-effector can be reached with static ensured conditions. In [16], the wrench feasible term is used that denotes the set of all poses of the end-effector where it can apply the required set of wrenches.

In cable based parallel manipulators, the workspace definition involves both geometrical and static parameters. The evaluation of different kinds of workspace can be achieved with several techniques i.e. it may be geometrical, analytical or numerical and it may depend upon the application requests.

The dimensions of the workspace can be determined by its area in case of a planar manipulator or by its volume in case of a spatial manipulator. While determining the workspace singular positions of the manipulator should be avoided.

### 3.2.2 Singularity Analysis

The manipulator is said to be in a singular configuration when it has uncontrollable degrees of freedoms (DOFs). The analysis of the singular configuration of the manipulator can be investigating the properties of the Jacobian matrix  $\mathbf{J}$ . If vector  $\mathbf{q}$  denotes the joint variables and  $\mathbf{x}$  denotes the position of the moving platform, the kinematic constraints imposed by the limbs can be written as:

$$\mathbf{f}(\mathbf{x}, \mathbf{q}) = \mathbf{0} \quad (3.19)$$

Where  $\mathbf{f}$  denotes the  $n$ -dimensional implicit function of  $\mathbf{x}$  and  $\mathbf{q}$  and  $\mathbf{0}$  is an  $n$ -dimensional zero vector. The relationship between end-effector output velocity and the input cable rates can be found by differentiating Eq. (3.19) as:

$$\mathbf{J}_x \dot{\mathbf{x}} = \mathbf{J}_q \dot{\mathbf{q}} \quad (3.20)$$

$$\text{Where } \mathbf{J}_x = \frac{\partial \mathbf{f}}{\partial \mathbf{x}} \text{ and } \mathbf{J}_q = - \frac{\partial \mathbf{f}}{\partial \mathbf{q}}$$

Hence the Jacobian matrix can be written as:

$$\dot{\mathbf{q}} = \mathbf{J}\dot{\mathbf{x}} \quad (3.21)$$

$$\text{Where } \mathbf{J} = \mathbf{J}_q^{-1} \mathbf{J}_x$$

In a parallel manipulator, singularities can be divided into three types due to the existence of two Jacobian matrices.

- An inverse kinematic singularity that occurs when the determinant of  $\mathbf{J}_q$  becomes zero. i.e.  $\text{Det}(\mathbf{J}_q) = 0$ . In this configuration, the manipulator loses one or more DOF.
- A direct kinematic singularity that occurs when the determinant of  $\mathbf{J}_x$  goes to zero. i.e.  $\text{Det}(\mathbf{J}_x) = 0$ . In this configuration, the manipulator gains one or more DOF.
- A combined singularity that occurs when the determinants of both  $\mathbf{J}_x$  and  $\mathbf{J}_q$  are zero. Generally, this type of singularity occurs for manipulators with special kinematic architectures.

Therefore it can be said that a cable based manipulator is singular if and only if the structure matrix has a rank smaller than the DOF of the manipulator.

$$\text{Rank}(\mathbf{J}) < n \quad (3.22)$$

For example, a cable based manipulator having 6 DOFs is singular if the rank of the matrix is less than six. Singularities can be avoided by adding additional links to the manipulator.



### **3.2.3 Maximizing Workspace**

The inverse kinematics for the proposed design is performed by applying formulations in Eq. (3.11), Eq. (3.15) and Eq. (3.18). By considering the configuration, a numerical algorithm is being implemented as depicted in figure 3.3 and results have been obtained. For every set of ship positions the proposed algorithm computes the workspace of the manipulator by verifying if the manipulator satisfies the imposed geometrical constraints, tensions in the cables are positive and the manipulator is not at a singular configuration.

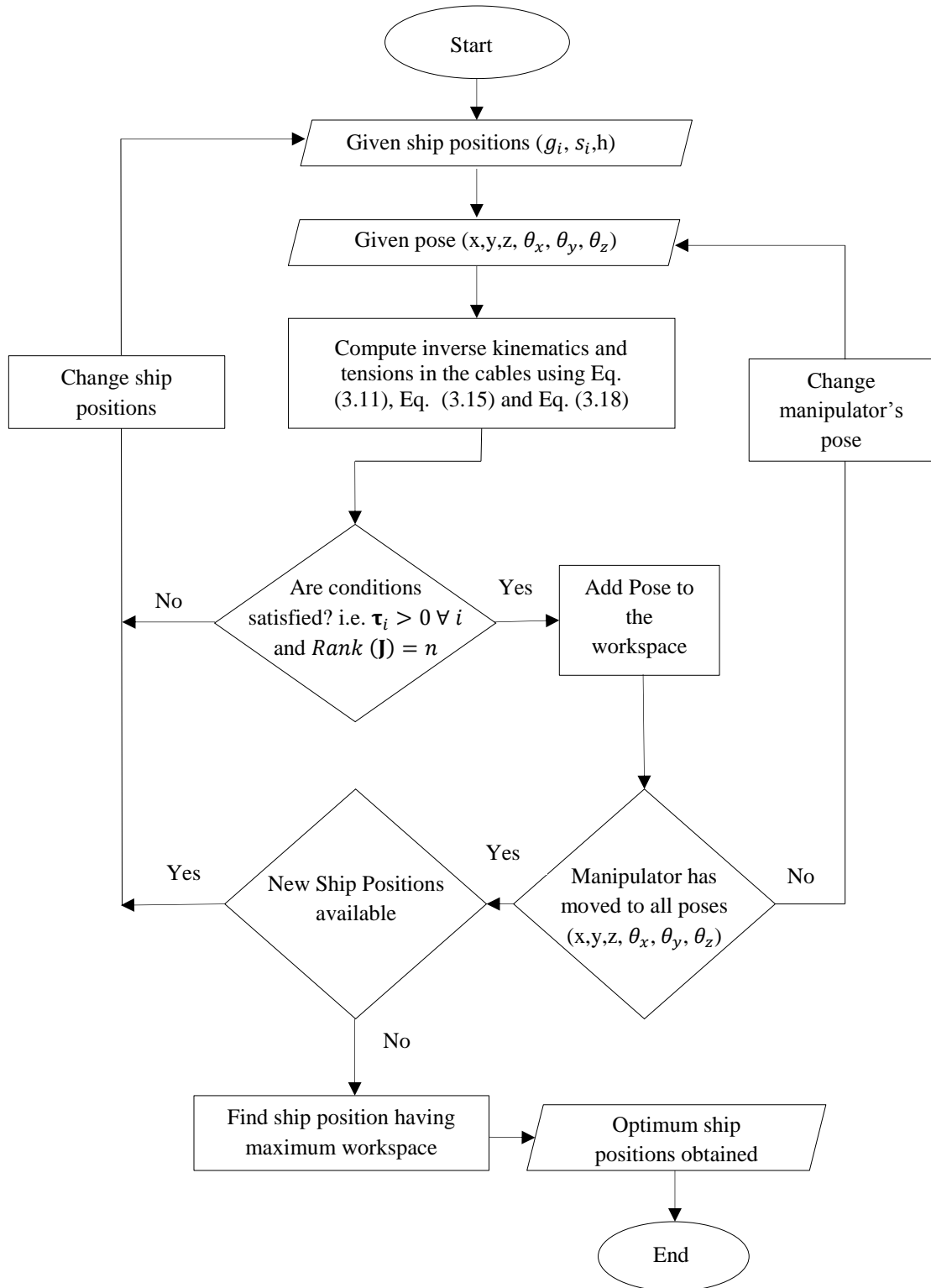


**Figure 3.3 A flow chart of the algorithm for computing the optimum ship positions based on maximum workspace of the manipulator.**

In order to determine the optimum positions of the ships, the workspace of the manipulator is maximized. The workspace is determined by the following conditions:

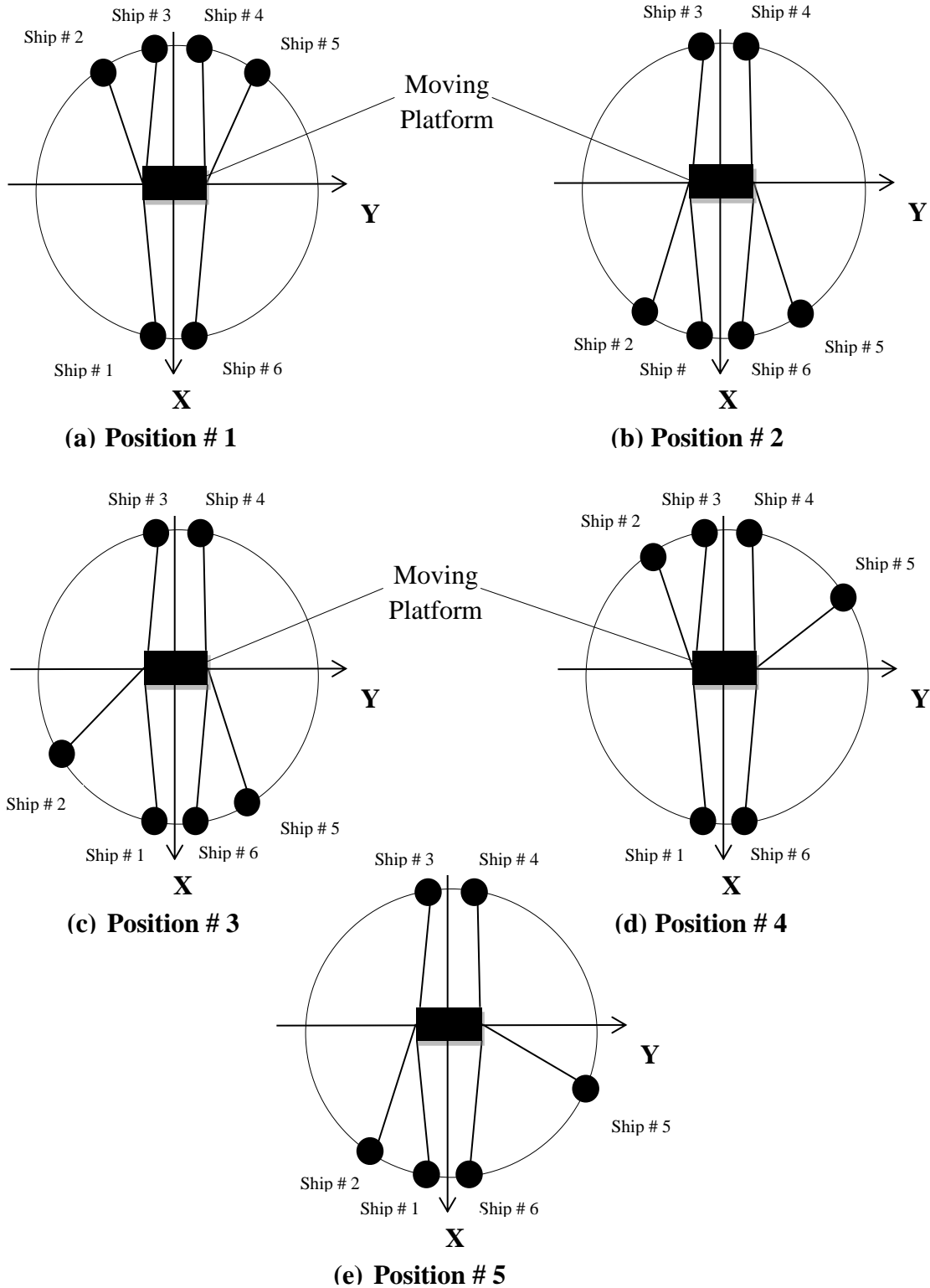
- The manipulator satisfies the imposed geometric constraints.
- Tensions should be positive in all cables i.e.  $\tau_i > 0 \forall i$
- The manipulator should avoid any singular position. i.e.  $Rank(\mathbf{J}) = n$

The workspace of the manipulator that satisfies the above conditions is determined. The algorithm in figure 3.3 computes the workspace of the manipulator for each possible position of the ships. For a given ship position and manipulator's pose, it computes the tension in the cables using Eq. (3.11), Eq. (3.15) and Eq. (3.18). If the required conditions are satisfied i.e.  $\tau_i > 0 \forall i$  and  $Rank(\mathbf{J}) = n$ , it adds the pose of the manipulator to the workspace. In order to determine the full workspace, the algorithm repeats the same procedure for every pose of the manipulator. Finally, the above procedure is repeated for each combination of the ship position.

The position having maximum workspace is the optimum position of the ships. Table 3.1 summarizes the results obtained from the proposed algorithm in figure 3.3. It shows the number of workspace discrete points and their respective ship coordinates for the best five position sets of the ships. The top view of the cable based manipulator for these best five position sets of the ships are shown in figure 3.4. Solid circles denote the ships. It should be noted that the ship positions were optimized with the perimeter of a circle around the moving platform.

**Table 3.1 Computed Workspace for CPM with six cables by using the proposed algorithm with constraints expressed in Eq. (3.15), Eq. (3.16) and Eq. (3.18).**

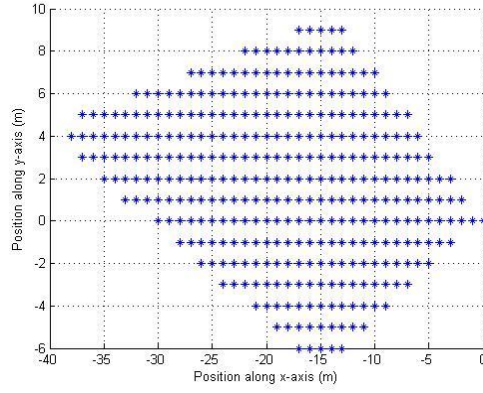
<b>Optimized Ship Position No.</b>	<b>1</b>	<b>2</b>	<b>3</b>	<b>4</b>	<b>5</b>
<b>x-y coordinate of Ship # 1 (m)</b>	49.8,-4.4	49.8,-4.4	49.8,-4.4	49.8,-4.4	49.8,-4.4
<b>x-y coordinate of Ship # 2 (m)</b>	-43.3,-25.0	38.3,-32.1	43.3,-25.0	-17.1,-47.0	38.3,-32.1
<b>x-y coordinate of Ship # 3 (m)</b>	-49.8,-4.4	-49.8,-4.4	-49.8,-4.4	-49.8,-4.4	-49.8,-4.4
<b>x-y coordinate of Ship # 4 (m)</b>	-49.8,4.4	-49.8,4.4	-49.8,4.4	-49.8,4.4	-49.8,4.4
<b>x-y coordinate of Ship # 5 (m)</b>	-38.3,32.1	43.3,25.0	17.1,47.0	-43.3,25.0	25.0,43.3
<b>x-y coordinate of Ship # 6 (m)</b>	49.8,4.4	49.8,4.4	49.8,4.4	49.8,4.4	49.8,4.4
<b>Workspace discrete points</b>	1704	1704	1692	1683	1600



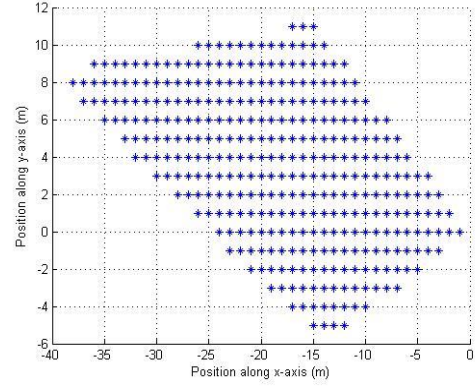
**Figure 3.4 Top five optimum ship positions for CPM with six cables based on maximizing workspace of the manipulator.**

Figure 3.4 is the pictorial representation of table 3.1. In table 3.1, number of discrete points of the workspace is shown for each set of position of the ships. The maximum points obtained are 1704 which shows the manipulator can move to 1704 distinct poses when the ship positions are given for ship position 1 in table 3.1. The pictorial representation of the manipulator for these ship coordinates are shown in figure 3.4(a). The manipulator can have the same 1704 distinct poses in the workspace when the ship coordinates are given for position 2 in table 3.1. The difference would be in the first case the manipulator's workspace is mostly at the upper portion of the semi-circle in figure 3.4(a) whereas in the second case, the workspace is at the lower portion of the semi-circle in figure 3.4(b). Similarly, for ship position number 3 in table 3.1, the manipulator can move to 1692 distinct poses and for position 4 and 5; the number of distinct poses reduces to 1683 and 1600 respectively. Since the objective was to determine the optimum positions of the ships based on maximizing workspace of the manipulator, therefore it can be concluded that the first two positions in table 3.1 or in figure 3.4(a) and (b) are the optimum positions of the ships.

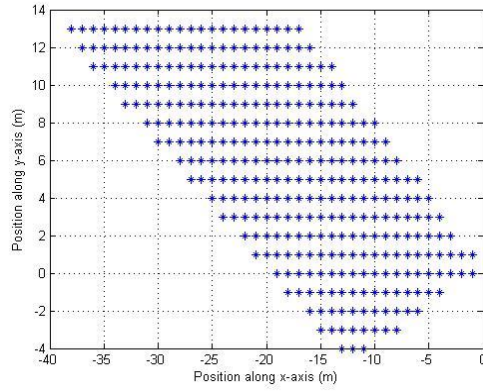
Considering the first position set of the ships in figure 3.4(a), the results of the numerical analysis are being reported in order to establish poses reachable by the manipulator by considering the given constraints. The position of the manipulator determined by keeping the values of the orientation angles  $\theta_x$   $\theta_y$   $\theta_z$  fixed. The range of values for angle  $\theta_x$   $\theta_y$   $\theta_z$  are assumed as  $[0, 85]$ ,  $[0, 60]$ ,  $[0, 40]$  respectively. By considering the values of  $\theta_x$  the poses of the manipulator obtained are shown in figure 3.5.



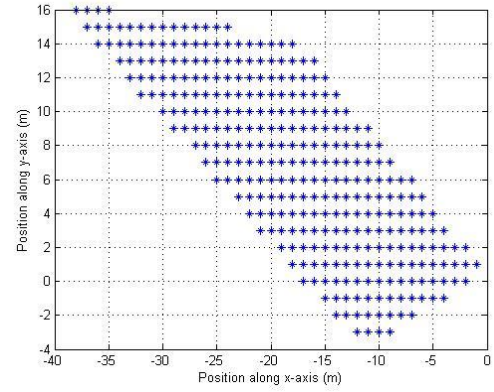
(a)  $\theta_x = 0$



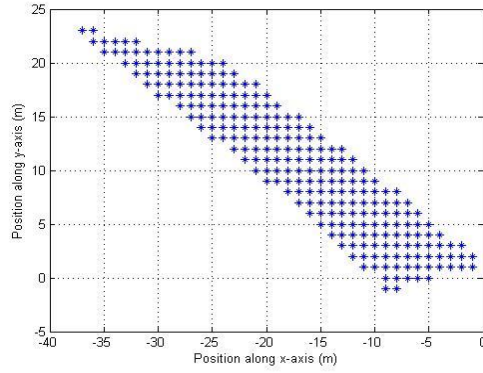
(b)  $\theta_x = 20$



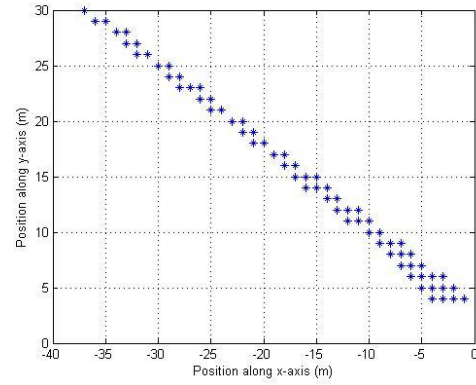
(c)  $\theta_x = 40$



(d)  $\theta_x = 50$



(e)  $\theta_x = 70$



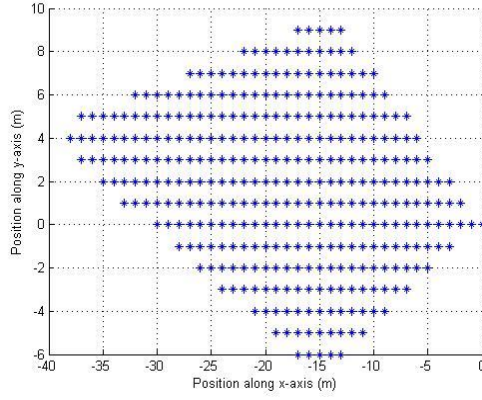
(f)  $\theta_x = 85$

**Figure 3.5 Manipulators planer workspace x-y by varying angular orientation  $\theta_x$  for position 1 in figure 3.4(a).**

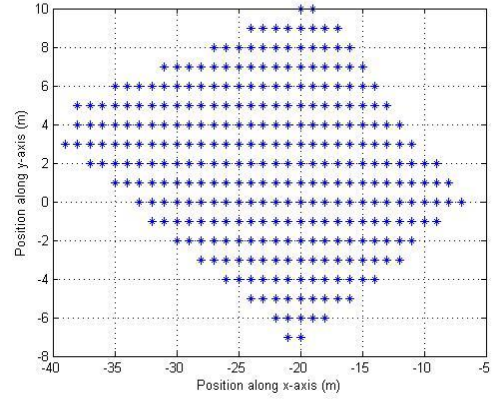
The results in figure 3.5 show that the manipulator gives the maximum workspace when  $\theta_x$  is equal to zero. The workspace continues to decrease by increasing the value of orientation angle  $\theta_x$  till it reaches value of  $85^\circ$  degrees where it tends towards a line representing its geometrical limit. The workspace changes shape and dimension by assuming values of the orientation angle between  $[0-85]$ .

Similarly, by varying the values of the orientation angle  $\theta_y$  the poses of the manipulator are being obtained. These results also show similar trend of the workspace as in case for the orientation angle  $\theta_x$ . The workspace decreases till it reaches the maximum allowable range of the orientation angle  $\theta_y$  which is  $60^\circ$  in this case. The obtained workspace is shown in figure 3.6 below. It should be noted that cable-driven manipulators allow limited rotations in their workspace. This is the reason for the decrease in the overall workspace volume at large orientation angles.

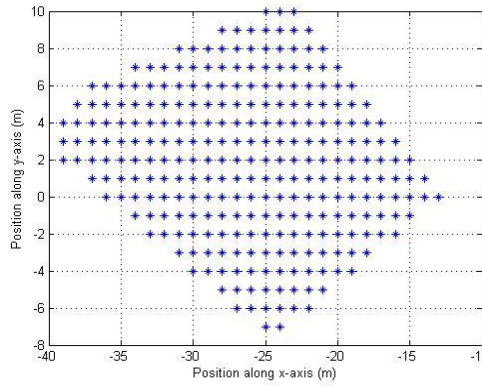




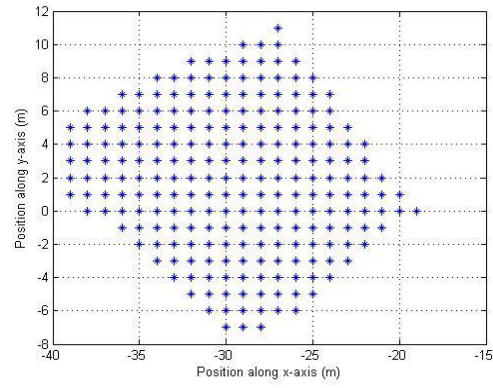
(a)  $\theta_y = 0$



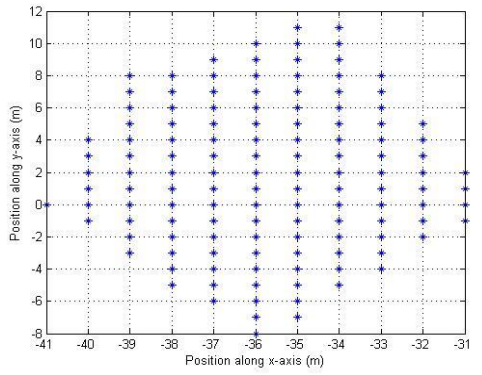
(b)  $\theta_y = 10$



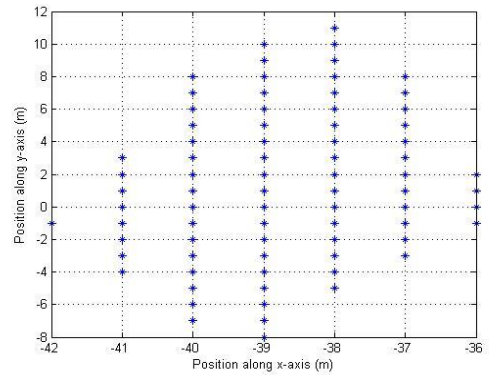
(c)  $\theta_y = 20$



(d)  $\theta_y = 30$



(e)  $\theta_y = 50$

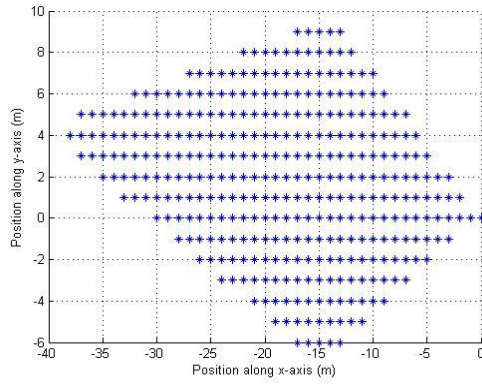


(f)  $\theta_y = 60$

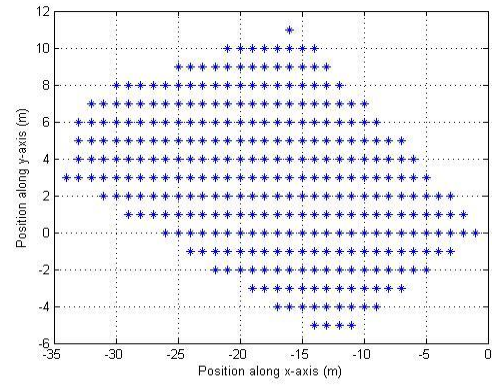
**Figure 3.6 Manipulators planer workspace x-y by varying angular orientation  $\theta_y$**

**for position 1 in figure 3.4(a).**

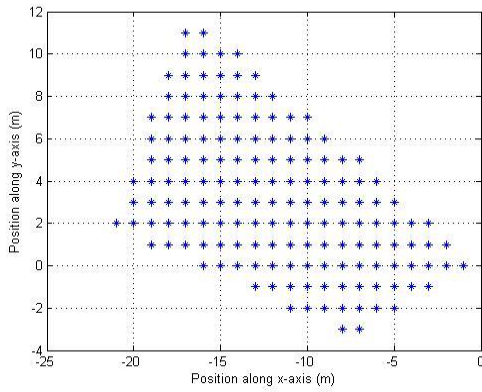
Finally, the poses of the manipulator are obtained by varying the values of the orientation angle  $\theta_z$ . In this case, the workspace area also decreases by increasing the value of the orientation angle  $\theta_z$ . Results are shown in figure 3.7. The maximum allowable range of orientation angle  $\theta_z$  is  $40^\circ$  where the dimensions of the manipulator's workspace area are reduced.



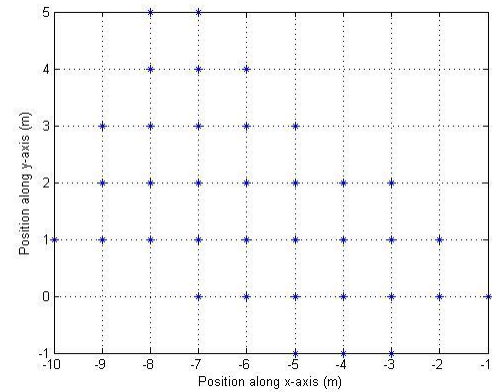
(a)  $\theta_z = 0$



(b)  $\theta_z = 10$



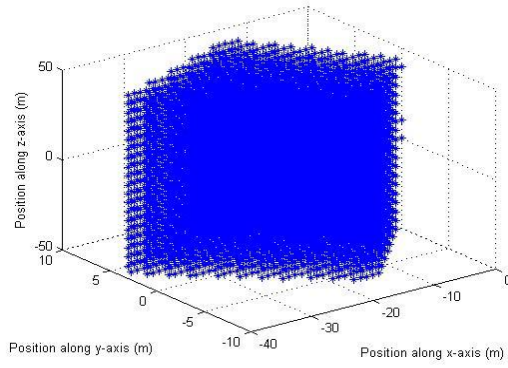
(c)  $\theta_z = 20$



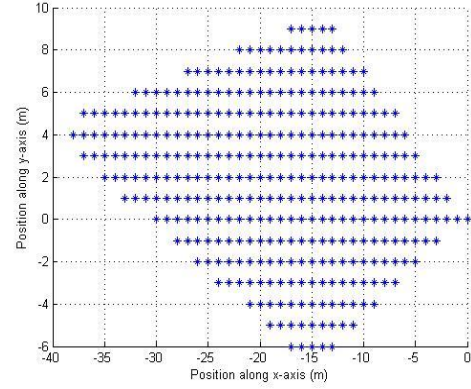
(d)  $\theta_z = 40$

**Figure 3.7 Manipulators planer workspace x-y by varying angular orientation  $\theta_z$  for position 1 in figure 3.4(a).**

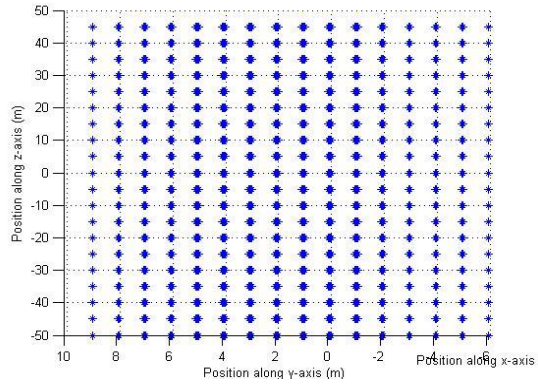
Figure 3.5 to 3.7 shows the manipulator's planar workspace where the manipulator is considered to move at a constant depth inside sea. It is possible to obtain the spatial workspace by moving the manipulator along the z-axis which is the depth of the sea. By considering the given constraints, the manipulator can be moved in a cubic volume to give the 3D workspace of the manipulator as shown in 3.8(a). It shows the workspace remains constant along the depth z-axis. Figure 3.8(b) and 3.8(c) shows the x-y and x-z workspace of the manipulator. As mentioned, it can be seen from figure 3.8(c) that the workspace remains the same along the z coordinate. The variation along the orientation of the manipulator can be seen in figure 3.8(d) to 3.8(f). Figure 3.8(d) depicts the variation along all three angles which shows the workspace is maximum when  $\theta_x\theta_y\theta_z$  are close to zero. As the values of the orientation angles  $\theta_x\theta_y\theta_z$  increase, the workspace is decreased showing its allowable limit. The planar workspace for the orientation angles are shown in figure 3.8(e) and 3.8(f). For the case of  $\theta_x\theta_y$  workspace in figure 3.8(e), the workspace remains constant i.e. for every value of  $\theta_x$ , there are almost same number of poses of  $\theta_y$  where the manipulator can reach with positive tension values. In figure 3.8(f), the  $\theta_x\theta_z$  workspace is shown. It can be seen from figure 3.8(f) that  $\theta_z$  is maximum when  $\theta_x$  is zero and it decreases with a constant rate on both sides of  $\theta_x$ .



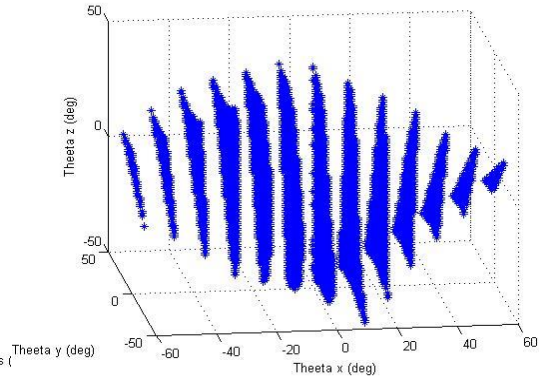
(a) 3D Workspace



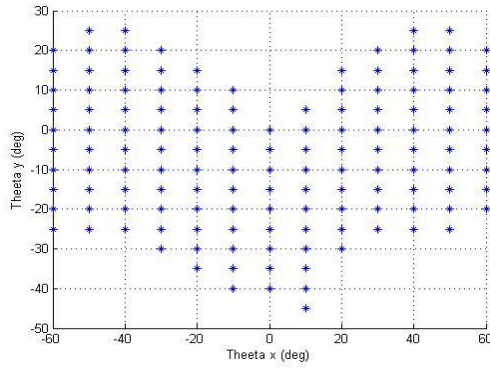
(b) x-y planer workspace



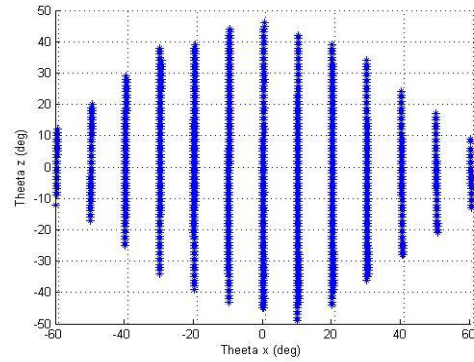
(c) y-z planer workspace



(d) Workspace by varying  $\theta_x \theta_y \theta_z$



(e) Workspace by varying  $\theta_x \theta_y$



(f) Workspace by varying  $\theta_x \theta_z$

**Figure 3.8 Manipulators workspace for position 1 in figure 3.4(a).**

### 3.2.4 Maximizing Stiffness in the Workspace

In this section, the stiffness of the manipulator is incorporated in the optimization such that the optimization objective is not limited to the workspace volume but also includes the stiffness of the manipulator in the workspace.

During the manipulation, the compliance of the manipulator structure causes a displacement of the end effector. This displacement does not only depend upon the external wrench applied but also on the stiffness of the manipulator. The accuracy of the manipulator pose is strongly affected by the stiffness of the manipulator structure.

The manipulator stiffness depends upon several parameters including material, links dimensions, transmission system, actuation system etc. Based on the work of Behzadipour and Khajepour [5], the stiffness of the cable based manipulator can be given as:

$$K = \frac{dw}{d\rho} = K_k + K_\tau$$

$$K_k = \sum_{i=1}^6 \left( k_i \begin{bmatrix} \hat{l}_i \hat{l}_i^T & \hat{l}_i \hat{l}_i^T [r_i \times]^T \\ [r_i \times] \hat{l}_i \hat{l}_i^T & [r_i \times] \hat{l}_i \hat{l}_i^T [r_i \times]^T \end{bmatrix} \right);$$

$$K_\tau = \sum_{i=1}^6 \left( \frac{\tau_i}{l_i} \begin{bmatrix} I - \hat{l}_i \hat{l}_i^T & (I - \hat{l}_i \hat{l}_i^T) [r_i \times]^T \\ [r_i \times] (I - \hat{l}_i \hat{l}_i^T) & [r_i \times] (I - \hat{l}_i \hat{l}_i^T) [r_i \times]^T - l_i [\hat{l}_i \times] [r_i \times] \end{bmatrix} \right); (3.23)$$

where  $\rho = [P_x \ P_y \ P_z \ \theta_x \ \theta_y \ \theta_z]$  is the position vector of the manipulator coordinates in fixed frame.  $k_i$  is the  $i$ th cable stiffness which is the combination of cable material stiffness and stiffness of the actuator system.  $K_k$  is the moving platform stiffness as a result of cable stiffness and  $K_\tau$  is the moving platform stiffness as a result of cable

tensions.  $I$  is an identity matrix,  $[r_i \times]$  and  $[\hat{l}_i \times]$  represents the cross product and is given as:

$$[r_i \times] = \begin{bmatrix} 0 & -r_{iz} & r_{iy} \\ r_{iz} & 0 & -r_{ix} \\ -r_{iy} & r_{ix} & 0 \end{bmatrix} \text{ and } [\hat{l}_i \times] = \begin{bmatrix} 0 & -\hat{l}_{iz} & \hat{l}_{iy} \\ \hat{l}_{iz} & 0 & -\hat{l}_{ix} \\ -\hat{l}_{iy} & \hat{l}_{ix} & 0 \end{bmatrix} \quad (3.24)$$

The stiffness of the manipulator can be determined from Eq. (3.23). In order to find the optimum positions of the ships, the maximum value of the lower stiffness value is to be determined. However, translational and rotational stiffness values cannot be compared because they have different physical units. Instead natural frequencies are used because they have common physical units and are indicative of the stiffness matrix. The formula to calculate the natural frequency of the system considering cables as springs is given by:

$$f_j^k = \frac{\sqrt{eig_j(M^{-1}K^k)}}{2\pi} \quad (3.25)$$

where  $f_j^k$  is the  $j$ th natural frequency calculated at  $k$ th pose.  $eig_j$  is the  $j$ th eigen value of the stiffness matrix.  $K^k$  is the stiffness value of the moving platform at  $k$ th pose.

$\mathbf{M}$  is the inertia matrix which is given by assuming the values of the manipulator as:

$$M = \begin{bmatrix} 100 & 0 & 0 & 0 & 0 & 0 \\ 0 & 100 & 0 & 0 & 0 & 0 \\ 0 & 0 & 100 & 0 & 0 & 0 \\ 0 & 0 & 0 & 8.4 & 0 & 0 \\ 0 & 0 & 0 & 0 & 5.4 & 0 \\ 0 & 0 & 0 & 0 & 0 & 13.6 \end{bmatrix} \quad (3.26)$$

The value of  $f_j^k$  depends upon the pose of the manipulator and therefore the entire workspace is to be considered when investigating the natural frequency of the manipulator. As mentioned before, in order to find the optimum position of the ships, sum of the natural frequencies is calculated for all poses of the manipulator at a particular set of position of the ships. The function showing the summation of the natural frequencies is expressed as:

$$\text{Sum of } f_{min} = \sum_{j=1}^n \min_j(f_j^k) \quad (3.27)$$

where  $\min_j(f_j^k)$  is the smallest natural frequency at the  $k$ th pose of the manipulator. Usually, higher values of natural frequencies imply higher stiffness value. Therefore, in order to maximize the manipulator stiffness, sum of the lowest natural frequency should be maximized. So at each set of ship position, sum of  $f_{min}$  is calculated for all poses of the manipulator. The position of the ships where sum of  $f_{min}$  is maximum would be the optimum position of the ships. The flow chart of this algorithm is shown in figure 3.9.



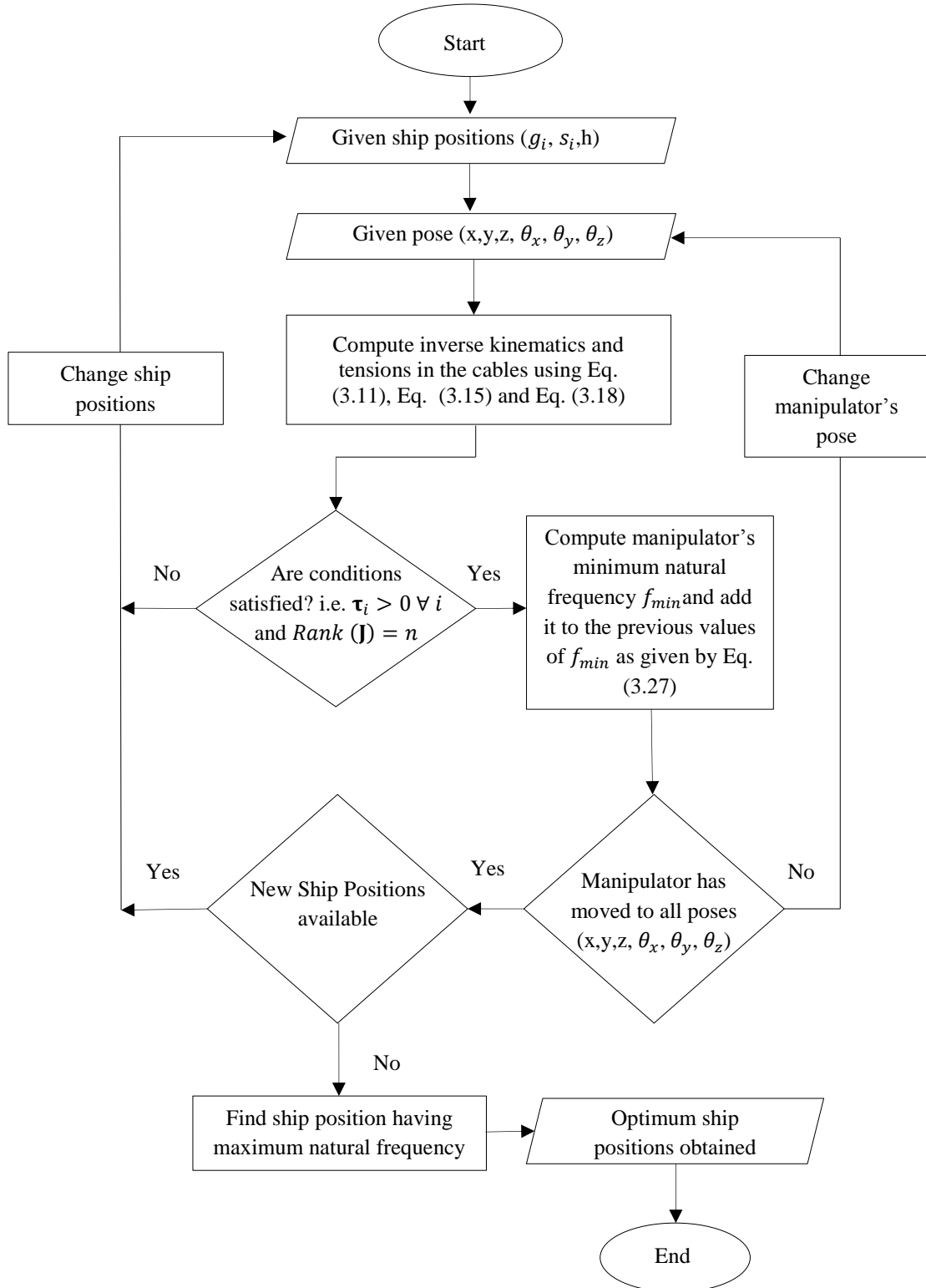


**Figure 3.9 A flow chart of the algorithm for computing the optimum ship positions based on maximizing manipulator's stiffness and natural frequency.**

The algorithm computes the summation of the lowest natural frequencies in the workspace for a given position set of the ships. For a given ship position and manipulator's pose, it computes the tension in the cables using Eq. (3.11), Eq. (3.15) and Eq. (3.18). If the required conditions are satisfied i.e.  $\tau_i > 0 \forall i$  and  $Rank(\mathbf{J}) = n$ , it computes the manipulator's stiffness and natural frequencies using Eq. (3.23) and Eq. (3.25). As the manipulator is a six DOF system, therefore six natural frequencies are obtained at a given pose in the workspace. The program computes the minimum among the natural frequencies and adds this value to the previous minimum value if there is any. It then computes the minimum natural frequency for all poses of the manipulator and gives the result in the form of summation of lowest natural frequency calculated at each pose of the manipulator. The same procedure is repeated for each combination of the ship position till it computes the summation of lowest natural frequency for all ship positions. Maximizing this minimum natural frequency sum leads to maximizing the stiffness of the manipulator in the workspace.

The results obtained from the algorithm shown in figure 3.9 are summarized in table 3.2. It shows the sum of the lowest natural frequencies obtained with their respective ship positions. The five best positions of the ships and their natural frequencies are shown here. The ship positions having the highest value among the sum of  $f_{min}$  are the most optimum positions of the ships. These results are shown graphically in figure 3.10.

**Table 3.2 Computed summation of minimum natural frequencies  $f_{min}$  for CPM with six cables by using the proposed algorithm and using Eq. (3.27).**

<b>Optimized Ship Position No.</b>	<b>1</b>	<b>2</b>	<b>3</b>	<b>4</b>	<b>5</b>
<b>x-y coordinate of Ship # 1 (m)</b>	49.8,-4.4	49.8,-4.4	49.8,-4.4	49.8,-4.4	49.8,-4.4
<b>x-y coordinate of Ship # 2 (m)</b>	-43.3,-25.0	17.1,-47.0	38.3,-32.1	-25.0,-43.3	-43.3,-25.0
<b>x-y coordinate of Ship # 3 (m)</b>	-49.8,-4.4	-49.8,-4.4	-49.8,-4.4	-49.8,-4.4	-49.8,-4.4
<b>x-y coordinate of Ship # 4 (m)</b>	-49.8,4.4	-49.8,4.4	-49.8,4.4	-49.8,4.4	-49.8,4.4
<b>x-y coordinate of Ship # 5 (m)</b>	-17.1,47.0	43.3,25.0	25.0,43.3	-38.3,32.1	0,50
<b>x-y coordinate of Ship # 6 (m)</b>	49.8,4.4	49.8,4.4	49.8,4.4	49.8,4.4	49.8,4.4
<b>Sum of <math>f_{min}</math> (Hz)</b>	2038.1	2017.5	1995.9	1992.0	1947.1

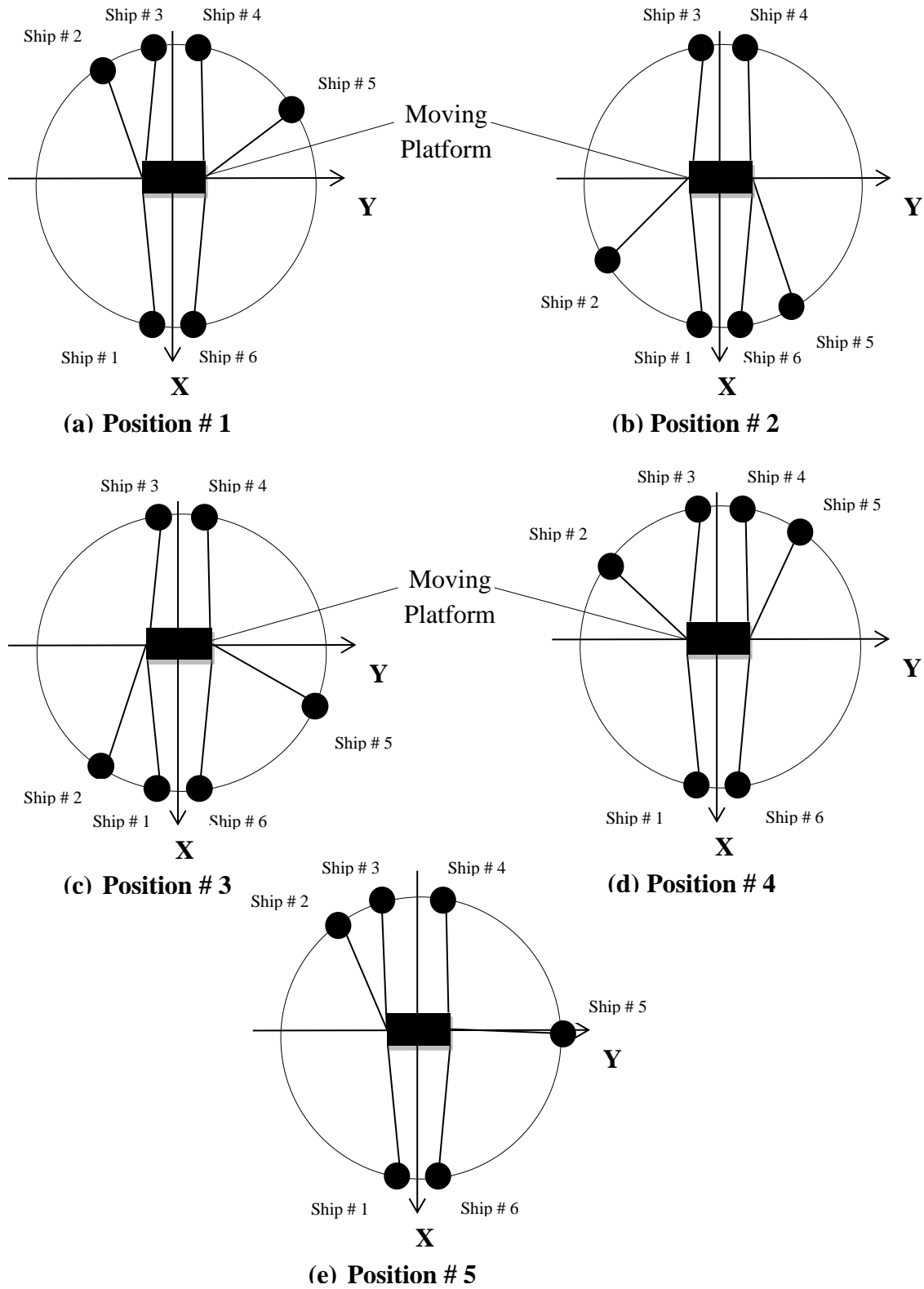


**Figure 3.10 Top five optimum ship positions for CPM with six cables based on maximizing stiffness of the manipulator.**

The results in table 3.2 shows the summation of the lowest natural frequencies of the manipulator calculated at each pose in the workspace with the respective ship positions as well. The maximum value of the summation is 2038 Hz. Therefore, the respective ship positions with the highest value of sum which is 2038 Hz are the optimum positions whose coordinates are given in table 3.2 under ship position 1. The pictorial representation for these ship positions are shown in figure 3.10(a). With these ship positions, the manipulator can have maximum stiffness. The summation of the lowest natural frequencies is slightly reduced to 2017 Hz, when the ship positions are moved to position set 2 as given in table 3.2 and shown pictorially in figure 3.10(b). Similarly, with ship position set 3, 4 and 5, the summation value is further decreased to values 1995 Hz, 1992 Hz and 1947 Hz respectively. These ship positions are shown pictorially in figure 3.10 (c) to (e). Therefore, figure 3.10(a) to (e) depicts the top five optimum ship positions based on maximizing stiffness of the manipulator.

### **3.3 Results and Discussions**

In this chapter, the ship position optimization has been performed for a cable based parallel manipulator operating inside deep sea. In section 3.1, a cable based manipulator for subsea applications have been proposed and the kinematic and force analysis of the system is performed. The layout optimization was conducted in section 3.2. This optimization was based on maximizing the workspace of the manipulator and it also incorporated the stiffness analysis in the optimization. The problem of workspace evaluation has been discussed and formulated. The singularity and stiffness analysis has been conducted.

The system studied is a six DOF cable based manipulator operating inside sea connected by six ships on sea surface via cables. The optimization of the ship positions was based on maximizing the workspace and stiffness of the manipulator. An algorithm was presented that computes the workspace of the manipulator by verifying if the manipulator satisfied the imposed geometrical constraints, tensions in the cables were positive and the manipulator was not at a singular configuration. Top five positions of the ships calculated from the proposed algorithm were presented and discussed. The workspace of the manipulator was presented for the most optimum position of the ships. The workspace evaluation shows the manipulator can operate in a considerable volume given the wrench acting on the platform. This wrench also includes the buoyancy force acting on the manipulator. This shows that the cable based manipulator is capable for translating as well as rotating along all three axis  $x$ - $y$ - $z$  inside deep sea.

The optimization part was not just limited to maximizing workspace but it also included the stiffness of the manipulator in the workspace. Since the manipulator can translate as well as rotate, therefore the translational and rotational stiffness cannot be compared. Instead natural frequencies were used. The top five positions of the ships were obtained based on maximizing the summation of lowest natural frequency of the system. Therefore, the optimization was conducted using the proposed algorithm to increase the workspace as well as the stiffness of the manipulator.

# **CHAPTER 4**

## **SHIP POSITION OPTIMIZATION FOR REDUNDANT CABLES**

### **4.1 Introduction**

When more than six cables (redundant cables) are used to operate a cable driven parallel manipulator (CPM), multiple solutions exist for the cable tensions given a certain wrench at the end effector. In this chapter, the positions of the ships will be optimized utilizing cable tension minimization scheme developed by Dykstra [41] and applied by [11] in cable manipulators. The optimization will consider eight and ten cables as shown in figure 4.1 and figure 4.2 respectively.

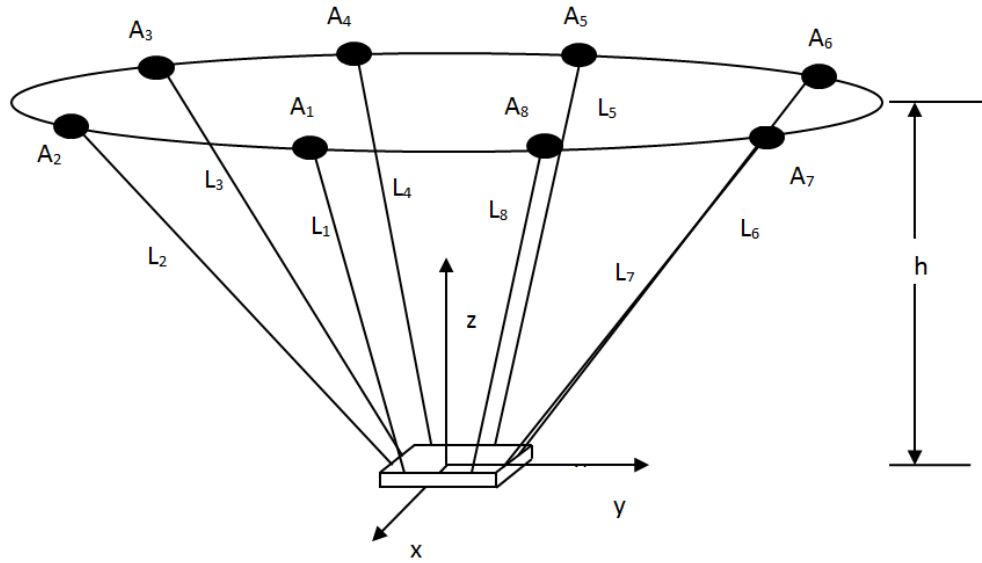


**Figure 4.1 Schematic Diagram of the CPM layout with eight cables.**

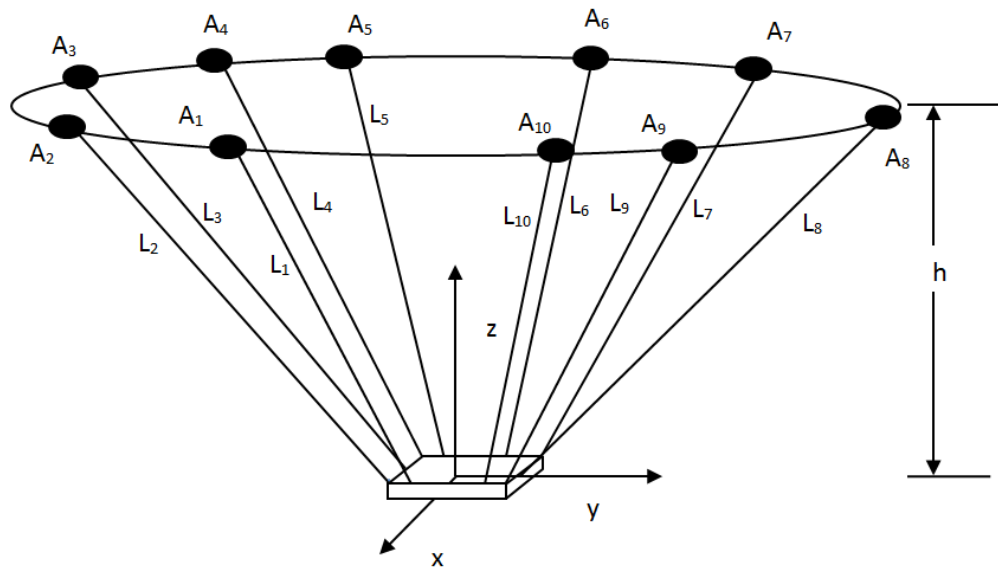


**Figure 4.2 Schematic Diagram of the CPM layout with ten cables.**



For the CPM's shown in figure 4.1 and figure 4.2, tensions of the cables at each pose of the manipulator are minimized based on a 2-norm minimization convex scheme. Then the ship positions will be optimized for workspace and stiffness of the manipulator.

## 4.2 Inverse Kinematic Analysis

As explained in Chapter 3, the position and velocity analysis was conducted using inverse kinematics. In Chapter 3, the layout of the CPM included six cables. The CPM shown in figure 4.1 consists of eight cables so two additional equations are formulated in the position analysis in order to calculate the lengths of the cables given the position of the manipulator and the ships. These eight equations for each cable are given as:

$$\begin{aligned}
 l_1^2 = & \left( p_x + (\cos \emptyset \cos \theta) \frac{m}{2} - (\cos \emptyset \sin \theta \sin \psi - \sin \emptyset \cos \psi) \frac{n}{4} \right. \\
 & \left. + (\cos \emptyset \sin \theta \cos \psi + \sin \emptyset \sin \psi) \frac{o}{2} - g_1 \right)^2 \\
 & + \left( p_y + (\sin \emptyset \cos \theta) \frac{m}{2} - (\sin \emptyset \sin \theta \sin \psi + \cos \emptyset \cos \psi) \frac{n}{4} \right. \\
 & \left. + (\sin \emptyset \sin \theta \cos \psi - \cos \emptyset \sin \psi) \frac{o}{2} - s_1 \right)^2 \\
 & + \left( p_z + (-\sin \theta) \frac{m}{2} - (\cos \theta \sin \psi) \frac{n}{4} + (\cos \theta \cos \psi) \frac{o}{2} - h_1 \right)^2
 \end{aligned}$$

$$\begin{aligned}
l_2^2 = & \left( p_x + (\cos \emptyset \cos \theta) \frac{m}{4} - (\cos \emptyset \sin \theta \sin \psi - \sin \emptyset \cos \psi) \frac{n}{2} \right. \\
& \left. + (\cos \emptyset \sin \theta \cos \psi + \sin \emptyset \sin \psi) \frac{o}{2} - g_2 \right)^2 \\
& + \left( p_y + (\sin \emptyset \cos \theta) \frac{m}{4} - (\sin \emptyset \sin \theta \sin \psi + \cos \emptyset \cos \psi) \frac{n}{2} \right. \\
& \left. + (\sin \emptyset \sin \theta \cos \psi - \cos \emptyset \sin \psi) \frac{o}{2} - s_2 \right)^2 \\
& + \left( p_z + (-\sin \theta) \frac{m}{4} - (\cos \theta \sin \psi) \frac{n}{2} + (\cos \theta \cos \psi) \frac{o}{2} - h_2 \right)^2
\end{aligned}$$

$$\begin{aligned}
l_3^2 = & \left( p_x - (\cos \emptyset \cos \theta) \frac{m}{4} - (\cos \emptyset \sin \theta \sin \psi - \sin \emptyset \cos \psi) \frac{n}{2} \right. \\
& \left. + (\cos \emptyset \sin \theta \cos \psi + \sin \emptyset \sin \psi) \frac{o}{2} - g_3 \right)^2 \\
& + \left( p_y - (\sin \emptyset \cos \theta) \frac{m}{4} - (\sin \emptyset \sin \theta \sin \psi + \cos \emptyset \cos \psi) \frac{n}{2} \right. \\
& \left. + (\sin \emptyset \sin \theta \cos \psi - \cos \emptyset \sin \psi) \frac{o}{2} - s_3 \right)^2 \\
& + \left( p_z + (\sin \theta) \frac{m}{4} - (\cos \theta \sin \psi) \frac{n}{2} + (\cos \theta \cos \psi) \frac{o}{2} - h_3 \right)^2
\end{aligned}$$

$$\begin{aligned}
l_4^2 = & \left( p_x - (\cos \emptyset \cos \theta) \frac{m}{2} + (\cos \emptyset \sin \theta \sin \psi - \sin \emptyset \cos \psi) \frac{n}{4} \right. \\
& \left. + (\cos \emptyset \sin \theta \cos \psi + \sin \emptyset \sin \psi) \frac{o}{2} - g_4 \right)^2 \\
& + \left( p_y - (\sin \emptyset \cos \theta) \frac{m}{2} + (\sin \emptyset \sin \theta \sin \psi + \cos \emptyset \cos \psi) \frac{n}{4} \right. \\
& \left. + (\sin \emptyset \sin \theta \cos \psi - \cos \emptyset \sin \psi) \frac{o}{2} - s_4 \right)^2 \\
& + \left( p_z + (\sin \theta) \frac{m}{2} + (\cos \theta \sin \psi) \frac{n}{4} + (\cos \theta \cos \psi) \frac{o}{2} - h_4 \right)^2
\end{aligned}$$

$$\begin{aligned}
l_5^2 = & \left( p_x - (\cos \emptyset \cos \theta) \frac{m}{2} + (\cos \emptyset \sin \theta \sin \psi - \sin \emptyset \cos \psi) \frac{n}{4} \right. \\
& + \left. (\cos \emptyset \sin \theta \cos \psi + \sin \emptyset \sin \psi) \frac{o}{2} - g_5 \right)^2 \\
& + \left( p_y - (\sin \emptyset \cos \theta) \frac{m}{2} + (\sin \emptyset \sin \theta \sin \psi + \cos \emptyset \cos \psi) \frac{n}{4} \right. \\
& + \left. (\sin \emptyset \sin \theta \cos \psi - \cos \emptyset \sin \psi) \frac{o}{2} - s_5 \right)^2 \\
& + \left( p_z + (\sin \theta) \frac{m}{2} + (\cos \theta \sin \psi) \frac{n}{4} + (\cos \theta \cos \psi) \frac{o}{2} - h_5 \right)^2
\end{aligned}$$

$$\begin{aligned}
l_6^2 = & \left( p_x - (\cos \emptyset \cos \theta) \frac{m}{4} + (\cos \emptyset \sin \theta \sin \psi - \sin \emptyset \cos \psi) \frac{n}{2} \right. \\
& + \left. (\cos \emptyset \sin \theta \cos \psi + \sin \emptyset \sin \psi) \frac{o}{2} - g_6 \right)^2 \\
& + \left( p_y - (\sin \emptyset \cos \theta) \frac{m}{4} + (\sin \emptyset \sin \theta \sin \psi + \cos \emptyset \cos \psi) \frac{n}{2} \right. \\
& + \left. (\sin \emptyset \sin \theta \cos \psi - \cos \emptyset \sin \psi) \frac{o}{2} - s_6 \right)^2 \\
& + \left( p_z + (\sin \theta) \frac{m}{4} + (\cos \theta \sin \psi) \frac{n}{2} + (\cos \theta \cos \psi) \frac{o}{2} - h_6 \right)^2
\end{aligned}$$

$$\begin{aligned}
l_7^2 = & \left( p_x + (\cos \emptyset \cos \theta) \frac{m}{4} + (\cos \emptyset \sin \theta \sin \psi - \sin \emptyset \cos \psi) \frac{n}{2} \right. \\
& + \left. (\cos \emptyset \sin \theta \cos \psi + \sin \emptyset \sin \psi) \frac{o}{2} - g_6 \right)^2 \\
& + \left( p_y + (\sin \emptyset \cos \theta) \frac{m}{4} + (\sin \emptyset \sin \theta \sin \psi + \cos \emptyset \cos \psi) \frac{n}{2} \right. \\
& + \left. (\sin \emptyset \sin \theta \cos \psi - \cos \emptyset \sin \psi) \frac{o}{2} - s_6 \right)^2 \\
& + \left( p_z - (\sin \theta) \frac{m}{4} + (\cos \theta \sin \psi) \frac{n}{2} + (\cos \theta \cos \psi) \frac{o}{2} - h_6 \right)^2
\end{aligned}$$

$$\begin{aligned}
l_8^2 = & \left( p_x + (\cos \emptyset \cos \theta) \frac{m}{2} + (\cos \emptyset \sin \theta \sin \psi - \sin \emptyset \cos \psi) \frac{n}{2} \right. \\
& \left. + (\cos \emptyset \sin \theta \cos \psi + \sin \emptyset \sin \psi) \frac{o}{2} - g_6 \right)^2 \\
& + \left( p_y + (\sin \emptyset \cos \theta) \frac{m}{2} + (\sin \emptyset \sin \theta \sin \psi + \cos \emptyset \cos \psi) \frac{n}{2} \right. \\
& \left. + (\sin \emptyset \sin \theta \cos \psi - \cos \emptyset \sin \psi) \frac{o}{2} - s_6 \right)^2 \\
& + \left( p_z - (\sin \theta) \frac{m}{2} + (\cos \theta \sin \psi) \frac{n}{2} + (\cos \theta \cos \psi) \frac{o}{2} - h_6 \right)^2
\end{aligned} \tag{4.1}$$

Eq. (4.1) gives the lengths of the cables required to move the platform to any desired position and orientation.

### 4.3 Static Analysis: Bounded Cable tensions

When a task is performed by the manipulator, the end effector exerts force and moment on the external environment. In order to make sure that cables do not lose tensions during operation, a certain amount of pretension i.e. lower bound needs to be maintained in each cable. Considering minimum bound on cable tensions, the wrench exerted on the moving platform to the cable tensions is written as:

$$\mathbf{w} = \begin{bmatrix} \mathbf{f} \\ \mathbf{m} \end{bmatrix} = -\mathbf{A}\boldsymbol{\tau} \tag{4.2}$$

Where

$$\mathbf{A} = \begin{bmatrix} \hat{\mathbf{I}}_1 & \cdots & \hat{\mathbf{I}}_i & \cdots & \hat{\mathbf{I}}_n \\ (\mathbf{r}_1 \times \hat{\mathbf{I}}_1) & \cdots & (\mathbf{r}_i \times \hat{\mathbf{I}}_i) & \cdots & (\mathbf{r}_n \times \hat{\mathbf{I}}_n) \end{bmatrix}$$

And

$$\boldsymbol{\tau}_i > 0 \forall i$$

Here  $\mathbf{f}$  and  $\mathbf{m}$  are the external force and moment applied to the moving platform. 'n' are the number of cables;  $\boldsymbol{\tau}$  is an n-dimensional vector of cable tensions;  $\tau_i$  is the value of tension in the  $i$ th cable.  $\hat{\mathbf{l}}_i$  is a unit vector in the direction of the force applied by the  $i$ th cable and  $\mathbf{r}_i$  is the position of the  $i$ th cable connection point on the moving platform with respect to its center.

Eq. (4.2) can be written as

$$\boldsymbol{\tau} = -\mathbf{A}^+ \mathbf{w} + \mathbf{N} \mathbf{h} \quad (4.3)$$

Where  $\mathbf{A}^+$  is the Pseudo inverse of matrix  $\mathbf{A}$ , since matrix  $\mathbf{A}$  is not a square matrix, therefore, it is not invertible. So pseudo-inverse  $\mathbf{A}^+$  will be taken which is the generalization of the inverse of matrix  $\mathbf{A}$ . It is used to find the minimum (Euclidean) norm solution to a system of linear equations with multiple solutions. Later, Dykstra's algorithm will be used to minimize the cable tensions.  $\mathbf{N}$  represents the null space of matrix  $\mathbf{A}$  and  $\mathbf{h}$  is a vector of arbitrary real numbers. The term  $-\mathbf{A}^+ \mathbf{w}$  gives the solution without taking into account the minimum bound on the cable tensions.  $\mathbf{N} \mathbf{h}$  is the arbitrary vector in the null space of matrix  $\mathbf{A}$  and hence affects the distribution of cable tensions without affecting the wrench  $\mathbf{w}$  applied at the moving platform. The solution of Eq. (4.3) is obtained from the intersection of two convex sets, i.e.  $\boldsymbol{\tau} \in \mathcal{C} = \mathcal{G} \cap \mathcal{A}$ . The affine set  $\mathcal{A}$  is obtained by translating the null space of matrix  $\mathbf{A}$  from origin  $\boldsymbol{\tau} = \mathbf{0}$  by vector  $-\mathbf{A}^+ \mathbf{w}$  and is given by:

$$\mathcal{A} = \{\boldsymbol{\tau} | \boldsymbol{\tau} = -\mathbf{A}^+ \mathbf{w} + \mathbf{N} \mathbf{h}; \mathbf{h} \in \mathbb{R}^{n_r}\} \quad (4.4)$$

And set  $G$  represents an  $n$ -dimensional orthant in  $R^n$  and is expressed as:

$$G = \{\boldsymbol{\tau} | \tau_{i \min} \leq \tau_i \leq \infty \forall i\} \quad (4.5)$$

All solutions to  $\boldsymbol{\tau}$  in Eq. (4.2) must lie in the intersection set  $C$  for a given wrench  $\mathbf{w}$ . There exists no solution, if intersection set  $C$  is empty. The two cases will be discussed for the case of empty and a non-empty intersection. For case 1, set  $C$  is non-empty i.e. set  $A$  and  $G$  intersect. For case 2, set  $C$  is empty and therefore set  $A$  and  $G$  do not intersect. These cases are shown geometrically in figure 4.3.

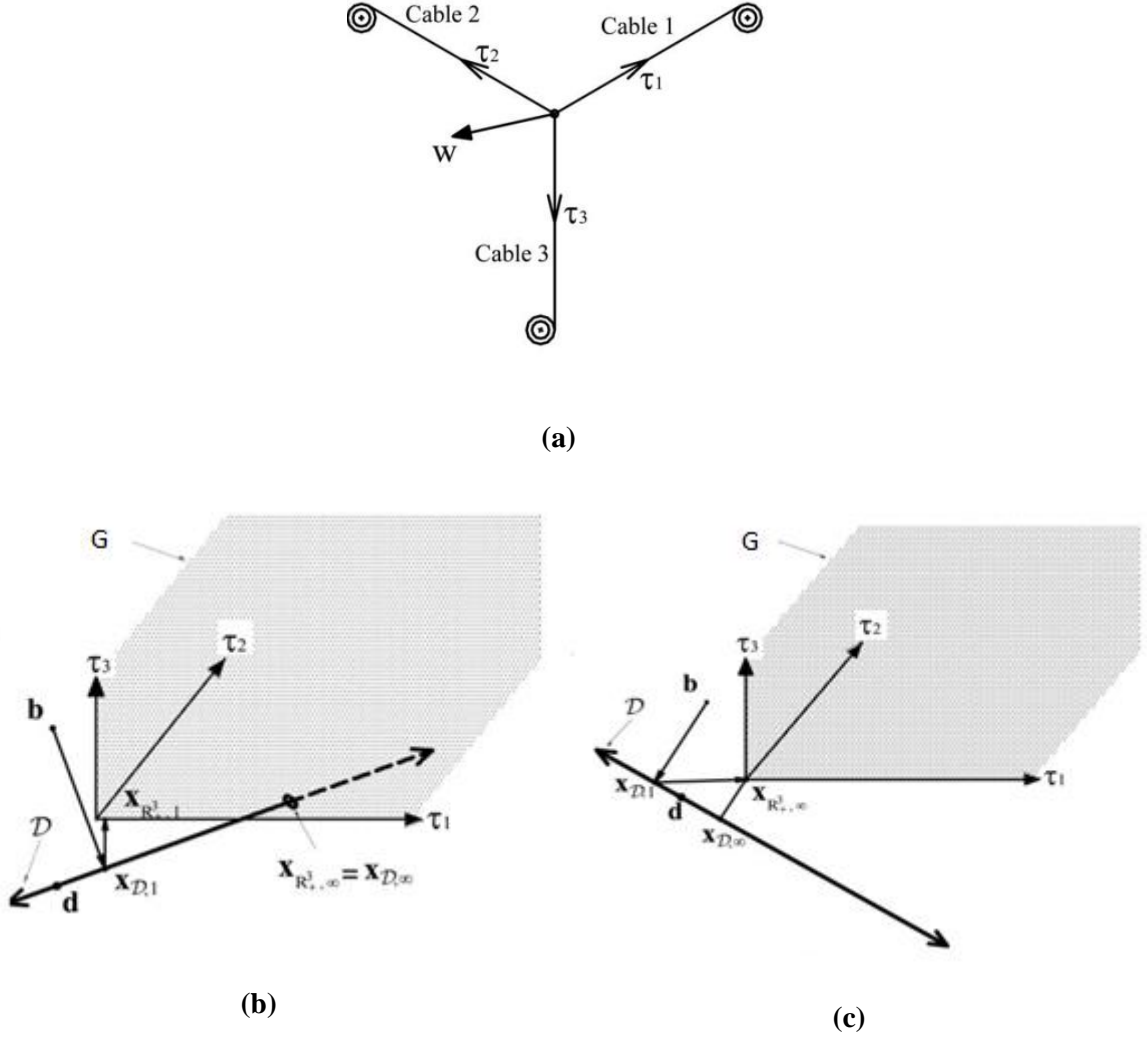


**Figure 4.3 (a) Planer translational CPM layout. (b) Non-empty intersection (Case 1). (c) Empty intersection (Case 2). [11].**

The CPM shown in figure 4.3(a) is a two DOF manipulator whose end-effector is driven by three cables. One of the three cables is redundant and at this configuration the null space dimension of matrix  $\mathbf{A}$  is 1, indicating the affine set  $A$  is a line in  $R^3$  as shown in figure 4.3(b) and (c). The CPM in figure 4.1 consists of eight cables and the manipulator is having six DOF. With this configuration, the dimension of null space of matrix  $\mathbf{A}$  is 2 which indicate that the affine set  $A$  is a plane. In addition, the orthant  $G$  has eight components because CPM has a total of eight cables. Figure 4.3(b) geometrically

illustrates case 1 where the affine set  $A$  passes through orthant  $G$  and the intersection set  $C$  is shown as the dotted line segment that is inside the orthant, which indicates that there exists multiple solutions to the cable tension  $\boldsymbol{\tau}$  that can balance the external wrench  $\mathbf{w}$ . On the other hand, figure 4.3(c) represents case 2 where affine set  $A$  does not intersect the orthant  $G$  and therefore it indicates that there exist no solution to  $\boldsymbol{\tau}$  that can balance the external wrench  $\mathbf{w}$ . The shortest distance from the origin to the affine set  $A$  is the magnitude of vector  $-\mathbf{A}^+\mathbf{w}$ . For the first case, we will find the minimum-2-norm solution to the cable tensions that is based on Dykstra's projection algorithm.

#### 4.4 Background on Dykstra's Algorithm

This is an iterative algorithm that can be used to find the minimum-Euclidean-distance projection of a point onto the intersection of a number of convex sets, provided that their intersection is a non-empty set [41].

Let there be a point  $\mathbf{b} \in R^m$  and  $S_1, \dots, S_L$  be  $L$  convex sets in  $R^m$  and their intersection is non-empty such that  $S_\cap = \cap_{k=1}^L (S_k)$ . The projection of point  $\mathbf{b}$  onto the intersection set  $S_\cap$  will be found from Dykstra's algorithm. The projection of point  $\mathbf{b}$  is denoted as  $Proj_{S_\cap}(\mathbf{b})$  and is the solution to the minimization problem  $\min_{\mathbf{v} \in S_\cap} \|\mathbf{b} - \mathbf{v}\|$  as

$$Proj_{S_\cap}(\mathbf{b}) = \arg \min_{\mathbf{v} \in S_\cap} \|\mathbf{b} - \mathbf{v}\| \quad (4.6)$$

In order to illustrate Dykstra's algorithm in finding the projection of point  $\mathbf{b}$   $Proj_{S_\cap}(\mathbf{b})$ , indicated in figure 4.3, let  $\mathbf{x}_{k,i}$  and  $\mathbf{y}_{k,i} \in R^m$ , where  $\mathbf{x}_{k,i}$  is the minimum Euclidean-distance projection of  $\mathbf{t} \in R^m$  onto convex set  $k$  at iteration  $i$ ; and  $\mathbf{y}_{k,i} =$



$(\mathbf{x}_{k,i} - \mathbf{t})$ , where the term  $k$  is an index that refers to the convex set  $S_k$ . In order to determine the projection of  $\mathbf{b}$  onto the intersection of sets  $S_1, \dots, S_L$ , the algorithm initializes at  $i=0$ , where  $\mathbf{x}_{1,0} = \mathbf{b}$ , which is the point to be projected and  $\mathbf{y}_{k,0} = \mathbf{0}$  for all  $k$ . The flow chart of the algorithm is shown in figure 4.4.

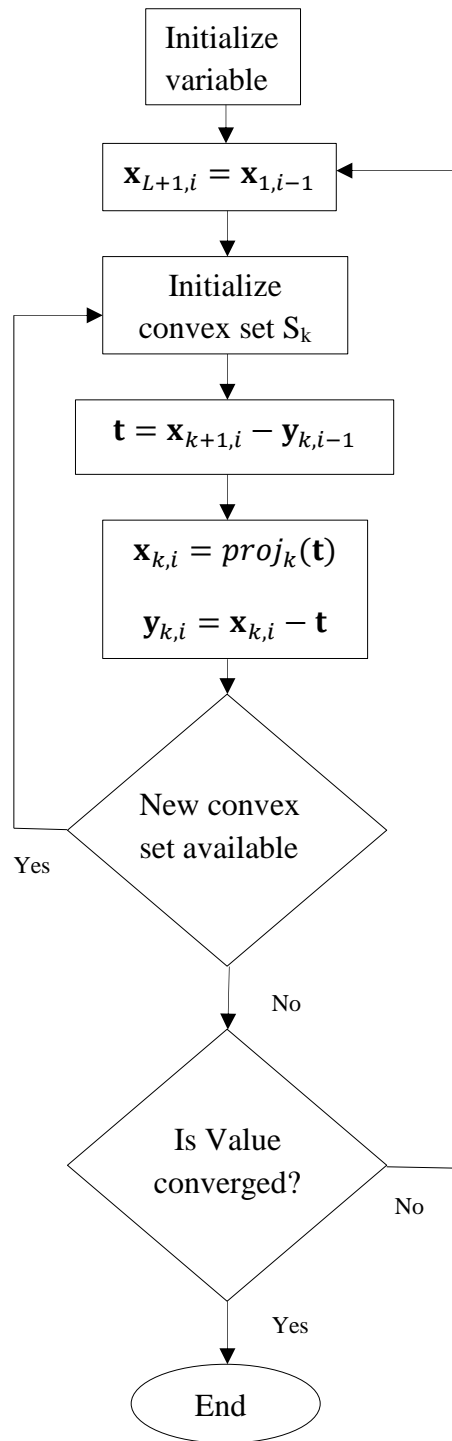


**Figure 4.4** Flow chart for Dykstra's Algorithm.

In this algorithm, the sequence initiates at point  $\mathbf{b}$  and proceeds by making successive projections of  $\mathbf{t}$  onto convex sets  $S_1, \dots, S_L$  until for the case where  $S_\cap$  is non-empty, all sequences  $\mathbf{x}_{k,i}$  converge to a single point on intersection set  $S_\cap$  which is the minimum Euclidean-distance from the initial point  $\mathbf{b}$ . The convergence point can be represented as:

$$\mathbf{x}_{1,\infty}, \mathbf{x}_{2,\infty}, \dots, \mathbf{x}_{L,\infty} = \text{proj}_{S_\cap}(\mathbf{b}) \quad (4.7)$$

## 4.5 Optimizing Cable tensions using Dykstra's algorithm

The tensions obtained from Eq. (4.3) are not the minimum cable tensions we are interested in. A minimum-2-norm solution to  $\boldsymbol{\tau}$  should be found from amongst the solutions in set  $C$ . For this, Dykstra's algorithm will be used as explained in Section 4.3 to find this minimum-2-norm solution. The 2-norm of  $\boldsymbol{\tau}$  is the minimum Euclidean distance from origin to point  $\boldsymbol{\tau} \in C$  which is expressed as  $\|\mathbf{0} - \boldsymbol{\tau}\|$  i.e. the point on  $C$  which is closest to origin in Euclidean distance sense. The projection of this minimum Euclidean distance can be expressed as:

$$\boldsymbol{\tau}_{\min\|\boldsymbol{\tau}\|} = \text{proj}_C(\mathbf{0}) = \arg \min_{\boldsymbol{\tau} \in C} \|\mathbf{0} - \boldsymbol{\tau}\| \quad (4.8)$$

Where  $\text{proj}_C(\mathbf{0})$  is the minimum-Euclidean distance projection of the origin onto convex set  $C$ .

As Eq. (4.8) is similar to Eq. (4.6), therefore Dykstra's algorithm can be applied in order to calculate  $\boldsymbol{\tau}_{\min\|\boldsymbol{\tau}\|}$ . The Dykstra's algorithm is applied to the manipulator shown in figure 4.1 & 4.2. The sequences initiate at the origin and proceed by making successive projections of point  $\mathbf{t}$  in each iteration. If  $C$  is a non-empty set, all sequences

will converge to a single point onto  $C$  as  $i \rightarrow \infty$  which is the minimum Euclidean distance from the initial point. Therefore the solution can be expressed as:

$$\boldsymbol{\tau}_{\min||\boldsymbol{\tau}||} = \text{proj}_C(\mathbf{0}) = \mathbf{x}_{G,\infty} = \mathbf{x}_{A,\infty} \quad (4.9)$$

At each iteration the algorithm computes  $\mathbf{x}_{A,i} = \text{proj}_A(\mathbf{t})$  and  $\mathbf{x}_{G,i} = \text{proj}_G(\mathbf{t})$  of  $\mathbf{t}$  onto  $A$  and  $G$  respectively.  $\text{proj}_A(\mathbf{t})$  can be found as:

$$\text{proj}_A(\mathbf{t}) = (\mathbf{I} - \mathbf{A}^+\mathbf{A})\mathbf{t} - \mathbf{A}^+\mathbf{w} \quad (4.10)$$

In Eq. (4.10),  $\mathbf{t}$  is projected onto the null space of matrix  $\mathbf{A}$  and the result is translated by  $-\mathbf{A}^+\mathbf{w}$ . Similarly,  $\text{proj}_G(\mathbf{t})$  can be calculated as:

$$\text{proj}_G(\mathbf{t}) = [\bar{t}_1 \dots \bar{t}_n]^T$$

$$\bar{t}_i = \begin{cases} \tau_{i \min} & t_i \leq \tau_{i \min} \\ t_i & \tau_{i \min} \leq t_i \leq \infty \\ \tau_{i \max} & t_i \geq \infty \end{cases} \quad (4.11)$$

Eq. (4.11) therefore trims all coordinates of  $\mathbf{t}$  that are outside the bounds of the orthant  $G$  i.e. those values of  $\bar{t}_i$  that are less than the minimum value bounded on cable tensions.

In the second case shown in figure 4.3(c), when set  $C$  is a non-intersecting set, the sequences  $\mathbf{x}_{k,i}$  will not converge to only one point but instead it will converge to two distinct points and therefore Dykstra's algorithm can be applied to check whether a solution exists to  $\boldsymbol{\tau}$  in equation (4.2) or not for a given wrench  $\mathbf{w}$ , i.e. when  $\mathbf{x}_{G,\infty} = \mathbf{x}_{A,\infty}$ , applied wrench  $\mathbf{w}$  is feasible and infeasible otherwise.

An algorithm termination rule should be specified because it is not known prior whether the algorithm converges to a single point or to two distinct points. Hence the following equation is established in order to determine the termination of the algorithm.

$$\begin{aligned} \left\| \mathbf{x}_{A,i} - \mathbf{x}_{A,i-1} \right\| + \left\| \mathbf{x}_{G,i} - \mathbf{x}_{G,i-1} \right\| &\leq \epsilon_x \\ \left\| \hat{\mathbf{y}}_{A,i} - \hat{\mathbf{y}}_{A,i-1} \right\| + \left\| \hat{\mathbf{y}}_{G,i} - \hat{\mathbf{y}}_{G,i-1} \right\| &\leq \epsilon_y \end{aligned} \quad (4.12)$$

Where  $\hat{\mathbf{y}}_{A,i}$  and  $\hat{\mathbf{y}}_{G,i}$  are the unit vectors in the direction of  $\mathbf{y}_{A,i}$  and  $\mathbf{y}_{G,i}$  respectively and  $\epsilon_x$  and  $\epsilon_y$  are the small tolerances specified.

## 4.6 Layout Optimization

Following the optimization of cable tensions, workspace of CPM will be determined in order to perform layout optimization. The optimization includes determining the best possible positions of the ships shown in figure 4.1 and figure 4.2 that will give the maximum workspace. Since the workspace is the set of all poses a manipulator can reach with all conditions satisfied, the optimum positions of the ships will be based on maximizing workspace of the manipulator. Moreover, the optimization will also be performed using stiffness and natural frequencies of the manipulator so that it is not just limited to workspace volume but also incorporates stiffness of the manipulator.

### 4.6.1 Maximizing workspace volume

This section is devoted to determining the optimized position of the ships so that the manipulator can have maximum volume of the workspace. The workspace of a cable-driven manipulator includes the set of all poses a manipulator can reach such that:

- The tensions in the cables are positive i.e.  $\tau_i > 0 \forall i$
- The end-effector must avoid any singular condition i.e.  $Rank(\mathbf{J}) = n$

### **Case 1: CPM with eight cables**

The inverse kinematics of CPM having eight cables is formulated using Eq. (4.1) and Eq. (4.3). Dykstra's algorithm as explained in Section 4.3 is applied in order to calculate the minimum-2-norm solution to the cable tensions and determine whether or not a solution exists to  $\tau$  in Eq. (4.2) for a given wrench  $\mathbf{w}$ . The flow chart of the algorithm to compute the workspace using Dykstra's algorithm and to determine the optimum positions of the ships is shown in figure 4.5.

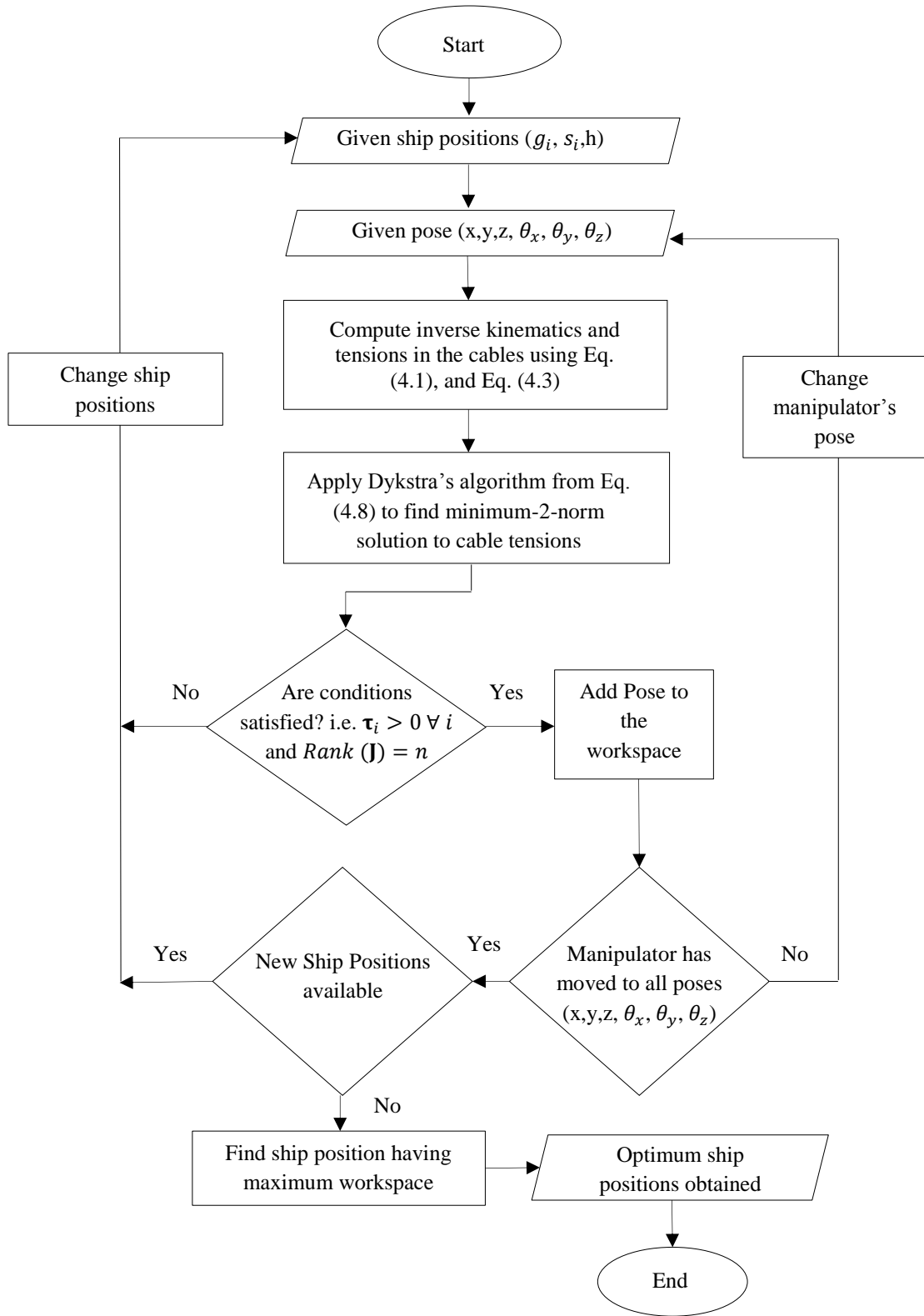


**Figure 4.5 A flow chart of the algorithm for computing the optimum ship positions based on maximum workspace of the manipulator.**

The flow chart applies the formulations in Eq. (4.1) and Eq. (4.3). Dykstra's algorithm is applied as given by Eq. (4.8) to find the minimum-2-norm solution to the cable tensions. If the required conditions are met i.e.  $\tau_i > 0 \forall i$  and  $Rank(\mathbf{J}) = n$ , it adds the pose of the manipulator to the workspace. In order to determine the full workspace, the algorithm repeats the same procedure for every pose of the manipulator. Finally, the above procedure is repeated for each combination of the ship position.

The position having maximum workspace is the optimum position of the ships. Table 4.1 summarizes the results obtained from the proposed algorithm in figure 4.5 for the cable based manipulator shown in figure 4.1. It shows the number of workspace discrete points and their respective ship coordinates for the best five position sets of the ships. The top view of the cable based manipulator for these best five position sets of the ships are shown in figure 4.6. Solid circles denote the ships. It should be noted that the ship positions were optimized with the perimeter of a circle around the moving platform.



**Table 4.1 Computed Workspace for CPM with eight cables by using the proposed algorithm with constraints expressed in Eq. (4.1) and Eq. (4.3).**

<b>Optimized Ship Position No.</b>	<b>1</b>	<b>2</b>	<b>3</b>	<b>4</b>	<b>5</b>
<b>(r- <math>\theta</math>) coordinate of Ship # 1 (m,deg)</b>	(50,260)	(50,260)	(50,260)	(50,260)	(50,260)
<b>(r- <math>\theta</math>) coordinate of Ship # 2 (m,deg)</b>	(50,185)	(50,200)	(50,215)	(50,185)	(50,185)
<b>(r- <math>\theta</math>) coordinate of Ship # 3 (m,deg)</b>	(50,175)	(50,145)	(50,145)	(50,145)	(50,175)
<b>(r- <math>\theta</math>) coordinate of Ship # 4 (m,deg)</b>	(50,125)	(50,125)	(50,125)	(50,125)	(50,125)
<b>(r- <math>\theta</math>) coordinate of Ship # 5 (m,deg)</b>	(50,55)	(50,55)	(50,55)	(50,55)	(50,80)
<b>(r- <math>\theta</math>) coordinate of Ship # 6 (m,deg)</b>	(50,5)	(50,5)	(50,5)	(50,5)	(50,5)
<b>(r- <math>\theta</math>) coordinate of Ship # 7 (m,deg)</b>	(50,355)	(50,355)	(50, 355)	(50, 355)	(50, 355)
<b>(r- <math>\theta</math>) coordinate of Ship # 8 (m,deg)</b>	(50,280)	(50,280)	(50,280)	(50,280)	(50,280)
<b>Workspace discrete points</b>	2428	2317	2301	2297	2231

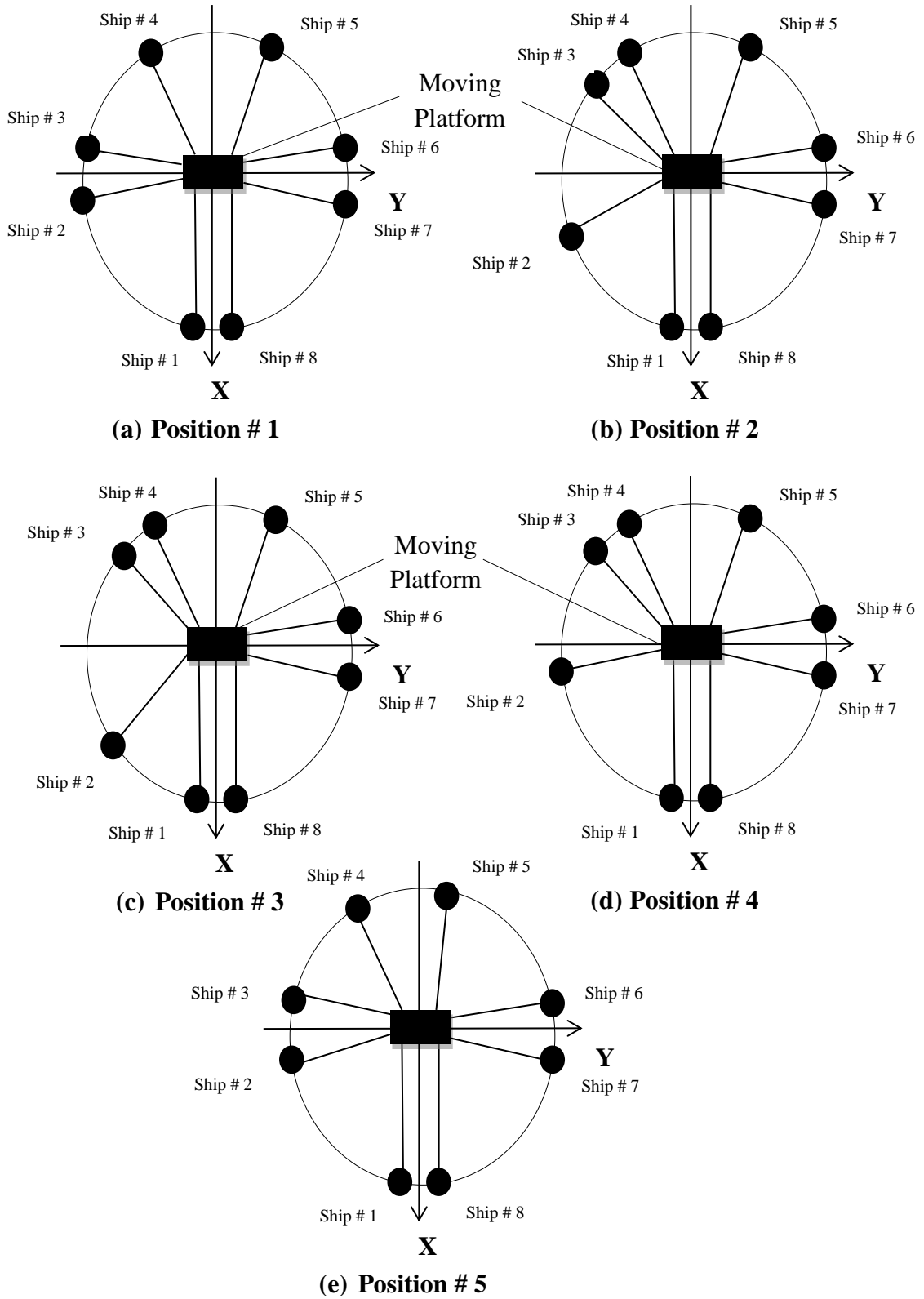
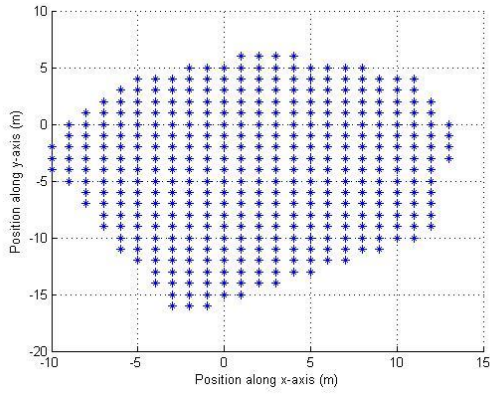


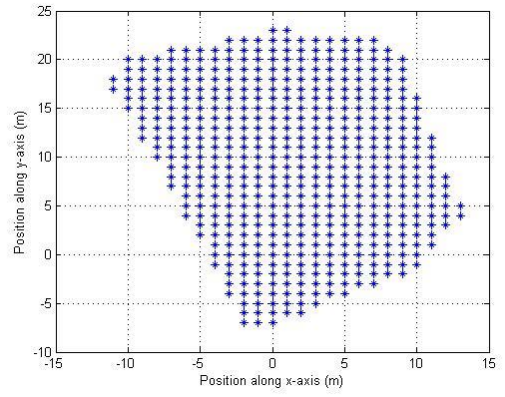
**Figure 4.6 Top five optimum ship positions for CPM with eight cables based on maximizing workspace of the manipulator.**

The pictorial representation of table 4.1 is shown in figure 4.6. The discrete points of the workspace are shown for each set of position of the ships. The maximum points obtained are 2428 which shows the manipulator can move to 2428 poses when the ship positions are given for ship position 1 in Table 4.1. The pictorial representation of the manipulator for these ship coordinates are shown in figure 4.6(a). The manipulator can have the 2317 distinct poses in the workspace when the ship coordinates are given for position 2 in Table 4.1. This is almost similar to position 1 with only a slight difference in position of ship 2 and ship 3. Similarly, for ship position number 3 in table 4.1, the manipulator can move to 2301 poses and for position 4 and 5; the number of distinct poses reduces to 2297 and 2231 respectively. Since the objective was to determine the optimum positions of the ships based on maximizing workspace of the manipulator, therefore it can be concluded that the first position in Table 4.1 or in Figure 4.6(a) are the optimum positions of the ships as with these positions the manipulator will have maximum workspace.

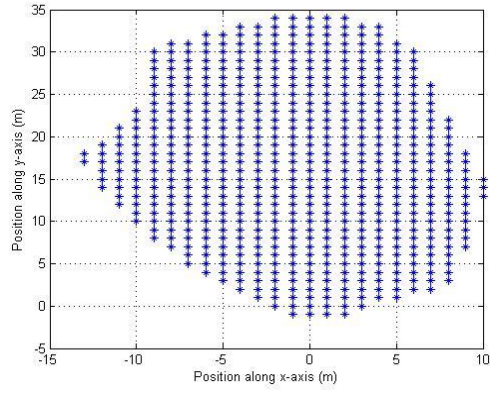
Considering the first position set of the ships in figure 4.6(a), the results of the numerical analysis are being reported in order to establish poses reachable by the manipulator by considering the given constraints. The workspace of the manipulator will be determined by keeping the values of the orientation angles  $\theta_x$   $\theta_y$   $\theta_z$  fixed. These orientation angle values will then be increased and the variation in the workspace will be observed. The range of values used for angles  $\theta_x$   $\theta_y$   $\theta_z$  are  $[0, 75]$ ,  $[0, 65]$ ,  $[0, 30]$  respectively. By considering the range of values of  $\theta_x$  the poses of the manipulator obtained are shown in figure 4.7.



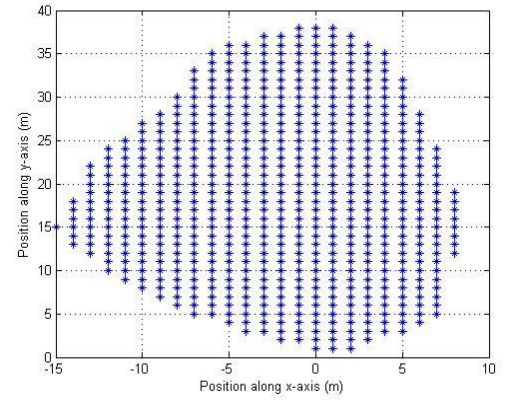
**(a)  $\theta_x=0$**



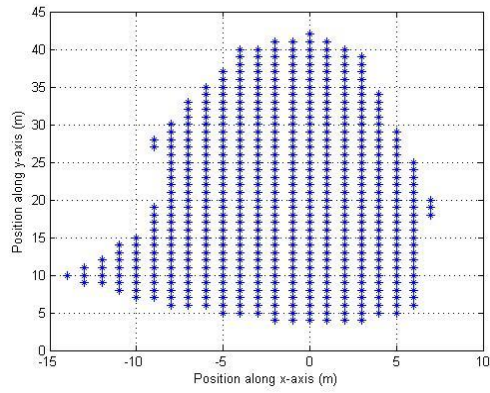
**(b)  $\theta_x=20$**



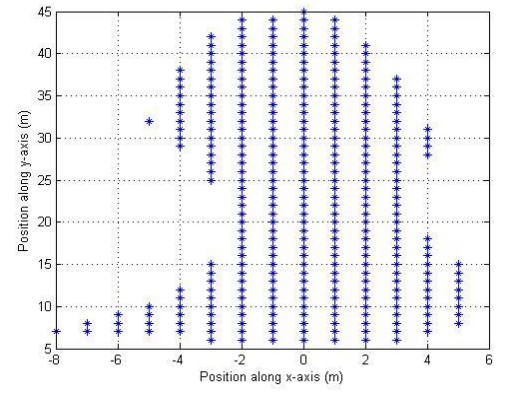
**(c)  $\theta_x=40$**



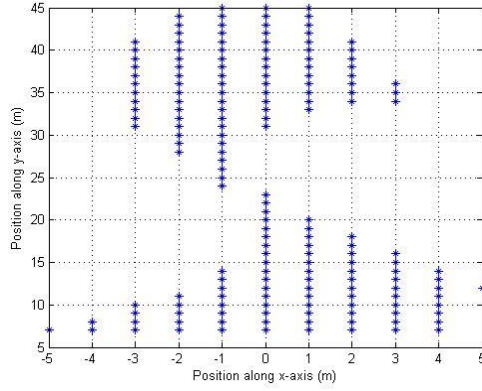
**(d)  $\theta_x=50$**



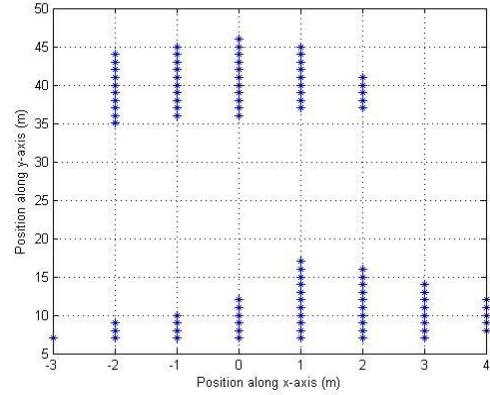
**(e)  $\theta_x=60$**



**(f)  $\theta_x=70$**



(g)  $\theta_x = 73$

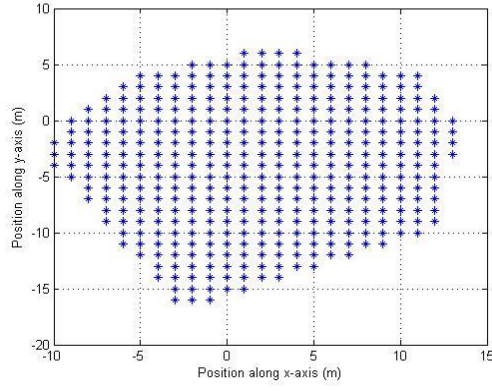


(h)  $\theta_x = 75$

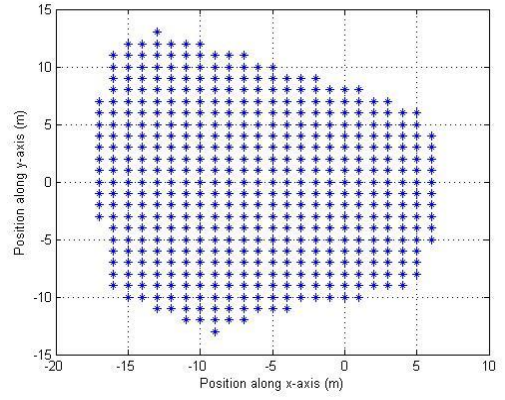
**Figure 4.7 (a)-(h) Manipulators planer workspace x-y by varying angular orientation  $\theta_x$  with  $\theta_y = \theta_z = 0$  for position 1(a) in figure 4.6.**

The workspaces shown in figure 4.7 at different orientation values of  $\theta_x$  show an increase in the workspace as  $\theta_x$  is increased from zero up to a certain value which is  $\theta_x = 50^\circ$ . As value of  $\theta_x$  is further increased workspace starts to decrease until it becomes almost zero at  $\theta_x = 75^\circ$ . The workspace changes shape and dimension by assuming values of the orientation angle between  $[0-75]$ .

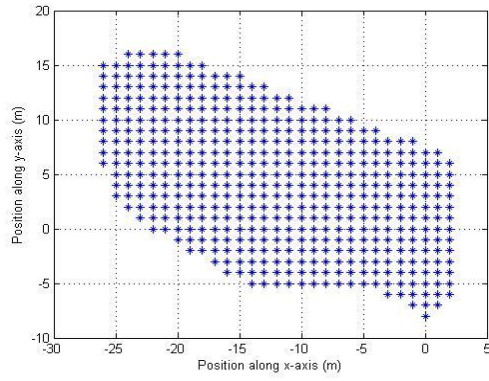
Similar results are obtained when workspace is studied when  $\theta_y$  is changed while keeping the other two orientation angles  $\theta_x$  and  $\theta_z$  equal to zero. The workspace increases upto  $\theta_y = 30^\circ$ . As value of  $\theta_y$  is increased further, workspace decreases till it reaches the maximum allowable range of the orientation angle  $\theta_y$  which is  $65^\circ$  in this case. These results are shown in figure 4.8.



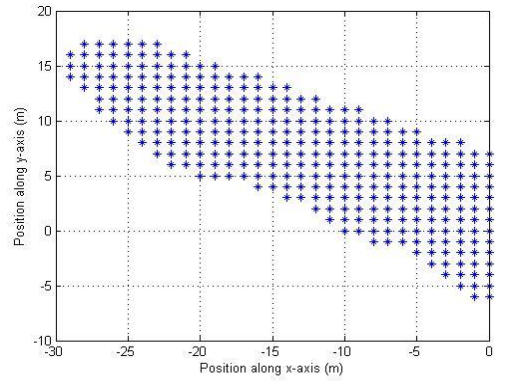
(a)  $\theta_y = 0$



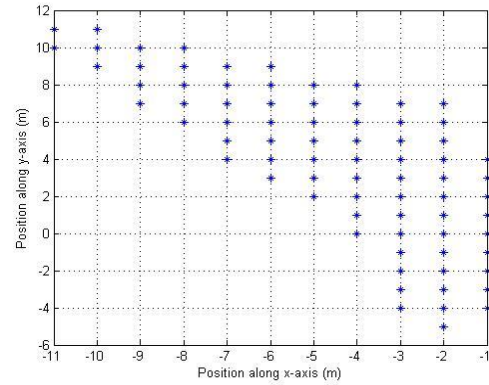
(b)  $\theta_y = 20$



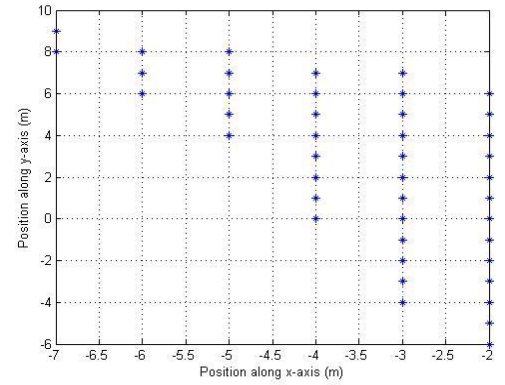
(c)  $\theta_y = 40$



(d)  $\theta_y = 50$



(e)  $\theta_y = 60$



(f)  $\theta_y = 65$

**Figure 4.8 Manipulators planer workspace x-y by varying angular orientation  $\theta_y$**

**with  $\theta_x = \theta_z = 0$  for position 1(a) in figure 4.6.**



Finally, the poses of the manipulator are obtained by varying the values of the orientation angle  $\theta_z$  and keeping  $\theta_x$  and  $\theta_y$  fixed. In this case, the workspace area also increases by increasing the value of the orientation angle  $\theta_z$  up to a certain value. After that workspace shows a decrease in shape and dimension similar to the previous cases of  $\theta_x$  and  $\theta_y$ . Results are shown in figure 4.9. The maximum allowable range of orientation angle  $\theta_z$  is  $30^\circ$  where the dimensions of the manipulator's workspace area are reduced.

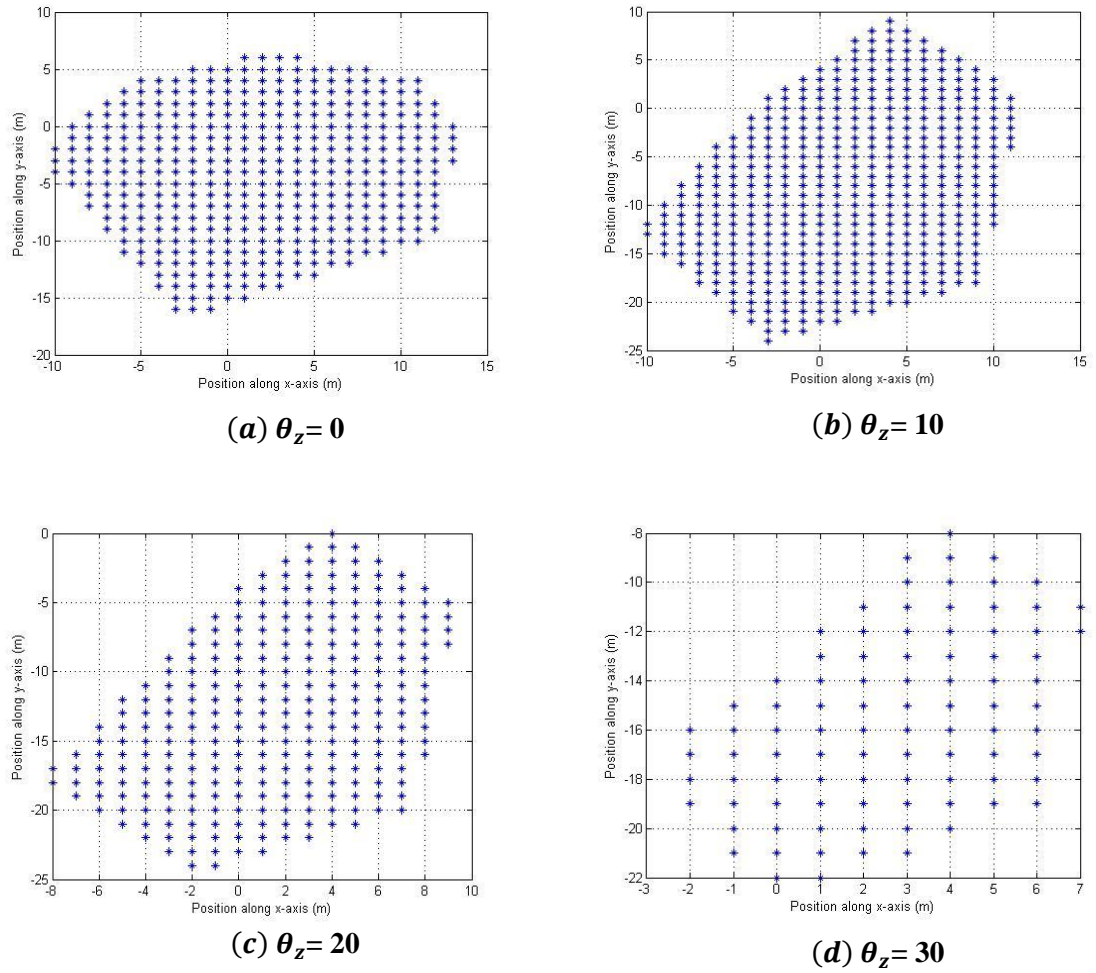


**Figure 4.9 Manipulators planer workspace x-y by varying angular orientation  $\theta_z$  with  $\theta_x = \theta_y = 0$  for position 1(a) in figure 4.6.**

## **Case 2: CPM with ten cables**

Ship position optimization will also be illustrated for CPM with ten cables. The schematic diagram is shown in figure 4.2. The basic mechanical structure is similar to the CPM with six or eight cables. The algorithm shown in figure 4.5 is also applied in this case to determine the optimum ship positions. The results obtained from this algorithm are summarized in table 4.2 and shown pictorially in figure 4.10.



**Table 4.2 Computed Workspace for CPM with ten cables by using the proposed algorithm with constraints expressed in Eq. (4.1) and Eq. (4.3).**

<b>Optimized Ship Position No.</b>	<b>1</b>	<b>2</b>	<b>3</b>	<b>4</b>	<b>5</b>
<b>(r- <math>\theta</math>) Position of Ship # 1 (m,deg)</b>	(50,260)	(50,260)	(50,260)	(50,260)	(50,260)
<b>(r- <math>\theta</math>) Position of Ship # 2 (m,deg)</b>	(50,210)	(50,210)	(50,210)	(50,210)	(50,225)
<b>(r- <math>\theta</math>) Position of Ship # 3 (m,deg)</b>	(50,195)	(50,195)	(50,165)	(50,165)	(50,165)
<b>(r- <math>\theta</math>) Position of Ship # 4 (m,deg)</b>	(50,150)	(50,150)	(50,150)	(50,150)	(50,150)
<b>(r- <math>\theta</math>) Position of Ship # 5 (m,deg)</b>	(50,100)	(50,100)	(50,100)	(50,100)	(50,100)
<b>(r- <math>\theta</math>) Position of Ship # 6 (m,deg)</b>	(50,80)	(50,80)	(50,80)	(50,80)	(50,80)
<b>(r- <math>\theta</math>) Position of Ship # 7 (m,deg)</b>	(50,30)	(50,30)	(50,30)	(50,30)	(50,30)
<b>(r- <math>\theta</math>) Position of Ship # 8 (m,deg)</b>	(50,15)	(50,345)	(50,15)	(50,345)	(50,15)
<b>(r- <math>\theta</math>) Position of Ship # 9 (m,deg)</b>	(50,330)	(50,330)	(50,330)	(50,330)	(50,330)
<b>(r- <math>\theta</math>) Position of Ship # 10 (m,deg)</b>	(50,280)	(50,280)	(50,280)	(50,280)	(50,280)
<b>Workspace discrete points</b>	3823	3717	3652	3586	3491

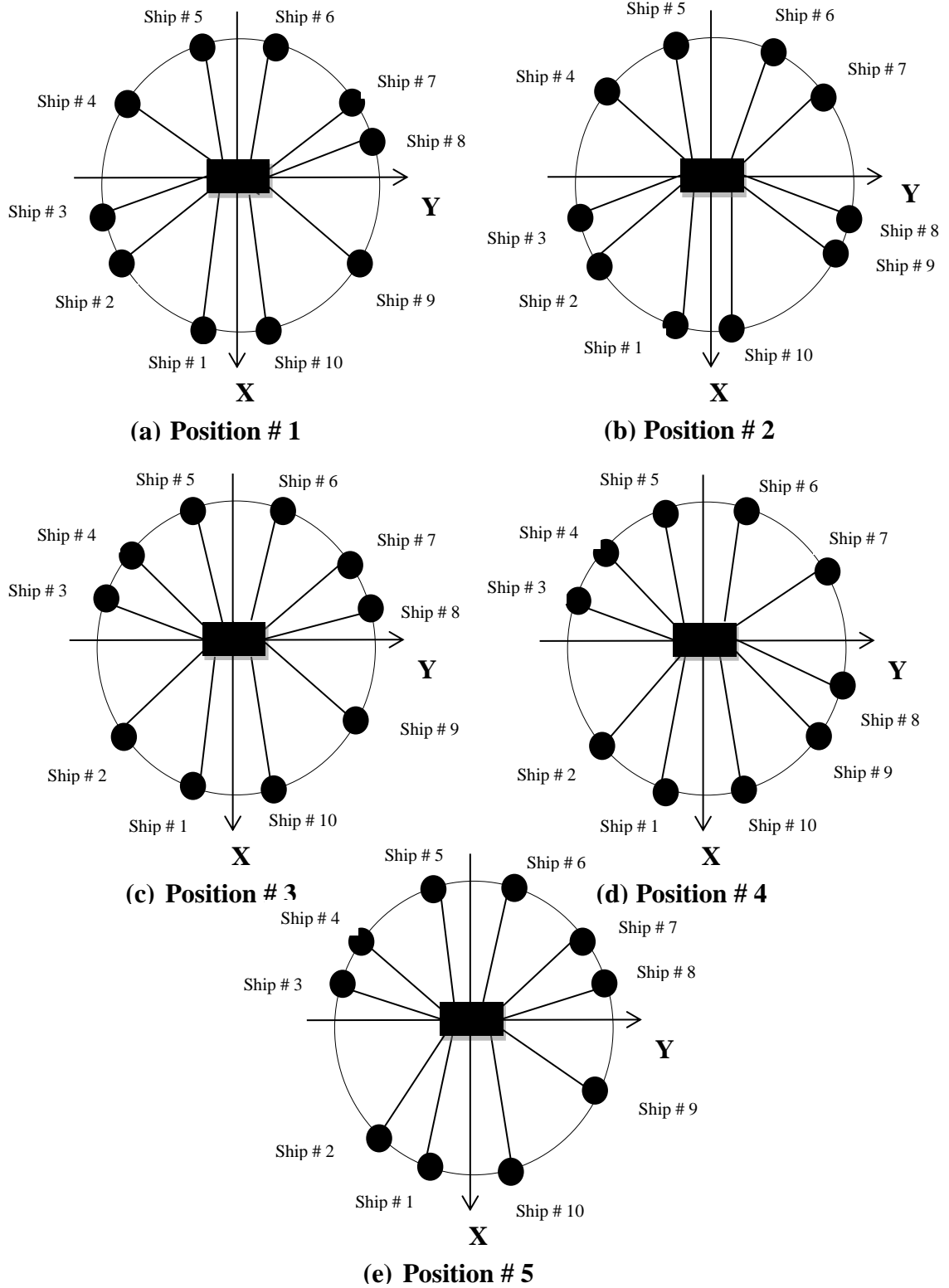


**Figure 4.10 Top five optimum ship positions for CPM with ten cables based on maximizing workspace of the manipulator.**

In the case of ten cables, the algorithm shown in figure 4.5 is applied to determine the workspace and the optimum ship positions. The ship positions giving the maximum workspace are the ship optimum positions which are ship position set #1 in table 4.2 and its schematic diagram is shown in figure 4.10(a). With these ship position set, the workspace discrete points result in 3823 points. By comparing them with the workspace of optimum ship position sets of CPM with six and eight cables, this turns out to be greater, indicating that the workspace is increased by increasing the number of cables. In position set # 2 in table 4.2, the manipulator workspace is slightly decreased to 3717 points. Its schematic is shown in figure 4.10(b). The workspace of the manipulator is further decreased with position sets 3, 4, 5 in table 4.2 and shown pictorially in figure 4.10 (c), (d) and (e) respectively.

#### **4.6.2 Maximizing Stiffness in the workspace**

In this section, optimization will be performed to maximize the stiffness of the manipulator. The stiffness analysis is conducted using the same technique explained in Chapter 3 in Section 3.4.2. The stiffness of the manipulator is determined using Eq. (3.23) but this time it is obtained for eight as well as for ten cables.

After obtaining the cable tensions, stiffness of the manipulator is obtained. As explained before, translational and rotational stiffness values cannot be compared because they have different physical units. Instead natural frequencies are used. The natural frequency of the system will be determined by Eq. (3.26). The smallest value of the natural frequency will be maximized in order to determine the optimum positions of the ships. It is more accurate to consider summation of the lowest natural frequencies at all poses of the manipulator which is given by:

$$\text{Sum of } f_{min} = \sum_{j=1}^n \min_j(f_j^k) \quad (4.13)$$

where  $\min_j(f_j^k)$  is the smallest natural frequency at the  $k$ th pose of the manipulator. At each set of ship position, sum of  $f_{min}$  is calculated for all poses of the manipulator having positive cable tensions. The position of the ships where sum of  $f_{min}$  is maximum would be the optimum position of the ships. The flow chart of this algorithm is shown in figure 4.11.

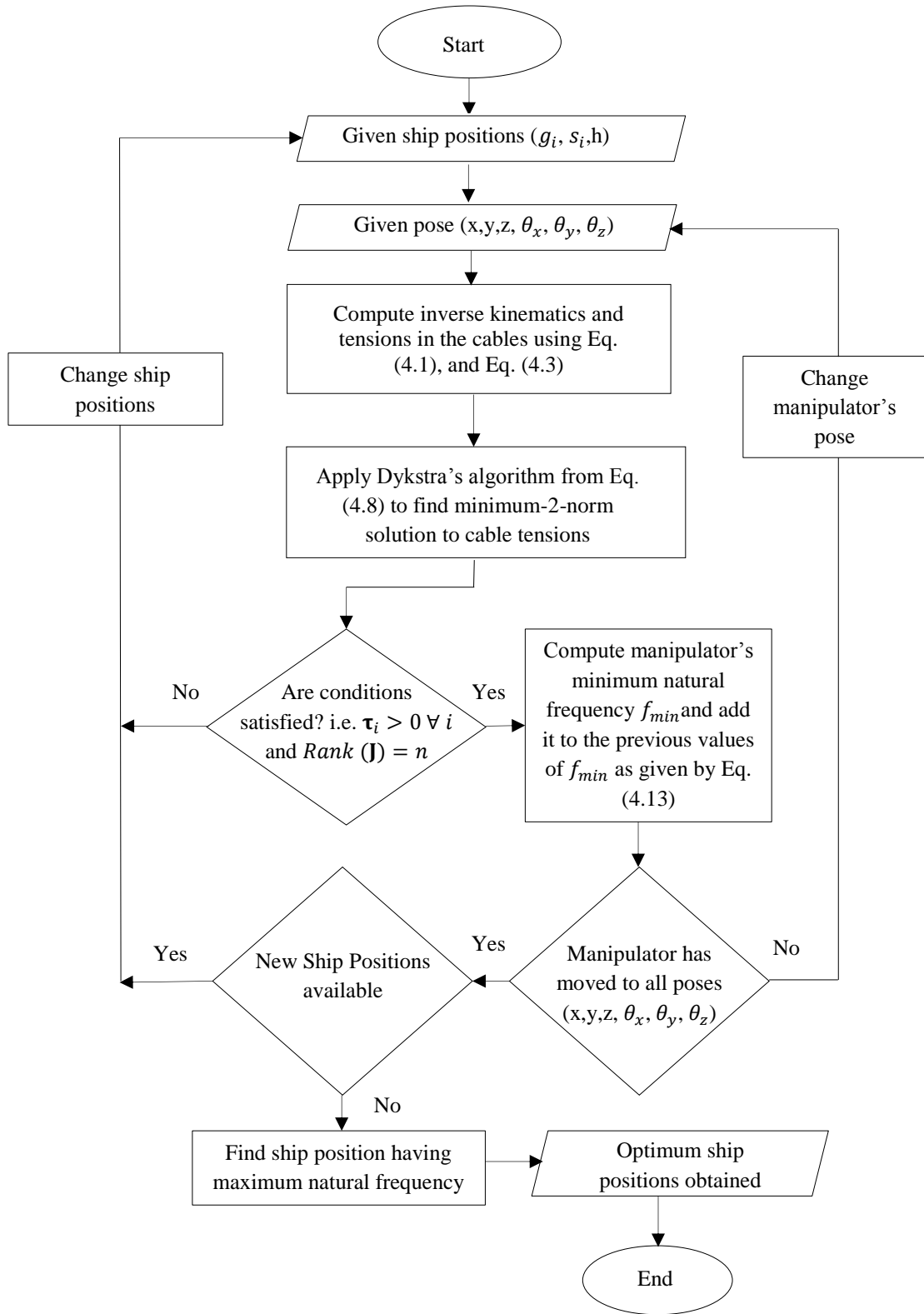


**Figure 4.11 A flow chart of the algorithm for computing the optimum ship positions based on maximizing manipulator's stiffness and natural frequency.**

The algorithm in figure 4.11 computes the summation of the lowest natural frequencies in the workspace for a given position set of the ships. For a given ship position and manipulator's pose, it computes the tension in the cables using Eq. (4.1), Eq. (4.3) and Dykstra's algorithm using Eq. (4.8). If the required conditions are satisfied i.e.  $\tau_i > 0 \forall i$  and  $Rank(J) = n$ , it computes the manipulator's stiffness and natural frequencies using Eq. (3.23) and Eq. (3.25). As the manipulator is a six DOF system, therefore six natural frequencies are obtained at a given pose in the workspace. The algorithm computes the minimum of the natural frequencies and adds this value to the previous minimum value if there is any. It then computes the minimum natural frequency for all poses of the manipulator and gives the result in the form of summation of lowest natural frequency calculated at each pose of the manipulator. The same procedure is repeated for each combination of the ship position till it computes the summation of lowest natural frequency for all ship positions. Maximizing this minimum natural frequency sum leads to maximizing the stiffness of the manipulator in the workspace.

### **Case 1: CPM with eight cables**

The results obtained for CPM with eight cables from the algorithm shown in figure 4.11 are summarized in table 4.3. It shows the sum of the lowest natural frequencies obtained with their respective ship positions. The five best positions of the ships and their natural frequencies are illustrated here. The ship positions having the highest value among the sum of  $f_{min}$  are the most optimum positions of the ships. These results are shown graphically in figure 4.12.

**Table 4.3 Computed summation of minimum natural frequencies  $f_{min}$  for CPM with eight cables by using the proposed algorithm and using Eq. (4.13).**

<b>Optimized Ship Position No.</b>	<b>1</b>	<b>2</b>	<b>3</b>	<b>4</b>	<b>5</b>
<b>(r- <math>\theta</math>) Position of Ship # 1 (m,deg)</b>	(50,260)	(50,260)	(50,260)	(50,260)	(50,260)
<b>(r- <math>\theta</math>) Position of Ship # 2 (m,deg)</b>	(50,190)	(50,185)	(50,185)	(50,200)	(50,185)
<b>(r- <math>\theta</math>) Position of Ship # 3 (m,deg)</b>	(50,165)	(50,175)	(50,145)	(50,145)	(50,175)
<b>(r- <math>\theta</math>) Position of Ship # 4 (m,deg)</b>	(50,125)	(50,125)	(50,125)	(50,125)	(50,125)
<b>(r- <math>\theta</math>) Position of Ship # 5 (m,deg)</b>	(50,55)	(50,80)	(50,55)	(50,55)	(50,55)
<b>(r- <math>\theta</math>) Position of Ship # 6 (m,deg)</b>	(50,5)	(50,5)	(50,5)	(50,5)	(50,40)
<b>(r- <math>\theta</math>) Position of Ship # 7 (m,deg)</b>	(50,355)	(50, 355)	(50, 355)	(50, 355)	(50, 355)
<b>(r- <math>\theta</math>) Position of Ship # 8 (m,deg)</b>	(50,280)	(50,280)	(50,280)	(50,280)	(50,280)
<b>Sum of <math>f_{min}</math> (Hz)</b>	3574	3410	3327	3288	3209

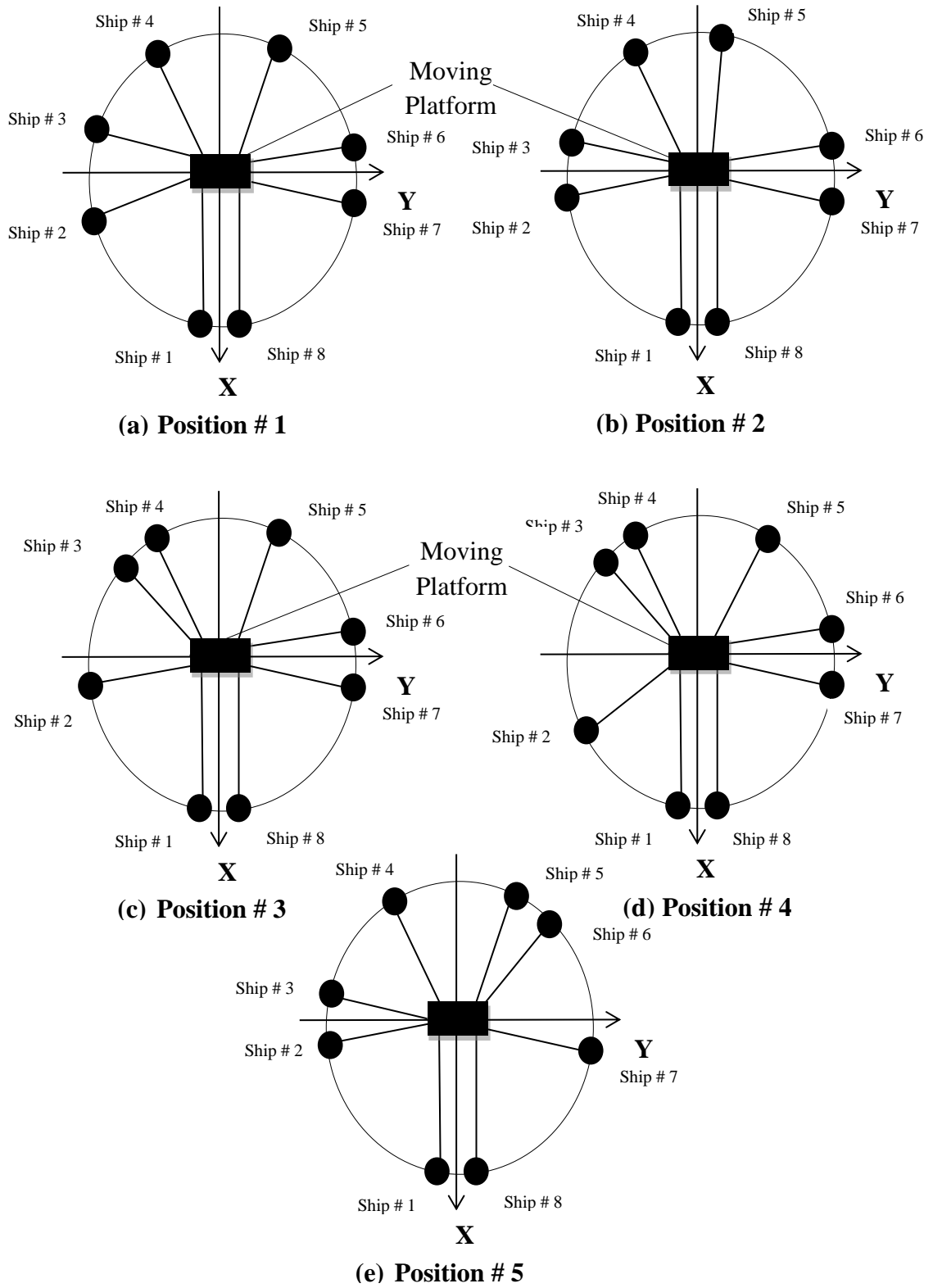


**Figure 4.12 Top five optimum ship positions for CPM with eight cables based on maximizing stiffness of the system.**



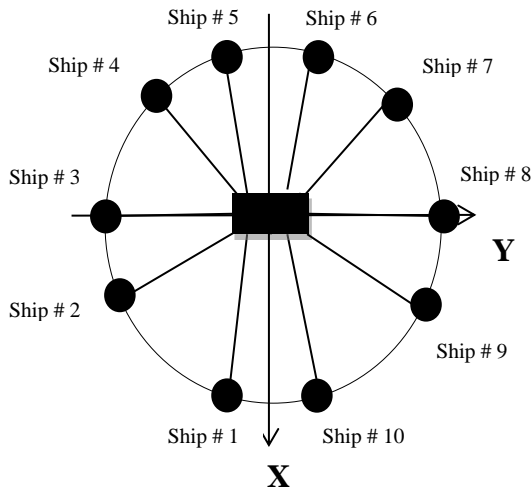
The results in table 4.3 shows the summation of the lowest natural frequencies of the manipulator calculated at each pose in the workspace with the respective ship positions as well. The maximum value of the summation is 3574 Hz. Therefore, the respective ship positions with the highest value of sum which is 3574 Hz are the optimum positions whose coordinates are given in table 4.3 under ship position 1. The pictorial representation for these ship positions are shown in figure 4.12(a). With these ship positions, the manipulator can have the maximum stiffness. The summation of the lowest natural frequency is slightly reduced to 3410 Hz, when the ship positions are moved to position set 2 as given in table 4.3 and shown pictorially in figure 4.12(b). Similarly, with ship position set 3, 4 and 5, the summation value is further decreased to values 3327 Hz, 3288 Hz and 3209 Hz respectively. These ship positions are shown pictorially in figure 4.12 (c) to (e). Therefore, figure 4.12(a) to (e) depicts the top five optimum ship positions based on maximizing stiffness of the manipulator.

### **Case 2: CPM with ten cables**

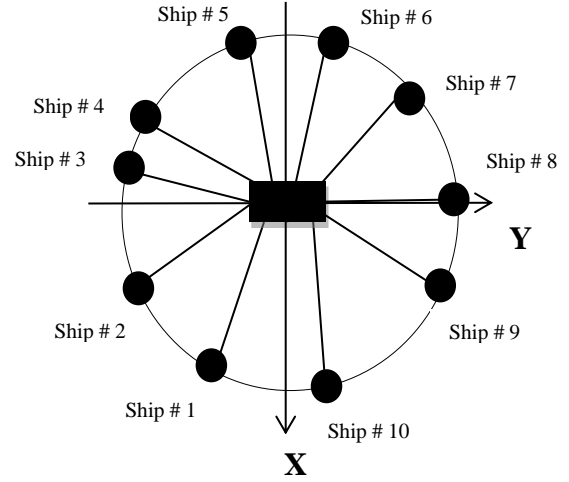
The results are also demonstrated for CPM with ten cables. The optimum ship positions for CPM with ten cables are also determined by maximizing the stiffness of the manipulator. The algorithm shown in figure 4.9 is used again to determine the natural frequency and hence the optimum ship positions. The results are summarized in table 4.4 and the schematic illustration of the CPM showing the ship positions are shown in figure 4.13.

**Table 4.4 Computed summation of minimum natural frequencies  $f_{min}$  for CPM with ten cables by using the proposed algorithm and using Eq. (4.13).**

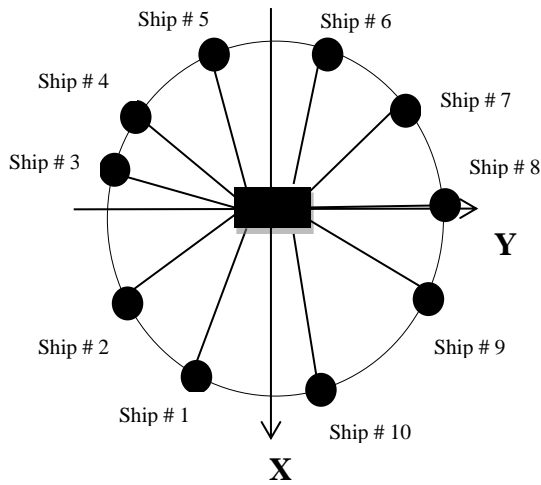
<b>Optimized Ship Position No.</b>	<b>1</b>	<b>2</b>	<b>3</b>	<b>4</b>	<b>5</b>
<b>(r- <math>\theta</math>) Position of Ship # 1 (m,deg)</b>	(50,260)	(50,245)	(50,245)	(50,260)	(50,260)
<b>(r- <math>\theta</math>) Position of Ship # 2 (m,deg)</b>	(50,210)	(50,210)	(50,210)	(50,210)	(50,210)
<b>(r- <math>\theta</math>) Position of Ship # 3 (m,deg)</b>	(50,180)	(50,165)	(50,165)	(50,180)	(50,195)
<b>(r- <math>\theta</math>) Position of Ship # 4 (m,deg)</b>	(50,135)	(50,150)	(50,150)	(50,135)	(50,135)
<b>(r- <math>\theta</math>) Position of Ship # 5 (m,deg)</b>	(50,100)	(50,100)	(50,115)	(50,115)	(50,115)
<b>(r- <math>\theta</math>) Position of Ship # 6 (m,deg)</b>	(50,80)	(50,80)	(50,80)	(50,80)	(50,80)
<b>(r- <math>\theta</math>) Position of Ship # 7 (m,deg)</b>	(50,45)	(50,45)	(50,45)	(50,45)	(50,45)
<b>(r- <math>\theta</math>) Position of Ship # 8 (m,deg)</b>	(50,0)	(50,0)	(50,0)	(50,0)	(50,0)
<b>(r- <math>\theta</math>) Position of Ship # 9 (m,deg)</b>	(50,330)	(50,330)	(50,330)	(50,330)	(50,330)
<b>(r- <math>\theta</math>) Position of Ship # 10 (m,deg)</b>	(50,280)	(50,280)	(50,280)	(50,280)	(50,280)
<b>Sum of <math>f_{min}</math> (Hz)</b>	3823	3790	3718	3653	3592



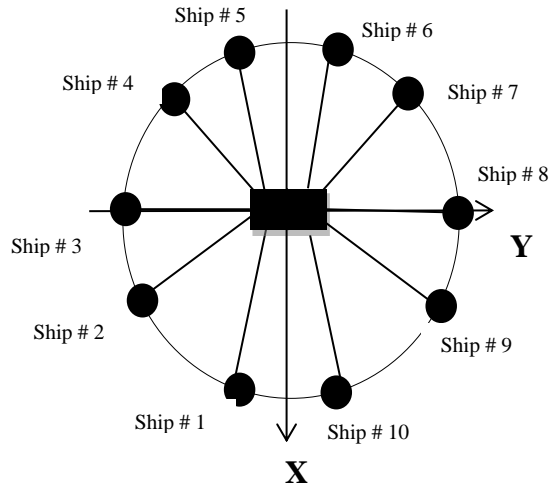
**(a) Position # 1**



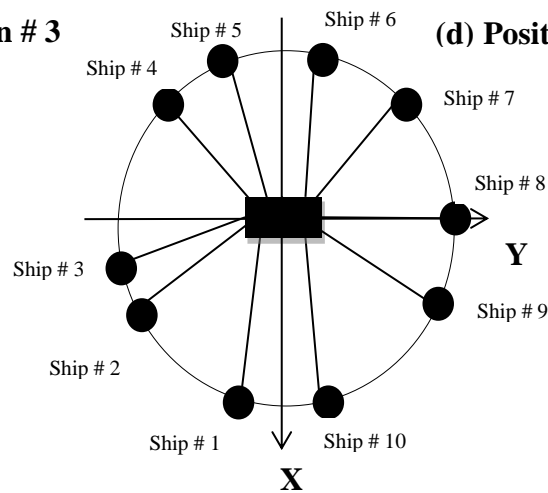
**(b) Position # 2**



**(c) Position # 3**



**(d) Position # 4**



**(e) Position # 5**

**Figure 4.13 Top five optimum ship positions based on maximizing stiffness of the system.**

In the case of ten cables, the algorithm shown in figure 4.11 is applied again in order to determine the manipulator's stiffness and hence the optimum ship positions. The ship positions giving the maximum stiffness and natural frequency are the ship optimum positions which are ship position set #1 in table 4.4 and its schematic diagram is shown in figure 4.13(a). With these ship position set, the summation of natural frequencies result in 3823 Hz. In position set # 2 in table 4.4, the summation value is slightly decreased to 3790 HZ. Its schematic is shown in figure 4.13(b). The value of summation is further decreased with position sets 3, 4, 5 in table 4.2 and shown pictorially in figure 4.13 (c), (d) and (e) respectively.

## **4.7 Results and Discussions**

In this chapter, the application of Dykstra's algorithm was studied to check whether a given wrench can be balanced without violating the cable tension limits and simultaneously calculate the minimum-2-norm solution for the cable tensions. Furthermore, cable tensions obtained were utilized to perform the workspace analysis and finally the layout optimization of CPM was conducted. In section 4.5, Dykstra's algorithm was applied to a six DOF manipulator connecting eight and ten ships via cables. It was illustrated that Dykstra's algorithm can be successfully applied to these manipulators in order to calculate the minimum-2-norm solution for the cable tensions. The problem was formulated as a projection of a point onto the intersection of convex sets. The manipulator was capable to be used for deep sea applications. Ship position optimization and the workspace analysis were reported in section 4.6. Based on maximizing the workspace of the manipulator, ship position optimization was performed.

This was further extended to incorporate stiffness of the manipulator i.e. optimum ship positions were determined so that the manipulator can have maximum stiffness.

**Table 4.5: Comparison of different CPM layouts for maximum workspace and stiffness of the manipulator.**

Optimized Ships positions	Workspace discrete points	Sum of $f_{min}$ (Hz)
For six ships CPM	1704	2038
For eight ships CPM	2852	3574
For ten ships CPM	3823	3718

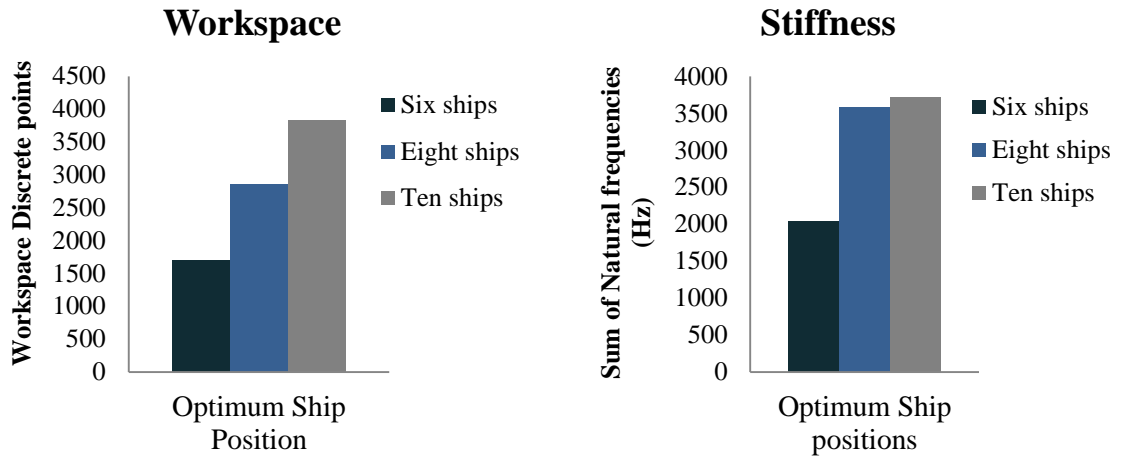


**Figure 4.14: Graph comparing CPM layouts with six, eight and ten ships for (a) Workspace and (b) Stiffness**

It was concluded from the layout optimization and workspace analysis that the moving platform can operate in a certain workspace under sea without losing the cable tensions. The workspace and stiffness of the manipulator with six, eight and ten ships

CPM is listed in table 4.4. The workspace of the manipulator was improved when eight cables were used to manipulate the moving platform compared to six cables CPM and it was further improved when number of cables used was ten. So it is concluded that the workspace of the manipulator is improved with higher number of cables. This is because with greater number of cables, each cable will support a fraction of the applied load at the manipulator, resulting in a better tension distribution among the cables and therefore less chance of having negative cable tensions. Similar conclusion is drawn for the stiffness of the manipulator. It was reported that the stiffness of the manipulator also increases with higher number of cables. This is due to the reason that all cables act like a spring and when more number of springs are connected in parallel, stiffness is found higher. These conclusions are depicted graphically in figure 4.14 where the workspace and stiffness of the manipulator is increased with higher number of ships in a cable based parallel manipulator.

## **CHAPTER 5**

### **FAILURE ANALYSIS**

In this chapter, the effect of cable failure on the position and force capability of cable based parallel manipulators is investigated. One of the important failures in cable based parallel manipulators can occur due to cable breakage. In section 5.1, the trajectory of the manipulator is reported when one of the cables is broken. The tensions in the remaining cables are determined in section 5.2. Based on the maximum tension in the cables, position optimization of the ships is performed such that the maximum tension after failure is minimized. The analysis is conducted on manipulators connected to ships via six, eight and ten cables.

#### **5.1 Theoretical background**

Cable based parallel manipulators can be used in remote areas such as inside deep sea to transport objects from one place to another. Damages occurring due to failure of a cable based parallel manipulator during its operation can be very costly. Failure of cable based parallel manipulators can occur because of the failure of a cable (cable breakage, cable jam or undesired flexibility of cable), sensor failure, actuator failure and transmission failure. These failures could result in the loss of DOF, loss of actuation and loss of motion constraint.

From the force point of view, failure of the manipulator occurs if the cable does not provide the required force/torque. For instance, when the actuator force/torque is lost partially or fully or the actuator is saturated. This could also happen when the cable is broken or slack (zero tension), cable is jammed (constant length), or its actuating

mechanism malfunctions such that a different (zero, constant or limited) force is provided by the cable.

For cable based parallel manipulators, research on failure analysis and fault tolerance has not been sufficiently explored. This study is aimed at analyzing the post failure trajectory of the CPM and calculating the actuator forces after failure in order to determine the optimum position of the ships such that the maximum tension in the cables after failure is minimized.

### 5.1.1 Effect of Cable Breakage on Manipulator Velocity

When a cable breakage occurs, the velocity equation can be written as:

$$\dot{\mathbf{l}}_a = \mathbf{J}_a \mathbf{v} \quad (5.1)$$

Where  $\mathbf{v} \in R^6$ ,  $\dot{\mathbf{l}}_a \in R^{n_a-1}$  and  $\mathbf{J}_a = R^{(n_a-1) \times 6}$

Here the Jacobian matrix  $\mathbf{J}_a$  and the velocity vector  $\dot{\mathbf{l}}_a$  denote the reduced Jacobian matrix and the rate of change of cable length vector respectively, after cable breakage.  $n_a$  denotes the number of rows of the matrix before failure. The Jacobian matrix  $\mathbf{J}_a$  in Eq. (5.1) losses the row corresponding to the cable that is broken. As the number of independent rows of  $\mathbf{J}_a$  in Eq. (5.1) becomes smaller than the number of columns after failure,  $\mathbf{J}_a$  has a null space, denoted as  $nsp(\mathbf{J}_a)$ , in which  $\dot{\mathbf{l}}_a = 0$  for all  $\mathbf{v} \in nsp(\mathbf{J}_a)$ , indicating that the end-effector could have an unconstrained motion of  $\mathbf{v} \in nsp(\mathbf{J}_a)$  even if all remaining cables are locked. To determine how the end-effector velocity  $\mathbf{v}$  lies in  $R^m$  relative to  $nsp(\mathbf{J}_a)$ ,  $\mathbf{v}$  could be divided into two orthogonal components shown in Eq. (5.2) below:



$$\mathbf{v} = \text{proj}_{\text{nsp}(\mathbf{J}_a)}(\mathbf{v}) + \text{proj}_{\text{nsp}(\mathbf{J}_a)^\perp}(\mathbf{v}) \quad (5.2)$$

Where  $\text{proj}_{\text{nsp}(\mathbf{J}_a)}(\mathbf{v})$  and  $\text{proj}_{\text{nsp}(\mathbf{J}_a)^\perp}(\mathbf{v})$  is given by:

$$\begin{aligned} \text{proj}_{\text{nsp}(\mathbf{J}_a)}(\mathbf{v}) &= N(\mathbf{J}_a)(N(\mathbf{J}_a))^T \mathbf{v} \\ \text{proj}_{\text{nsp}(\mathbf{J}_a)^\perp}(\mathbf{v}) &= B(\mathbf{J}_a)^T (B(\mathbf{J}_a)^T)^T \mathbf{v} \end{aligned} \quad (5.3)$$

Where  $\text{nsp}(\mathbf{J}_a)^\perp$  in Eq. (5.2) is the orthogonal complement of  $\text{nsp}(\mathbf{J}_a)$ ; In Eq. (5.3),  $\text{proj}_{\text{nsp}(\mathbf{J}_a)}(\mathbf{v})$  is the projection of  $\mathbf{v}$  onto  $\text{nsp}(\mathbf{J}_a)$ , which constitutes the velocity component that is unconstrained and cannot be controlled by the remaining actuators in the manipulator. Similarly,  $\text{proj}_{\text{nsp}(\mathbf{J}_a)^\perp}(\mathbf{v})$  is the projection of  $\mathbf{v}$  onto  $\text{nsp}(\mathbf{J}_a)^\perp$ , which constitutes the velocity component that is controllable by the remaining actuators in the manipulator.  $N(\mathbf{J}_a)$  is a matrix whose columns form an orthonormal basis of  $\text{nsp}(\mathbf{J}_a)$  and  $B(\mathbf{J}_a)^T$  is a matrix whose columns form an orthonormal basis of  $\text{csp}(\mathbf{J}_a)$ .

### 5.1.2 Effect of Cable Breakage on Manipulator Force

As a result of cable breakage, force equation can be written as:

$$\mathbf{F} = \mathbf{J}_a^T \boldsymbol{\tau}_a \quad (5.4)$$

Where  $\mathbf{F} \in R^6$ ;  $\boldsymbol{\tau}_a \in R^{n_a-1}$ ; and  $\mathbf{J}_a^T \in R^{6 \times (n_a-1)}$

The number of columns of the matrix  $\mathbf{J}_a^T$ , after cable breakage becomes smaller than the number of rows and therefore, the dimension of the column space  $n_a - 1$ , becomes smaller than the dimension of the desired task space,  $m$ . There is a unique solution of  $\boldsymbol{\tau}_a \in R^{n_a-1}$  only in case  $\mathbf{F} \in \text{csp}(\mathbf{J}_a^T)$ . Otherwise for  $\mathbf{F} \notin \text{csp}(\mathbf{J}_a^T)$ , there is no solution for  $\boldsymbol{\tau}_a \in R^{n_a-1}$ . Such vectors contain force components that belong to  $\text{csp}(\mathbf{J}_a^T)^\perp$ ,

which cannot be resisted by actuator forces and therefore cause unconstrained motion. Force applied on the end-effector,  $\mathbf{F} \in R^6$ , could be divided into two orthogonal components:

$$\mathbf{F} = proj_{csp(\mathbf{J}_a^T)}(\mathbf{F}) + proj_{csp(\mathbf{J}_a^T)^\perp}(\mathbf{F}) \quad (5.5)$$

Where

$$\begin{aligned} proj_{csp(\mathbf{J}_a)}(\mathbf{F}) &= B(\mathbf{J}_a)(B(\mathbf{J}_a))^T \mathbf{F} \\ proj_{csp(\mathbf{J}_a)^\perp}(\mathbf{F}) &= N(\mathbf{J}_a)^T (N(\mathbf{J}_a)^T)^T \mathbf{F} \end{aligned} \quad (5.6)$$

Here  $proj_{csp(\mathbf{J}_a^T)}(\mathbf{F})$  is the force component that is resisted by the actuator forces; Similarly,  $proj_{csp(\mathbf{J}_a^T)^\perp}(\mathbf{F})$  is the force component that cannot be resisted by the actuator forces;  $B(\mathbf{J}_a)$  is a matrix whose columns vectors form an orthonormal basis of  $csp(\mathbf{J}_a)$ ; and  $N(\mathbf{J}_a)^T$  is a matrix whose columns form an orthonormal basis for the null space of  $\mathbf{J}_a^T$ .

## 5.2 Post failure trajectory

The trajectory of a CPM after failure is investigated by examining the change in the Jacobian matrix, its inverse and transposes. When one of the cables fails, the Jacobian matrix becomes:

$$\mathbf{J}_a \in R^{(m-1) \times n} \quad (5.7)$$

Where  $m$  and  $n$  are the number of rows and columns respectively before failure. From Eq. (5.7), the Jacobian matrix loses its corresponding row when one of the cables

breaks. The post failure trajectory of the manipulator is determined by moving along the null-space of the reduced Jacobian matrix in Eq. (5.7).

The determination of the post failure velocity and static force capability of CPM is illustrated through a simulation conducted on a 6DOF manipulator connected to six ships via cables shown in figure 3.1 in chapter 3. The velocity equation for this CPM is given by Eq. (5.8) as:

$$\begin{bmatrix} \dot{l}_1 \\ \dot{l}_2 \\ \dot{l}_3 \\ \dot{l}_4 \\ \dot{l}_5 \\ \dot{l}_6 \end{bmatrix} = \begin{bmatrix} \hat{l}_{1x} \hat{l}_{1y} \hat{l}_{1z} (r_{1x} \times \hat{l}_{1x}) (r_{1y} \times \hat{l}_{1y}) (r_{1z} \times \hat{l}_{1z}) \\ \hat{l}_{1x} \hat{l}_{1y} \hat{l}_{1z} (r_{2x} \times \hat{l}_{2x}) (r_{2y} \times \hat{l}_{2y}) (r_{2z} \times \hat{l}_{2z}) \\ \hat{l}_{1x} \hat{l}_{1y} \hat{l}_{1z} (r_{3x} \times \hat{l}_{3x}) (r_{3y} \times \hat{l}_{3y}) (r_{3z} \times \hat{l}_{3z}) \\ \hat{l}_{1x} \hat{l}_{1y} \hat{l}_{1z} (r_{4x} \times \hat{l}_{4x}) (r_{4y} \times \hat{l}_{4y}) (r_{4z} \times \hat{l}_{4z}) \\ \hat{l}_{1x} \hat{l}_{1y} \hat{l}_{1z} (r_{5x} \times \hat{l}_{5x}) (r_{5y} \times \hat{l}_{5y}) (r_{5z} \times \hat{l}_{5z}) \\ \hat{l}_{1x} \hat{l}_{1y} \hat{l}_{1z} (r_{6x} \times \hat{l}_{6x}) (r_{6y} \times \hat{l}_{6y}) (r_{6z} \times \hat{l}_{6z}) \end{bmatrix} \begin{bmatrix} \dot{p}_x \\ \dot{p}_y \\ \dot{p}_z \\ \dot{\theta}_x \\ \dot{\theta}_y \\ \dot{\theta}_z \end{bmatrix} \quad (5.8)$$

Where  $\dot{\mathbf{p}} = \begin{bmatrix} \dot{p}_x \\ \dot{p}_y \\ \dot{p}_z \end{bmatrix}$  and  $\dot{\boldsymbol{\theta}} = \begin{bmatrix} \dot{\theta}_x \\ \dot{\theta}_y \\ \dot{\theta}_z \end{bmatrix}$

All vectors are expressed in  $x$ - $y$ - $z$  coordinates. The simulations presented in this section illustrate how the projection equations shown in section 5.1 can be used to determine the post failure position and orientation trajectories of the CPM discussed above. For simplification, it is assumed that the manipulator moves with a very low velocity and therefore the dynamic behavior is neglected. The algorithm to calculate the position and orientation trajectory of the end effector after failure is shown in figure 5.1. The velocities,  $\dot{\mathbf{p}}$  and  $\dot{\boldsymbol{\theta}}$  in Eq. (5.8) are substituted by the infinitesimal displacements  $\Delta \mathbf{p}$  and  $\Delta \boldsymbol{\theta}$  respectively, and the position  $\mathbf{p} = [p_x \ p_y \ p_z]^T$  and orientation  $\boldsymbol{\theta} = [\theta_x \ \theta_y \ \theta_z]^T$  were calculated by summing the preceding infinitesimal displacements  $\Delta \mathbf{p}$  and  $\Delta \boldsymbol{\theta}$

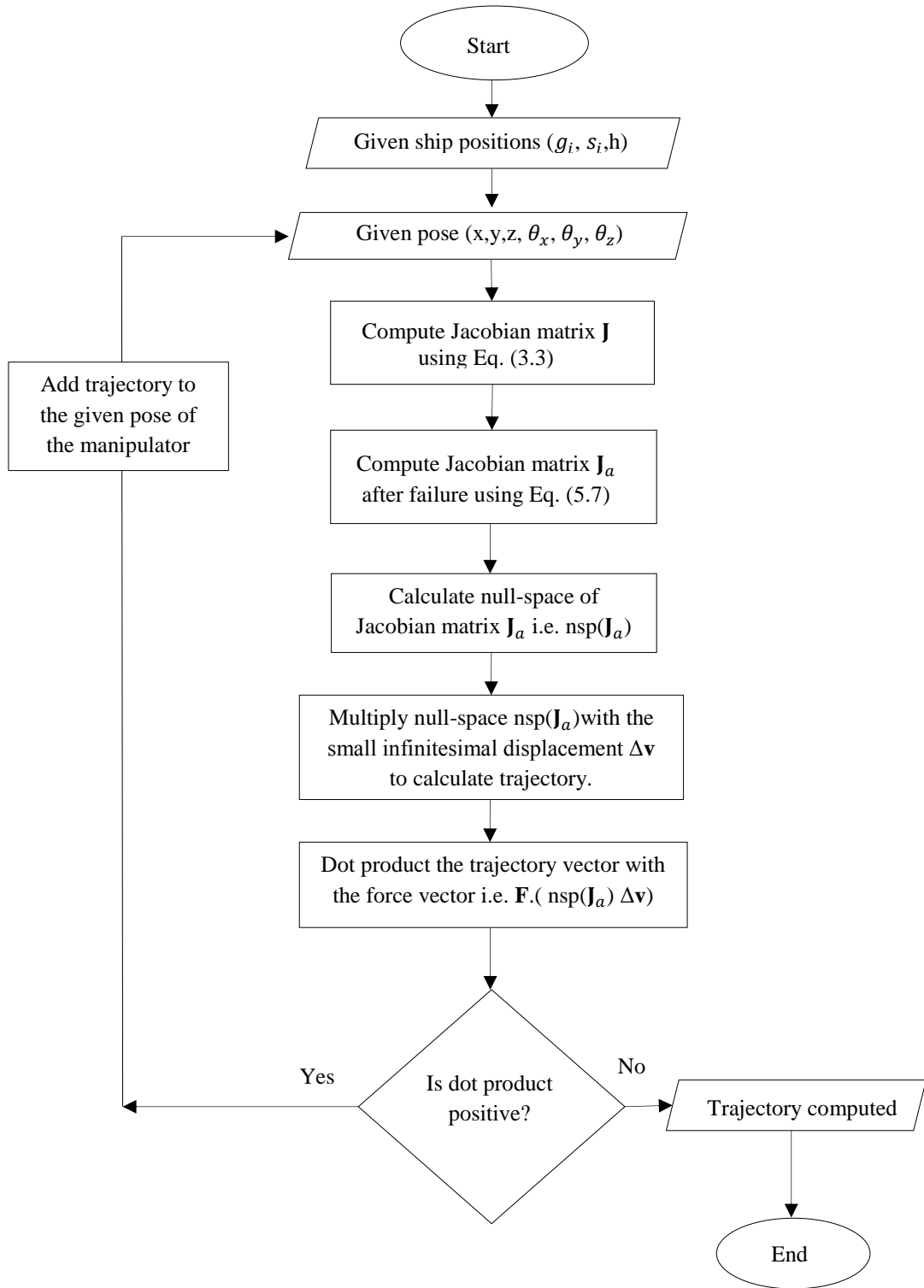
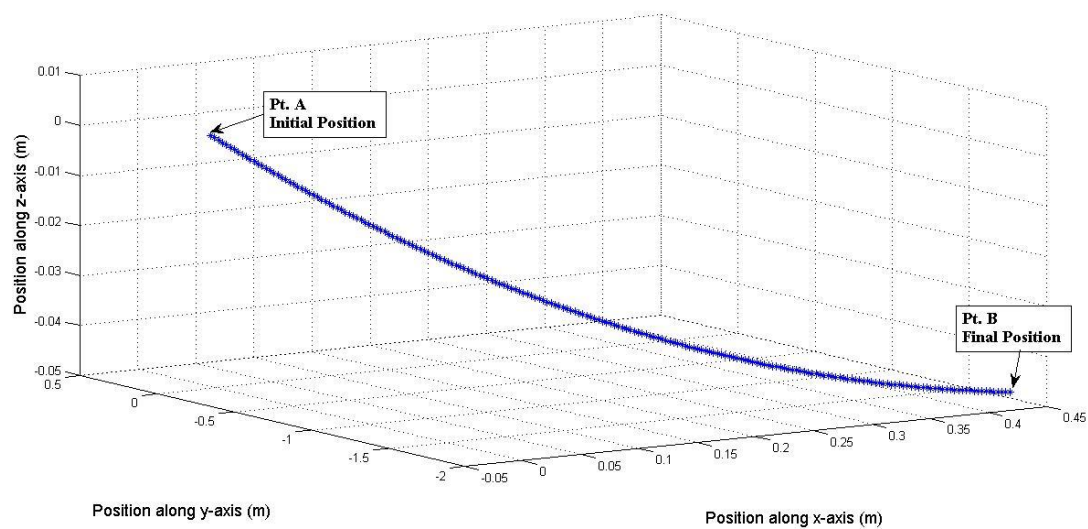


**Figure 5.1 A flow chart of the algorithm for computing the post failure trajectory of the manipulator.**

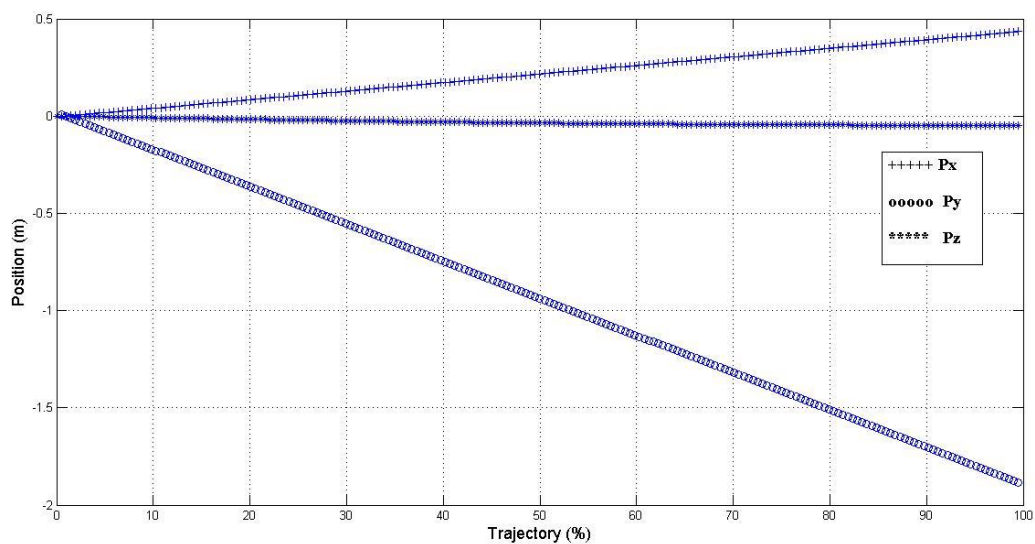
respectively after each displacement along the null space of the Jacobian matrix  $\mathbf{J}_a$ . In order to determine the final position of the manipulator after failure, the dot product of the force and the trajectory vector is obtained. If the dot product is positive, the small infinitesimal pose of the manipulator is summed again with the initial pose whereas the negative dot product indicates the manipulator has reached to its final position.

### **5.2.1 Simulation of cable 2 failure**

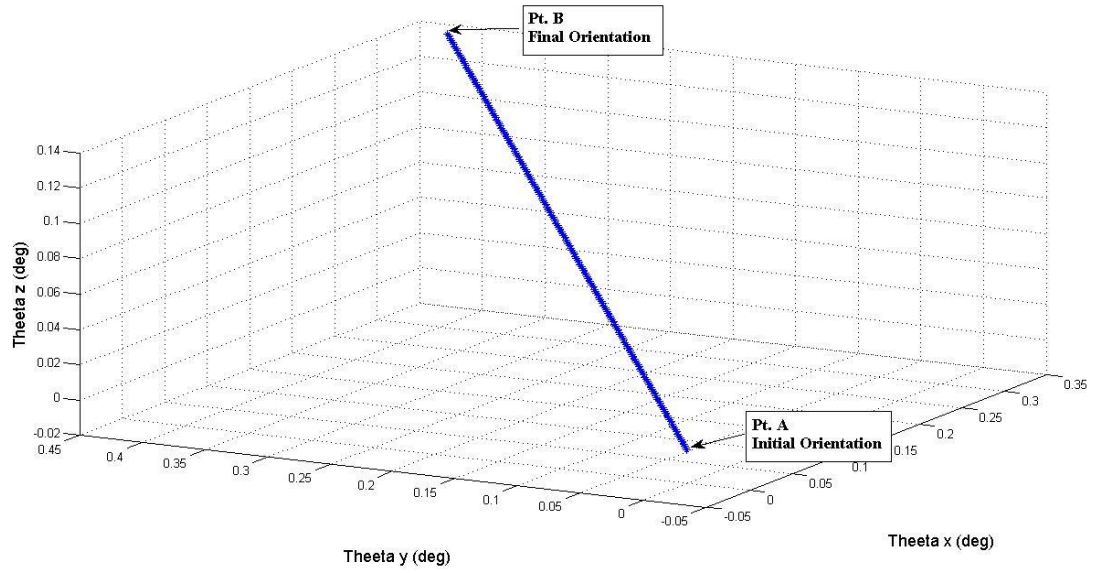
The algorithm in figure 5.1 is applied to calculate the post failure trajectory of the manipulator in case of cable no. 2 breakage. The simulations are presented in figure 5.2. The manipulator is at pose  $\mathbf{p} = [0 \ 0 \ 0]$ , and orientation  $\boldsymbol{\theta} = [0 \ 0 \ 0]$ , as shown by point A in figure 5.2(a) and (c) when cable no. 2 suddenly breaks. The trajectory followed by the manipulator after the breakage of cable no. 2 is shown in figure 5.2.



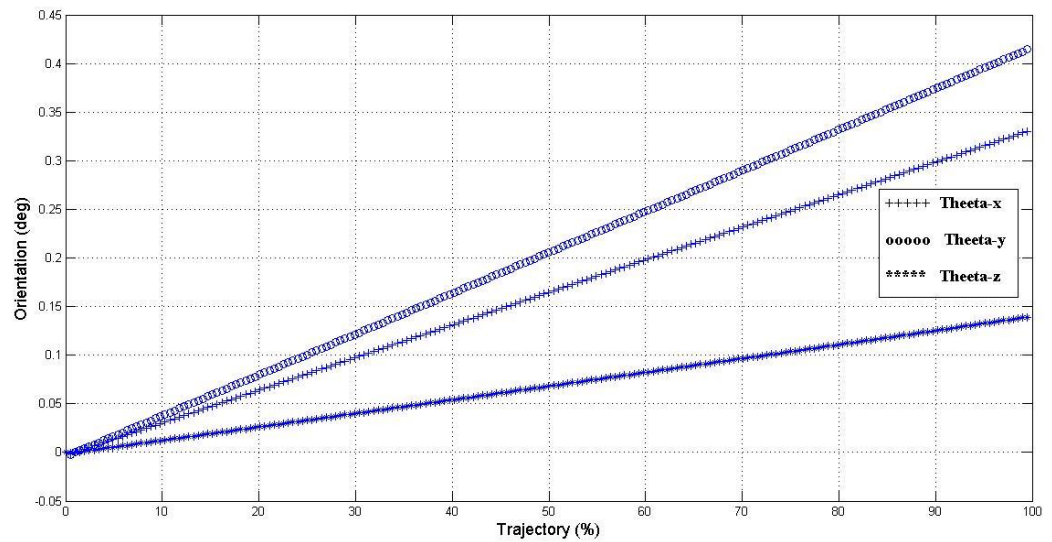
**(a) 3D Position trajectory of moving platform**



**(b) Position trajectory of moving platform**



(c) 3D Orientation trajectory of moving platform



(d) Orientation trajectory of moving platform

**Figure 5.2 (a)-(d) Trajectories of the example manipulator shown in figure 3.1 in case of cable no. 2 breakage.**

In figure 5.2, the post failure trajectory of the manipulator is determined by moving infinitesimal displacements onto the null space of  $\mathbf{J}_a$ . It should be noted that, as a result of cable no. 2 breakage, the Jacobian matrix  $\mathbf{J}$  in Eq. (5.8), is reduced by eliminating its second row. From figure 5.2, Point A indicates the manipulator's initial pose before failure. When cable 2 breaks, the manipulator follows the trajectory from point A till it reaches the new static equilibrium position  $\mathbf{p} = [0.45 \ -1.97 \ -0.05]$  (meters) and new orientation  $\boldsymbol{\theta} = [0.35 \ 0.43 \ 0.15]$  (degrees) at point B as shown in figure 5.2(a). The movement of the manipulator along  $x$ - $y$ - $z$  direction can be more clearly seen in figure 5.2(b). It is observed from figure that there is a small movement of the manipulator along  $z$ -direction compared with the movement along  $x$  and  $y$  direction. Apart from the translational movement, the manipulator also undergoes rotational movement along  $x$ - $y$ - $z$  axis as indicated in figure 5.2(c). Point A shows the orientation before failure and point B indicates the new static orientation of the platform after cable 2 failure. As shown in figure 5.2(d),  $\theta_x$  undergoes a rotation of 0.35 deg whereas  $\theta_y$  and  $\theta_z$  rotates 0.43 deg and 0.15 deg respectively.

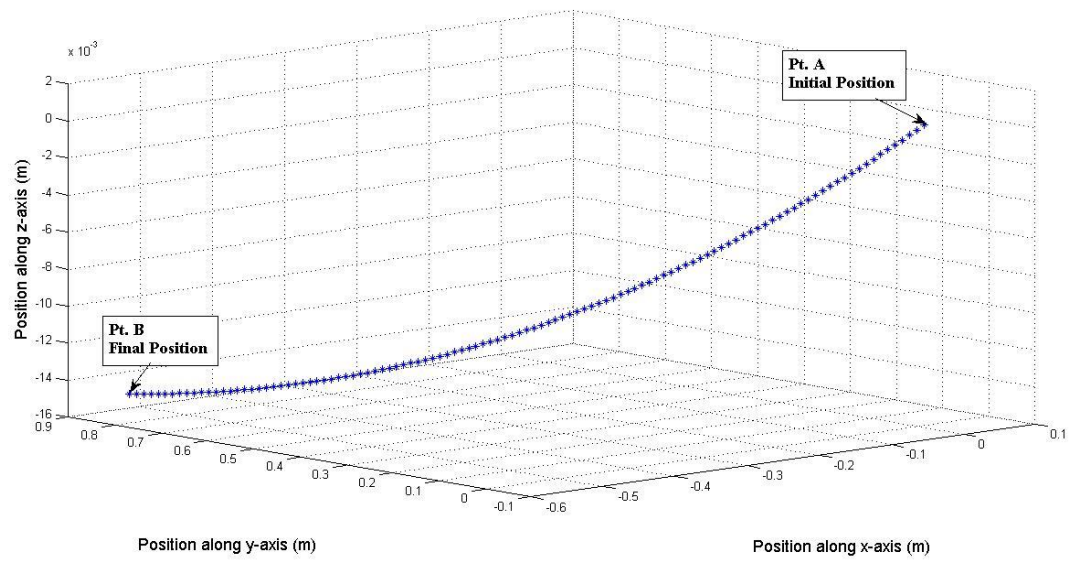
### 5.2.2 Simulation of cable 6 failure

The simulations shown in figure 5.3 show post trajectory failure of the example CPM the manipulator could follow in the case when cable 6 breaks.

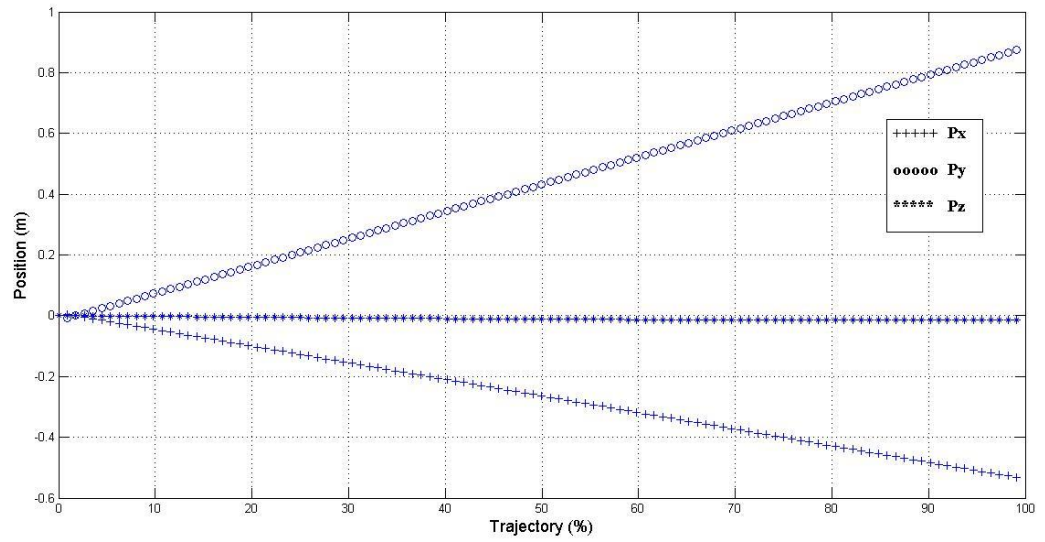
The initial position and orientation of the manipulator is  $\mathbf{p} = [0 \ 0 \ 0]$ (meters) and  $\boldsymbol{\theta} = [0 \ 0 \ 0]$ (degrees), respectively. This is indicated by point A in figure 5.3(a). When a breakage occurs in cable no. 6 the manipulator follows a trajectory calculated from the



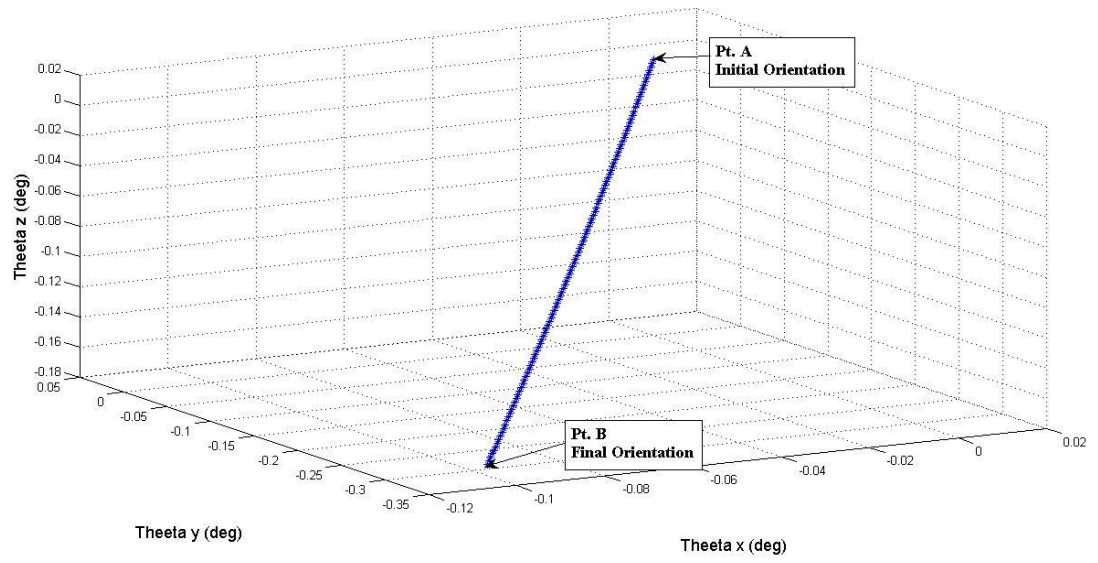
algorithm in figure 5.1 to its new static equilibrium position, indicated by point B in figure 5.3(a).



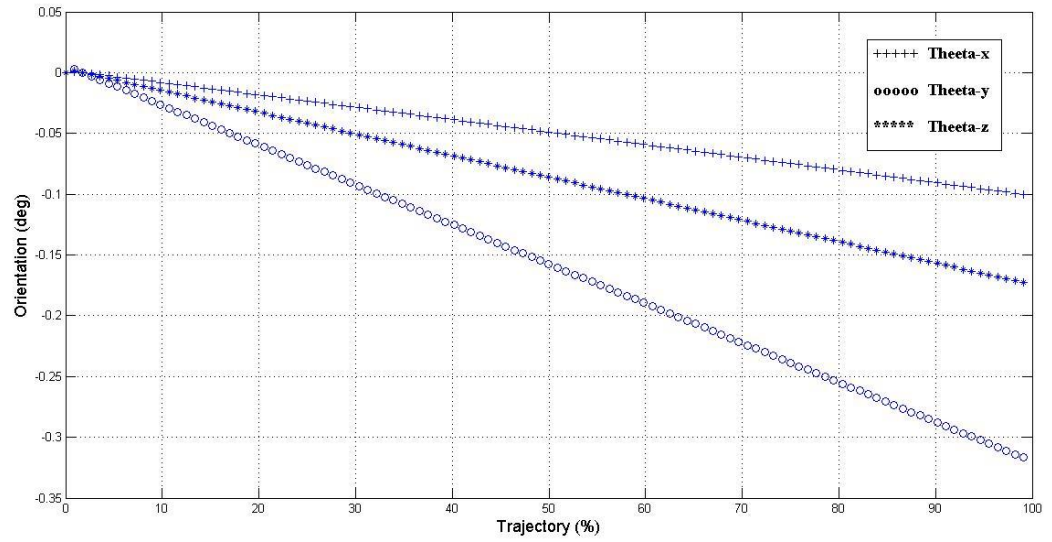
(a) 3D Position trajectory of moving platform



(b) Position trajectory of moving platform



(c) 3D Orientation trajectory of moving platform



(d) Orientation trajectory of moving platform

**Figure 5.3 (a)-(d) Trajectories of the example manipulator shown in figure 3.1 in case of cable no. 6 breakage.**

The trajectory obtained in figure 5.3 is determined by moving small infinitesimal displacements along the null space of  $\mathbf{J}_a$ . In case of cable no. 6 breakage,  $\mathbf{J}_a$  is obtained by eliminating its sixth row. From the initial position  $\mathbf{p} = [0 \ 0 \ 0]$  (meters) and orientation  $\boldsymbol{\theta} = [0 \ 0 \ 0]$  (degrees), shown by point A in figure 5.3(a) and (c), the manipulator now moves to its new static equilibrium position and orientation. The new static equilibrium position and orientation obtained in case of cable no. six breakage is  $\mathbf{p} = [-0.53 \ 0.87 \ -0.02]$  (meters) and  $\boldsymbol{\theta} = [-0.1 \ -0.32 \ -0.17]$  (degrees) respectively. This is indicated by point B in figure 5.3(a) and (c). Figure 5.2(b) shows the translational movements along  $x$ - $y$ - $z$  axis. As can be seen in the figure the  $z$ -axis movement is small as compared to  $x$  and  $y$ -axis movement. Similarly, the 3D orientation trajectory can be seen in figure 5.3(c). The individual rotations along  $x$ - $y$ - $z$  axis are depicted in figure 5.3(d). With the breakage of cable 6, the platform undergoes rotation in  $x$ - $y$ - $z$  axis in the negative direction.

Similarly, with other cable breakages, the manipulator follows the trajectory trend similar to the above ones shown. With the breakage of one of the cables, the manipulator gains an unconstrained motion in a specific portion of the task space in which an externally applied force cannot be resisted by the cable tensions. In the simulations,  $\mathbf{J}_a$  is updated after each displacement along the trajectory, and therefore, the smaller the displacement step is, the less error exists in the simulation.

With the breakage of one of the cables, apart from the trajectory that is followed by the manipulator, tensions in the remaining cables also vary after failure. This is explained in detail in the next section.

### 5.3 Post failure tension in the cables

When a cable breaks in CPM's, the tensions in the remaining cables differ from their previous value before cable  $i$  failure. Determining the tension values in the remaining cables is necessary for the safe operation of the system. The maximum tension after failure will be minimized in section 5.4. In this section, different designs of CPM will be used to study the post failure tensions in the cables. The designs will include six, eight and ten cables.

#### 5.3.1 Post failure tensions in CPM with six cables

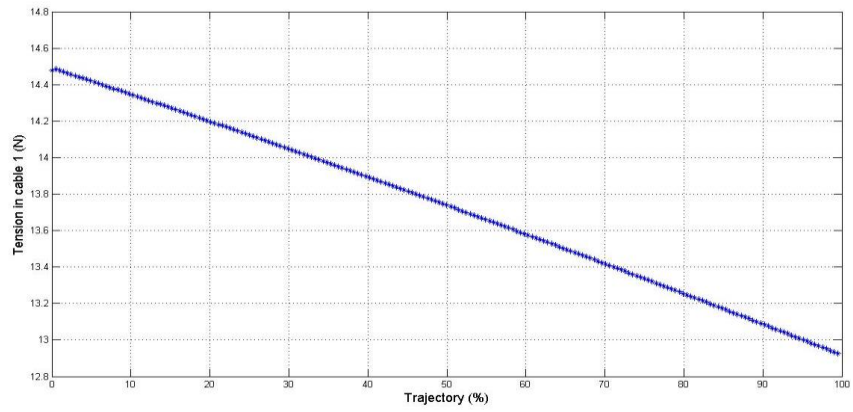
The design of the CPM with six cables is similar to the one shown in figure 3.1 in chapter 3. Its post failure trajectory is obtained in the previous section. In this section, the post failure variation in the cable tensions will be analyzed. The post failure tension in the cables can be determined from Eq. (5.4).

##### Example 1: Post failure tensions in case of cable 2 failure

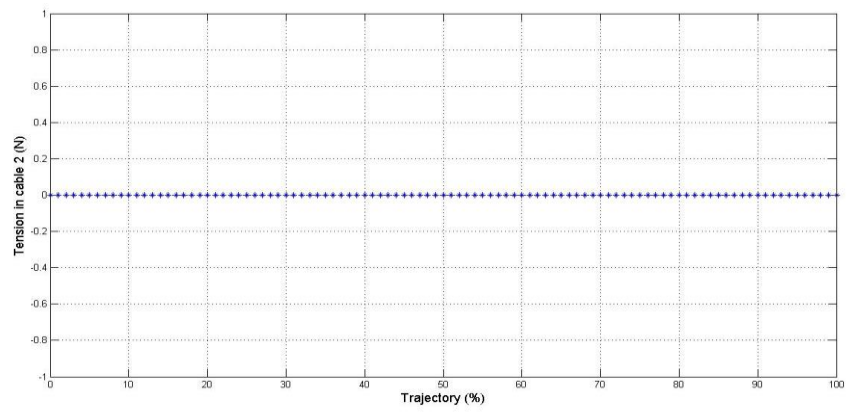
In case of cable 2 breakage, the tensions in cable 2 will instantly become zero while tensions in the remaining cables also varies instantly. The equation to calculate the post failure tensions for the case of cable 2 breakage is given by:

$$\begin{bmatrix} \tau_1 \\ \tau_3 \\ \tau_4 \\ \tau_5 \\ \tau_6 \end{bmatrix} = \left( \begin{bmatrix} \hat{l}_{1x} \hat{l}_{1y} \hat{l}_{1z} (r_{1x} \times \hat{l}_{1x}) (r_{1y} \times \hat{l}_{1y}) (r_{1z} \times \hat{l}_{1z}) \\ \hat{l}_{3x} \hat{l}_{3y} \hat{l}_{3z} (r_{3x} \times \hat{l}_{3x}) (r_{3y} \times \hat{l}_{3y}) (r_{3z} \times \hat{l}_{3z}) \\ \hat{l}_{4x} \hat{l}_{4y} \hat{l}_{4z} (r_{4x} \times \hat{l}_{4x}) (r_{4y} \times \hat{l}_{4y}) (r_{4z} \times \hat{l}_{4z}) \\ \hat{l}_{5x} \hat{l}_{5y} \hat{l}_{5z} (r_{5x} \times \hat{l}_{5x}) (r_{5y} \times \hat{l}_{5y}) (r_{5z} \times \hat{l}_{5z}) \\ \hat{l}_{6x} \hat{l}_{6y} \hat{l}_{6z} (r_{6x} \times \hat{l}_{6x}) (r_{6y} \times \hat{l}_{6y}) (r_{6z} \times \hat{l}_{6z}) \end{bmatrix}^T \right)^+ \begin{bmatrix} F_x \\ F_y \\ F_z \\ M_x \\ M_y \\ M_z \end{bmatrix} \quad (5.9)$$

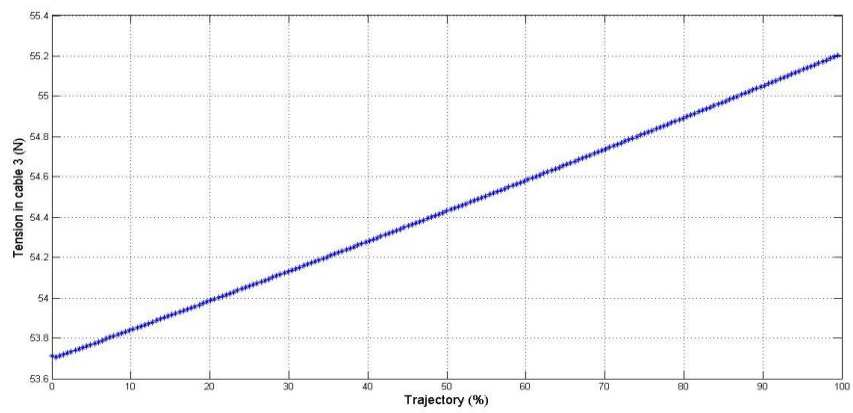
The variation in cable tensions is shown in figure 5.3.



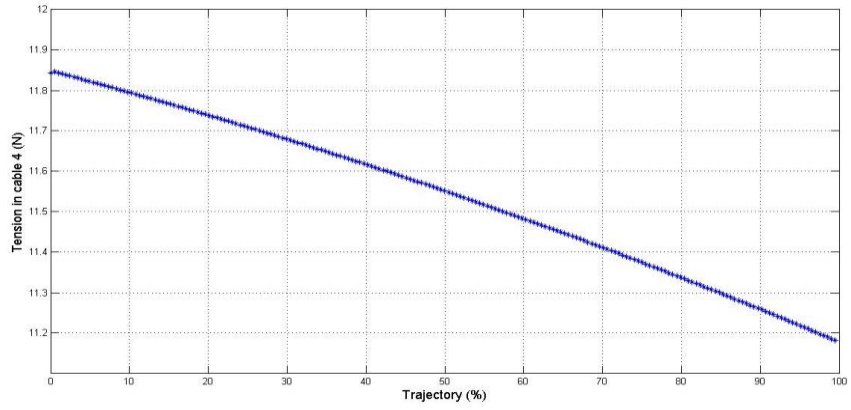
**(a) Tension variation in cable 1**



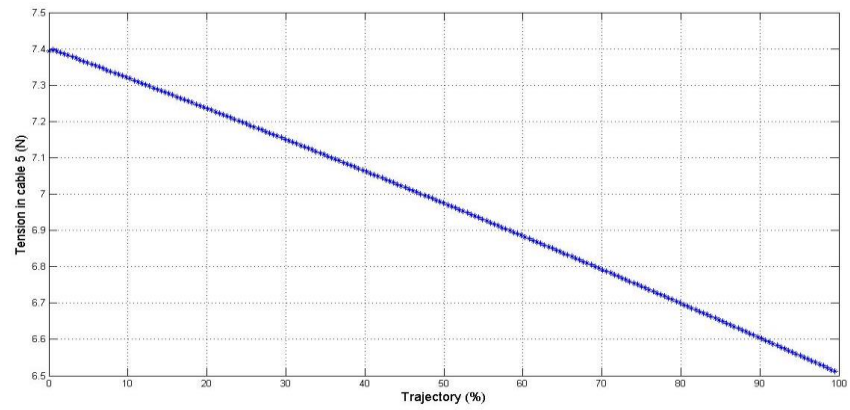
**(b) Tension variation in cable 2**



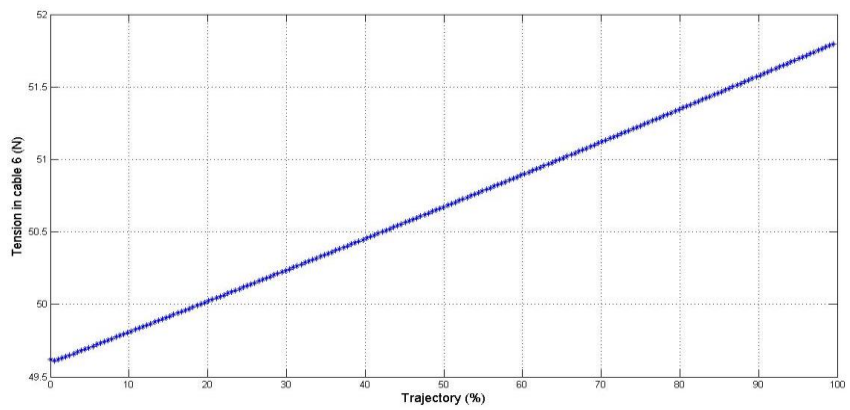
**(c) Tension variation in cable 3**



(d) Tension variation in cable 4



(e) Tension variation in cable 5



(f) Tension variation in cable 6

**Figure 5.4 (a)-(f) Tension variations along the trajectory of the example manipulator shown in figure 3.1 in case of cable no. 2 breakage.**

The tension variation in all of the cables along the trajectory can be observed in figure 5.4. When cable 2 breaks, there is an increase in the tension in cable no. 3 & 6 whereas tension in cable 1, 4 & 5 decreases along the manipulator's trajectory. The tensions exactly after failure are  $\tau = [14.4 \ 0 \ 53.7 \ 11.9 \ 7.4 \ 49.5]$ . As the manipulator moves along the trajectory to settle to its new static equilibrium pose shown in figure 5.2, tension in the cables continue to vary. This is due to an unbalanced force that is generated after the failure occurs. The magnitude of the unbalanced force continues to decrease till the manipulator reaches its final equilibrium position. At that position, the magnitude of the unbalanced force becomes zero and Eq. (5.9) is satisfied. The tension values at the new static equilibrium position are  $\tau = [12.9 \ 0 \ 55.2 \ 11.2 \ 6.5 \ 51.8]$  N.

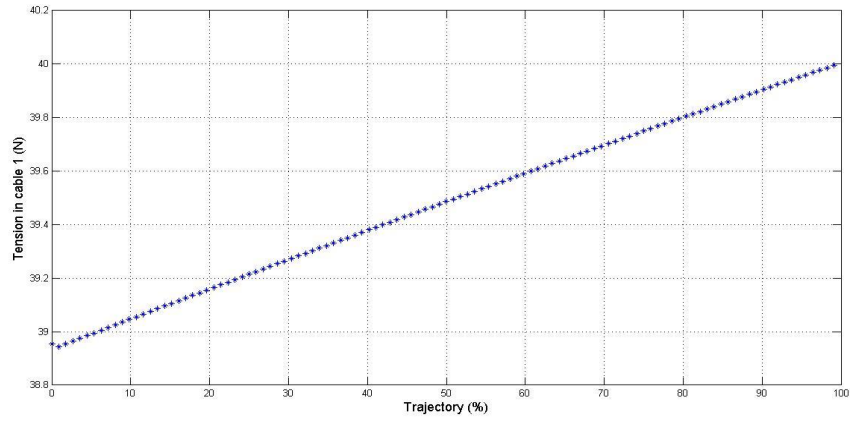
Knowledge of the post failure tension in the cables is useful for the safe operation of the CPM. In the above example, the maximum tension occurs in cable 3 which is  $\tau = 55.2$  N.

### Example 2: Post failure tensions in case of cable 6 failure

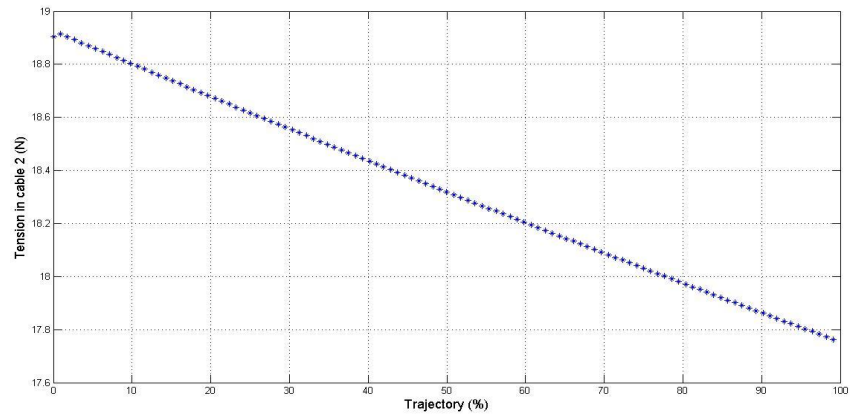
For the case of cable 6 breakage, the tension in cable 6 will instantly become zero while tensions in the remaining cables will vary. The equation to calculate the post failure tensions is obtained from Eq. (5.4) and is written for the case of cable no. 6 breakage in Eq. (5.10) and simulations for the cable tension variation is shown in figure 5.5.

$$\begin{bmatrix} \tau_1 \\ \tau_2 \\ \tau_3 \\ \tau_4 \\ \tau_5 \end{bmatrix} = \left( \begin{bmatrix} \hat{l}_{1x} \hat{l}_{1y} \hat{l}_{1z} (r_{1x} \times \hat{l}_{1x}) (r_{1y} \times \hat{l}_{1y}) (r_{1z} \times \hat{l}_{1z}) \\ \hat{l}_{2x} \hat{l}_{2y} \hat{l}_{2z} (r_{2x} \times \hat{l}_{2x}) (r_{2y} \times \hat{l}_{2y}) (r_{2z} \times \hat{l}_{2z}) \\ \hat{l}_{3x} \hat{l}_{3y} \hat{l}_{3z} (r_{3x} \times \hat{l}_{3x}) (r_{3y} \times \hat{l}_{3y}) (r_{3z} \times \hat{l}_{3z}) \\ \hat{l}_{4x} \hat{l}_{4y} \hat{l}_{4z} (r_{4x} \times \hat{l}_{4x}) (r_{4y} \times \hat{l}_{4y}) (r_{4z} \times \hat{l}_{4z}) \\ \hat{l}_{5x} \hat{l}_{5y} \hat{l}_{5z} (r_{5x} \times \hat{l}_{5x}) (r_{5y} \times \hat{l}_{5y}) (r_{5z} \times \hat{l}_{5z}) \end{bmatrix}^T \right)^+ \begin{bmatrix} F_x \\ F_y \\ F_z \\ M_x \\ M_y \\ M_z \end{bmatrix} \quad (5.10)$$

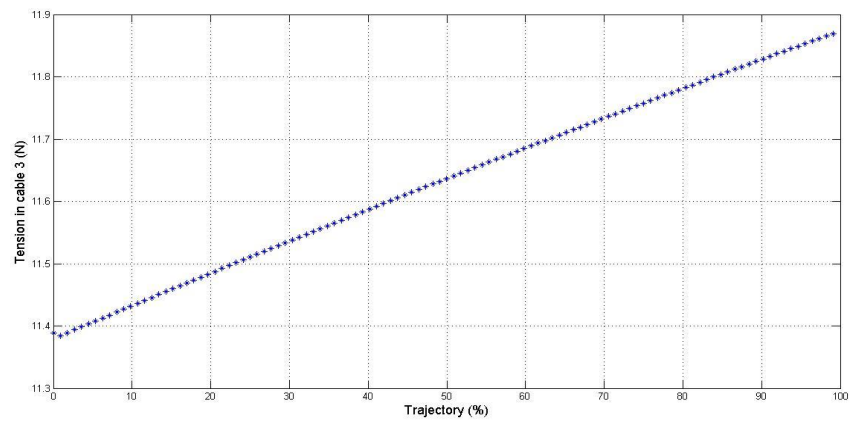




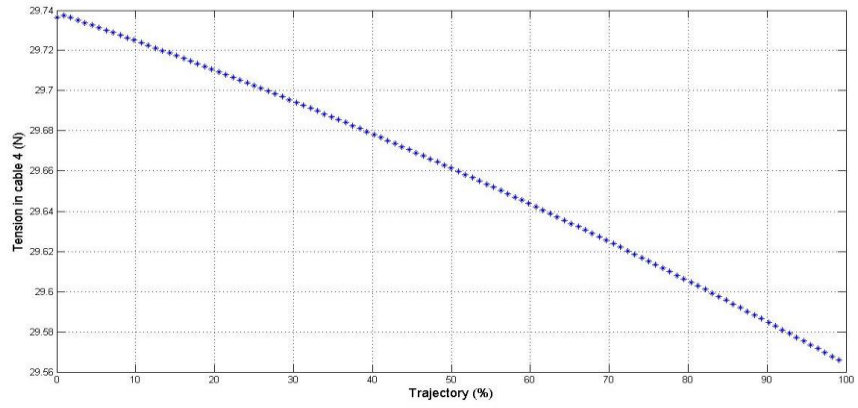
(a) Tension variation in cable 1



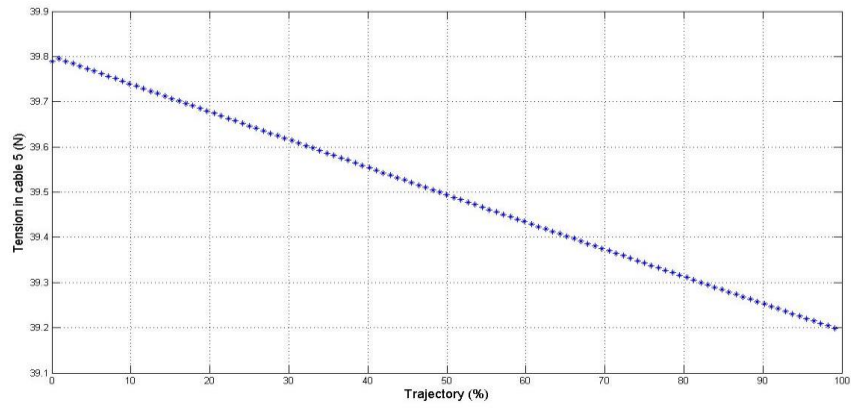
(b) Tension variation in cable 2



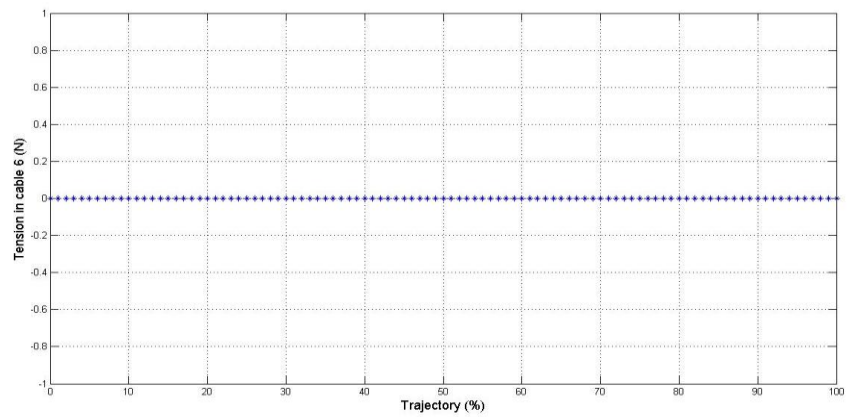
(c) Tension variation in cable 3



(d) Tension variation in cable 4



(e) Tension variation in cable 5



(f) Tension variation in cable 6

**Figure 5.5 (a)-(f) Tension variations along the trajectory of the example manipulator shown in figure 3.1 in case of cable no. 6 breakage.**

Figure 5.5 shows the variation of tension in the cables after the failure of cable no. 6. The tensions are determined during the trajectory of the manipulator reported in figure 5.3 using Eq. (5.10). As the manipulator moves along the trajectory, tensions in cable 1 & 3 increases while there is a decrease in tension values in cables 2, 4 & 5. The tension values at the instant of failure are  $\boldsymbol{\tau} = [38.9 \ 18.9 \ 11.4 \ 29.7 \ 39.8 \ 0]$  (N). They then vary along the path the manipulator follows due to the unbalanced force causing uncontrollable motion till the manipulator reaches the static equilibrium pose where the tension values obtained are  $\boldsymbol{\tau} = [39.9 \ 17.8 \ 11.9 \ 29.6 \ 39.2 \ 0]$  (N).

### 5.3.2 Post failure tensions in CPM with eight cables

In this section, the post failure tension in the cables will be analyzed for the CPM design having eight cables. The design is similar to the one shown in figure 4.1. The manipulator is operating inside sea having rectangular shape connected to eight ships on sea surface via cables. The manipulator is at pose  $\mathbf{p} = [0 \ 0 \ 0]$  (meters) and  $\boldsymbol{\theta} = [0 \ 0 \ 0]$  (degrees), when a failure occurs in one of the cables. The post failure tension values are obtained from Eq. (5.4) which can be written for eight cables as:

$$\begin{bmatrix} \tau_1 \\ \tau_2 \\ \tau_3 \\ \tau_4 \\ \tau_5 \\ \tau_6 \\ \tau_7 \\ \tau_8 \end{bmatrix} = \left( \begin{bmatrix} \hat{l}_{1x} \hat{l}_{1y} \hat{l}_{1z} (r_{1x} \times \hat{l}_{1x}) (r_{1y} \times \hat{l}_{1y}) (r_{1z} \times \hat{l}_{1z}) \\ \hat{l}_{2x} \hat{l}_{2y} \hat{l}_{2z} (r_{2x} \times \hat{l}_{2x}) (r_{2y} \times \hat{l}_{2y}) (r_{2z} \times \hat{l}_{2z}) \\ \hat{l}_{3x} \hat{l}_{3y} \hat{l}_{3z} (r_{3x} \times \hat{l}_{3x}) (r_{3y} \times \hat{l}_{3y}) (r_{3z} \times \hat{l}_{3z}) \\ \hat{l}_{4x} \hat{l}_{4y} \hat{l}_{4z} (r_{4x} \times \hat{l}_{4x}) (r_{4y} \times \hat{l}_{4y}) (r_{4z} \times \hat{l}_{4z}) \\ \hat{l}_{5x} \hat{l}_{5y} \hat{l}_{5z} (r_{5x} \times \hat{l}_{5x}) (r_{5y} \times \hat{l}_{5y}) (r_{5z} \times \hat{l}_{5z}) \\ \hat{l}_{6x} \hat{l}_{6y} \hat{l}_{6z} (r_{6x} \times \hat{l}_{6x}) (r_{6y} \times \hat{l}_{6y}) (r_{6z} \times \hat{l}_{6z}) \\ \hat{l}_{7x} \hat{l}_{7y} \hat{l}_{7z} (r_{7x} \times \hat{l}_{7x}) (r_{7y} \times \hat{l}_{7y}) (r_{7z} \times \hat{l}_{7z}) \\ \hat{l}_{8x} \hat{l}_{8y} \hat{l}_{8z} (r_{8x} \times \hat{l}_{8x}) (r_{8y} \times \hat{l}_{8y}) (r_{8z} \times \hat{l}_{8z}) \end{bmatrix}^T \right)^+ \begin{bmatrix} F_x \\ F_y \\ F_z \\ M_x \\ M_y \\ M_z \end{bmatrix} \quad (5.11)$$

In order to calculate the post failure tensions when cable  $i$  fails, the corresponding  $i$ th row of the Jacobian matrix  $\mathbf{J}_a$  is eliminated. Table 5.1 reports the tension values obtained with the corresponding failed cable.

**Table 5.1 Post Failure Tension values in the cables using Eq. (5.11).**

Failed Cable	Tension in cable 1 (N)	Tension in cable 2 (N)	Tension in cable 3 (N)	Tension in cable 4 (N)	Tension in cable 5 (N)	Tension in cable 6 (N)	Tension in cable 7 (N)	Tension in cable 8 (N)
Cable 1	0	35.66	31.83	0.12	5.16	29.59	34.84	0.83
Cable 2	-14.14	0	51.86	-15.92	70.93	-45.81	35.61	55.52
Cable 3	27.91	36.68	0	9.72	33.51	19.53	7.43	3.5
Cable 4	6.14	28.86	25.61	0	27.4	11.3	26.19	12.64
Cable 5	-0.77	37.55	32.5	0.47	0	34.27	36.31	-2.31
Cable 6	12.6	25.18	18.68	0.98	42.89	0	18.39	19.54
Cable 7	32.45	28.88	-4.29	8.75	56.26	-0.34	0	16.75
Cable 8	16.62	37.82	12.71	6.33	18.49	27.16	19.1	0

Results of post failure tension values are listed in table 5.1. The tension values before failure was given by  $\boldsymbol{\tau} = [13.5 \ 32.3 \ 16.81 \ 3.57 \ 27.5 \ 16.1 \ 20.1 \ 8.2]$  (N). Table 5.1 shows the tension values after failure of the respective cable. When cable no. 1 fails, its tension goes instantly to zero whereas there is an increase or decrease in the tension value in the remaining cables. When cable no. 2 breaks, apart from having an increase/decrease in the tension values of other cables, some of the cables become slack i.e. the tension becomes negative in those cables. This shows that the failure of cable no. 2 brings failure in some other cables as well since they become slack after failure. Similar trend is reported when cable no. 5 or cable no. 7 breaks. With the breakage of these

cables, some of the other cables become slack indicating the cable is failed since cables can only pull. This trend of negative tensions in some other cables after failure of one can be avoided by repositioning the ships which is performed in section 5.4.2. For the remaining cables failure, similar trend of either increase or decrease in tension values is reported as in the case of cable no. 1 failure.

### 5.3.3 Post failure tensions in CPM with ten cables

In this section, the post failure tension in the cables will be determined for the CPM design having ten cables. The design is shown in figure 4.5. The manipulator is operating under sea having rectangular shape connected to ten ships on sea surface via cables. The manipulator is at pose  $\mathbf{p} = [0 \ 0 \ 0]$  (meters) and  $\boldsymbol{\theta} = [0 \ 0 \ 0]$  (degrees), when one of the cables breaks. The post failure tension values can be obtained from Eq. (5.4) which is written for ten cables as:

$$\begin{bmatrix} \tau_1 \\ \tau_2 \\ \tau_3 \\ \tau_4 \\ \tau_5 \\ \tau_6 \\ \tau_7 \\ \tau_8 \\ \tau_9 \\ \tau_{10} \end{bmatrix} = \begin{bmatrix} \hat{l}_{1x} & \hat{l}_{1y} & \hat{l}_{1z} & (r_{1x} \times \hat{l}_{1x}) & (r_{1y} \times \hat{l}_{1y}) & (r_{1z} \times \hat{l}_{1z}) \\ \hat{l}_{2x} & \hat{l}_{2y} & \hat{l}_{2z} & (r_{2x} \times \hat{l}_{2x}) & (r_{2y} \times \hat{l}_{2y}) & (r_{2z} \times \hat{l}_{2z}) \\ \hat{l}_{3x} & \hat{l}_{3y} & \hat{l}_{3z} & (r_{3x} \times \hat{l}_{3x}) & (r_{3y} \times \hat{l}_{3y}) & (r_{3z} \times \hat{l}_{3z}) \\ \hat{l}_{4x} & \hat{l}_{4y} & \hat{l}_{4z} & (r_{4x} \times \hat{l}_{4x}) & (r_{4y} \times \hat{l}_{4y}) & (r_{4z} \times \hat{l}_{4z}) \\ \hat{l}_{5x} & \hat{l}_{5y} & \hat{l}_{5z} & (r_{5x} \times \hat{l}_{5x}) & (r_{5y} \times \hat{l}_{5y}) & (r_{5z} \times \hat{l}_{5z}) \\ \hat{l}_{6x} & \hat{l}_{6y} & \hat{l}_{6z} & (r_{6x} \times \hat{l}_{6x}) & (r_{6y} \times \hat{l}_{6y}) & (r_{6z} \times \hat{l}_{6z}) \\ \hat{l}_{7x} & \hat{l}_{7y} & \hat{l}_{7z} & (r_{7x} \times \hat{l}_{7x}) & (r_{7y} \times \hat{l}_{7y}) & (r_{7z} \times \hat{l}_{7z}) \\ \hat{l}_{8x} & \hat{l}_{8y} & \hat{l}_{8z} & (r_{8x} \times \hat{l}_{8x}) & (r_{8y} \times \hat{l}_{8y}) & (r_{8z} \times \hat{l}_{8z}) \\ \hat{l}_{9x} & \hat{l}_{9y} & \hat{l}_{9z} & (r_{9x} \times \hat{l}_{9x}) & (r_{9y} \times \hat{l}_{9y}) & (r_{9z} \times \hat{l}_{9z}) \\ \hat{l}_{10x} & \hat{l}_{10y} & \hat{l}_{10z} & (r_{10x} \times \hat{l}_{10x}) & (r_{10y} \times \hat{l}_{10y}) & (r_{10z} \times \hat{l}_{10z}) \end{bmatrix}^T + \begin{bmatrix} F_x \\ F_y \\ F_z \\ M_x \\ M_y \\ M_z \end{bmatrix} \quad (5.12)$$

In order to calculate the post failure tensions when cable  $i$  fails, the corresponding  $i$ th row of the Jacobian matrix  $\mathbf{J}_a$  is eliminated. Table 5.2 reports the tension values obtained with the corresponding failed cable.

**Table 5.2 Post Failure Tension values in the cables using Eq. (5.12).**

Failed Cable	Tension in cable 1 (N)	Tension in cable 2 (N)	Tension in cable 3 (N)	Tension in cable 4 (N)	Tension in cable 5 (N)	Tension in cable 6 (N)	Tension in cable 7 (N)	Tension in cable 8 (N)	Tension in cable 9 (N)	Tension in cable 10 (N)
Cable 1	0	13.53	9.08	4.31	42.05	3.55	10.02	9.16	7.65	38.68
Cable 2	2.08	0	14.6	7.44	47.78	0.99	0.99	9.18	17.37	37.68
Cable 3	0.99	16.22	0	9.79	39.79	6.09	11.25	4.16	6.38	43.31
Cable 4	0.99	14.06	11.48	0	43.21	3.68	11.38	10.12	5.43	37.71
Cable 5	-34.01	53.24	-11.25	35.28	0	21.30	-0.74	37.38	-8.89	45.32
Cable 6	0.99	12.21	10.23	3.45	44.20	0	13.13	6.24	10.56	36.97
Cable 7	0.99	7.31	9.93	6.48	42.79	8.42	0	12.91	7.76	41.56
Cable 8	1.83	14.99	0.99	9.49	42.18	0.99	15.81	0	10.68	40.97
Cable 9	0.99	17.7	6.82	0.99	40.27	8.88	9.96	11.14	0	41.34
Cable 10	-22.25	-2.77	74.38	-16.01	48.11	-22.99	-2.42	50.68	31.33	0

Table 5.2 summarizes the post failure tension values in the remaining cables when one of the cables fails. The initial tension in the cables before failure of any cable is given by  $\tau = [0.99 \ 12.9 \ 8.8 \ 3.7 \ 42.8 \ 3.9 \ 10.1 \ 8.4 \ 7.4 \ 39.1]$  (N). The results of table 5.2 show a similar trend to the results in table 5.1 for CPM having eight cables. When a failure occurs in anyone of the cables, the tension values in the remaining cables either increase or decrease. With the breakage of cable no. 5 or cable no. 10, apart from an increase/decrease tension values in the remaining cables, some of the cables become slack i.e. the tension values become negative after failure as observed previously in case of CPM having eight cables. This indicates the failure of those cables as well whose

tension values are negative. As discussed previously, this trend can be avoided by repositioning the ships and will be performed in section 5.4.2 for CPM having ten cables.

## **5.4 Layout Optimization**

It was observed that by repositioning the moving ships on sea surface, the performance of the CPM can be optimized. In this section, ship position optimization will be carried out. The optimized positions will be determined based on the following criteria.

- Minimizing the maximum tension in the cables after failure.
- Minimizing the maximum tension in the cables such that the negative tensions after failure are avoided.

In the former case, optimized positions of the ships will be determined such that when one of the cables fails, the remaining cables can have minimum value of the maximum tension after failure. It was reported in the previous section that with the failure of one cable, failure in other cables also takes place since values of tension in those cables went negative. In the latter case, ship position optimization is conducted such that none of the cables can have negative tension after one of the cables breaks. If negative value is obtained in any of the cables after failure, then that pose of the manipulator will not be included.

### **5.4.1 Minimizing post failure tension in the cables**

When one of the cables breaks in CPM's, there is an increase in the value of tension in the remaining cables. In this section, the optimized ship positions will be determined based on minimizing the maximum value of the tension after failure. This is

important for the stability of the ships supporting the moving platform via cables. The post failure tensions are calculated using Eq. (5.4) and the change in tension before and after failure is given by:

$$\Delta\tau = \tau_{new} - \tau_{old} \quad (5.13)$$

Where  $\tau_{new}$  is the tension in the cables after failure and is calculated by Eq. (5.4) and  $\tau_{old}$  is the tension in the cables before failure calculated by Eq. (3.18).

The value of  $\Delta\tau$  depends upon the pose of the manipulator and therefore the entire workspace will be considered when investigating the maximum tension in the cables. Moreover  $\Delta\tau$  will be calculated for each cable breakage. In order to determine the optimum positions of the ships, the maximum tension in the cables is calculated for each cable breakage at all poses of the manipulator at given positions of the ships. The function showing the maximum value of the tension at all poses of the manipulator is given by:

$$\Delta\tau_{max} = \max_k(\max_j(\Delta\tau_j^k)) \quad (5.14)$$

Where  $\max_j(\Delta\tau_j^k)$  is the maximum change in the value of the tension in the  $j$ th cable during the breakage of anyone of the cable calculated at the  $k$ th pose of the manipulator and  $\Delta\tau_{max}$  is the maximum change in the value of tension calculated globally in the entire workspace. When determining the optimum positions of the ships,  $\Delta\tau_{max}$  is calculated for each position of the ship. The optimum position of the ships will be the one in which  $\Delta\tau_{max}$  is minimum. The algorithm is illustrated in the flow chart in figure 5.6.



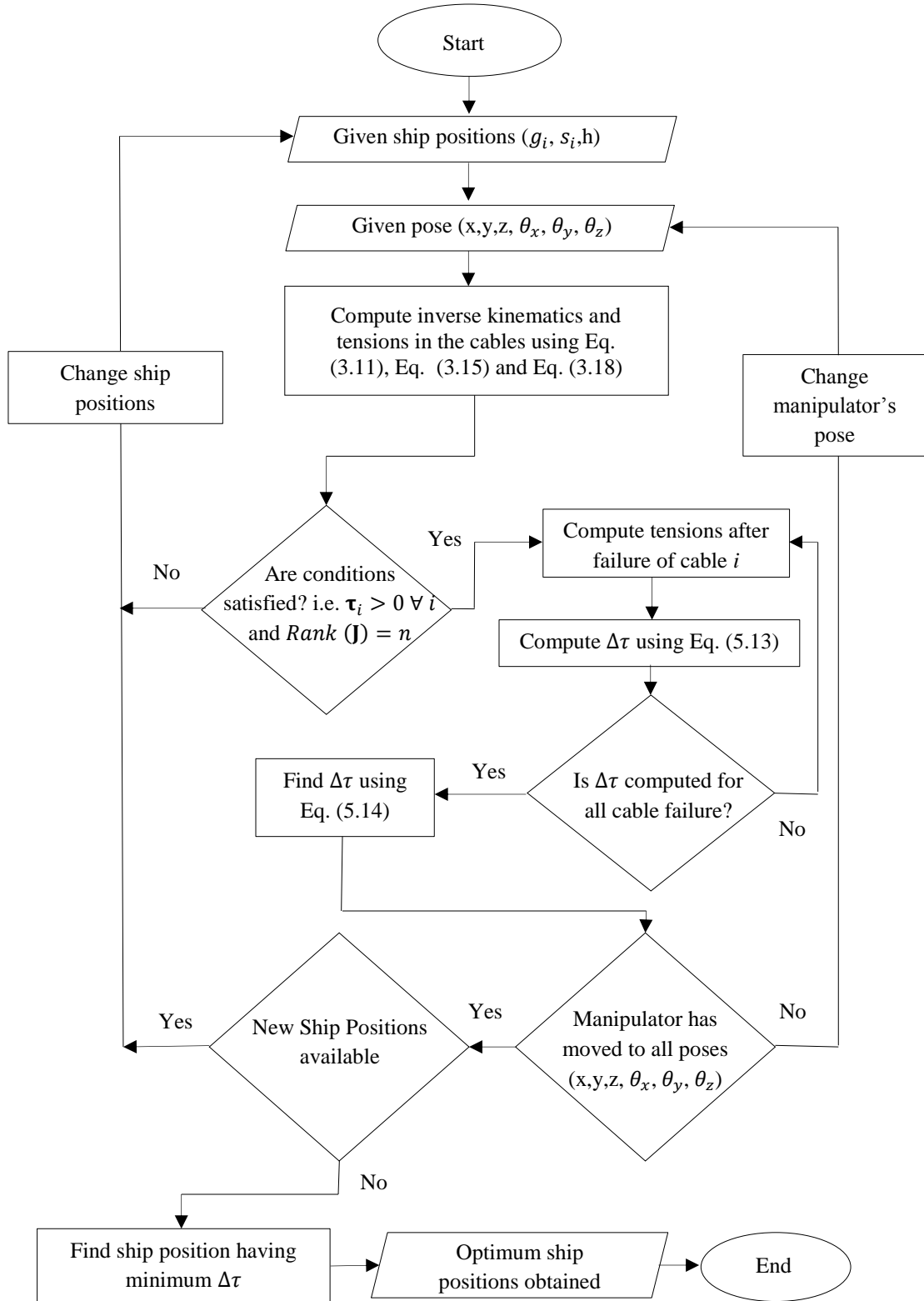


**Figure 5.6 A flow chart of the algorithm for computing the optimum ship positions based on minimizing the post failure change in the tensions.**

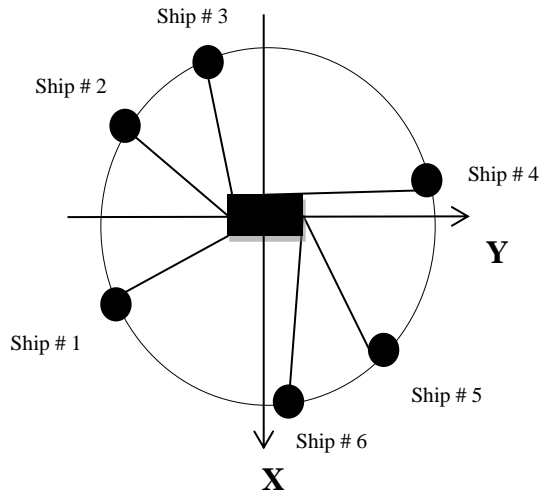
The algorithm in figure 5.6 computes the maximum change in the tension values when a failure occurs in one of the cables for a given position set of the ships. For a given ship position and manipulator's pose, it computes the tension in the cables before failure using Eq. (3.11), Eq. (3.15) and Eq. (3.18) and applying Dykstra's algorithm using Eq. (4.8) for the case of eight and ten cables. If the required conditions are satisfied i.e.  $\tau_i > 0 \forall i$  and  $Rank(\mathbf{J}) = n$ , it computes the tension in the cables after failure using Eq. (5.4). It then calculates the post failure tensions for every cable breakage case. The algorithm then computes the maximum value of  $\Delta\tau$  at a given pose of the manipulator. The manipulator is then moved to another position and same procedure is repeated such that the maximum change in the tension value after failure is calculated at all poses of the manipulator. The same procedure is repeated for each combination of the ship position till it computes the maximum change in tension value for all ship positions. By determining the minimum value of the maximum change in tension value, optimum positions of the ships will be determined. The ship position optimization is illustrated for CPM's with six, eight and ten cables.

#### ***5.4.1.1 Ship position optimization for CPM having six cables***

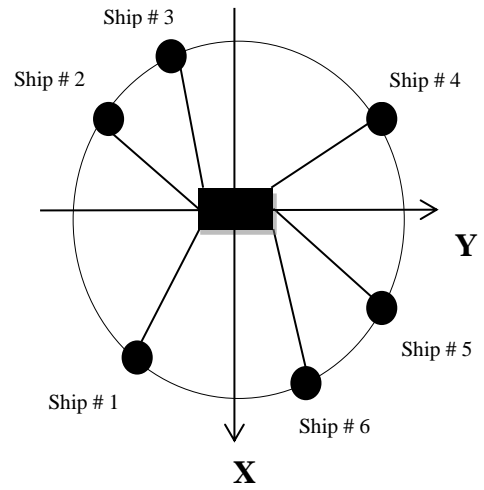
The procedure described above for determining the optimum ship positions is implemented in CPM having six cables. The CPM is depicted in figure 3.1. The manipulator is rectangular in shape which moves under sea connected to six ships on sea surface via cables. The algorithm shown in figure 5.6 is implemented for this CPM having six cables to determine the optimum positions of the ships. The results obtained from the algorithm are summarized in table 5.3. It shows the maximum change in tension value with the respective ship position.

**Table 5.3 Computed  $\Delta\tau_{max}$  for CPM with six cables by using the proposed algorithm in figure 5.6.**

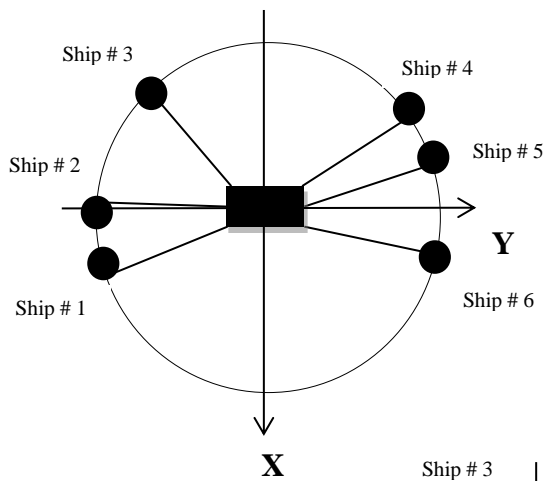
<b>Optimized Ship Position No.</b>	<b>1</b>	<b>2</b>	<b>3</b>	<b>4</b>	<b>5</b>
<b>(r- <math>\theta</math>) Position of Ship # 1 (m,deg)</b>	(50,205)	(50,235)	(50,185)	(50,265)	(50,235)
<b>(r- <math>\theta</math>) Position of Ship # 2 (m,deg)</b>	(50,150)	(50,150)	(50,180)	(50,180)	(50,180)
<b>(r- <math>\theta</math>) Position of Ship # 3 (m,deg)</b>	(50,115)	(50,115)	(50,145)	(50,175)	(50,115)
<b>(r- <math>\theta</math>) Position of Ship # 4 (m,deg)</b>	(50,5)	(50,25)	(50,25)	(50,55)	(50,5)
<b>(r- <math>\theta</math>) Position of Ship # 5 (m,deg)</b>	(50,300)	(50,330)	(50,20)	(50,20)	(50,330)
<b>(r- <math>\theta</math>) Position of Ship # 6 (m,deg)</b>	(50,275)	(50,295)	(50,355)	(50,355)	(50,295)
<b><math>\Delta\tau_{max}</math> (N)</b>	81	88	110	120	128



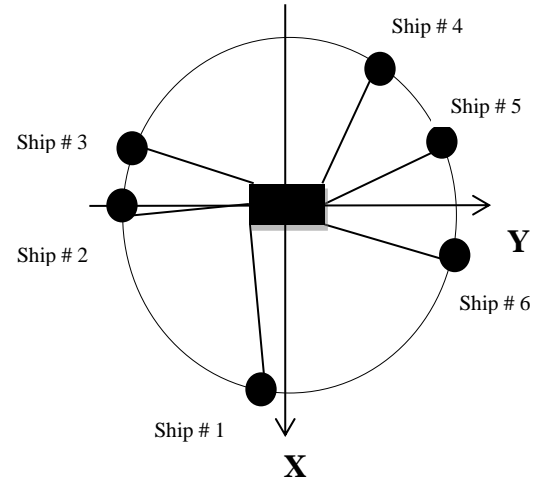
**(a) Position # 1**



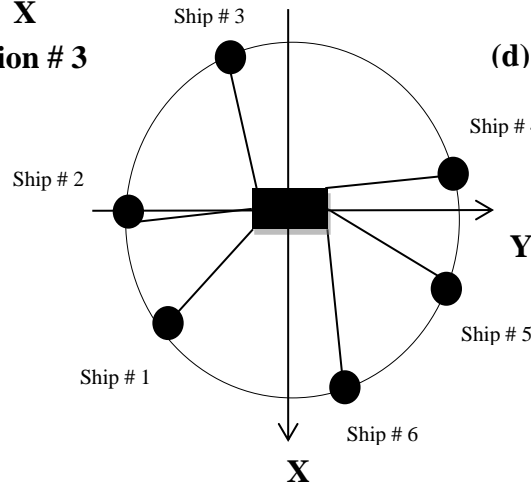
**(b) Position # 2**



**(c) Position # 3**



**(d) Position # 4**



**(e) Position # 5**

**Figure 5.7 Top five optimum ship positions based on minimizing post failure tensions in the CPM having six cables.**

The results in table 5.3 shows the maximum change in tension value after failure of one of the cables calculated at each pose in the workspace with the respective ship positions. The minimum value of  $\Delta\tau$  is 81 N. Therefore, the respective ship positions with the minimum value which is 81N are the optimum positions whose coordinates are given in table 5.3 under ship position 1. The pictorial representation for these ship positions are shown in figure 5.7(a). With these ship positions, the cable can have minimum value of the maximum tension. The value of  $\tau_{max}$  is slightly increased when the ship positions are moved to position set 2 as given in table 5.3 and shown pictorially in figure 5.7(b). Similarly, with ship position set 3, 4 and 5, the value of  $\tau_{max}$  is further increased to 110 N, 120 N and 128 N respectively. These ship positions are shown pictorially in figure 5.7 (c) to (e). Therefore, figure 5.7(a) to (e) depicts the top five optimum ship positions based on minimizing the maximum tension.

#### ***5.4.1.2 Ship position optimization for CPM having eight cables***

In this section, ship position optimization will be performed for CPM with eight cables. The CPM is shown in figure 4.1 in which eight ships are connected to the moving platform inside sea through eight cables. The platform is rectangular in shape and possesses 6DOF. The algorithm illustrated in figure 5.6 is used again to determine the optimum positions of the ships. Results obtained are shown in table 5.4 in which maximum change in tension value is shown against the respective ship positions.

**Table 5.4 Computed  $\Delta\tau_{max}$  for CPM with eight cables by using the proposed algorithm in figure 5.6.**

<b>Optimized Ship Position No.</b>	<b>1</b>	<b>2</b>	<b>3</b>	<b>4</b>	<b>5</b>
<b>(r- <math>\theta</math>) Position of Ship # 1 (m,deg)</b>	(50,235)	(50,260)	(50,235)	(50,235)	(50,235)
<b>(r- <math>\theta</math>) Position of Ship # 2 (m,deg)</b>	(50,200)	(50,215)	(50,185)	(50,185)	(50,215)
<b>(r- <math>\theta</math>) Position of Ship # 3 (m,deg)</b>	(50,175)	(50,175)	(50,100)	(50,145)	(50,175)
<b>(r- <math>\theta</math>) Position of Ship # 4 (m,deg)</b>	(50,100)	(50,100)	(50,100)	(50,100)	(50,100)
<b>(r- <math>\theta</math>) Position of Ship # 5 (m,deg)</b>	(50,80)	(50,80)	(50,80)	(50,80)	(50,80)
<b>(r- <math>\theta</math>) Position of Ship # 6 (m,deg)</b>	(50,25)	(50,40)	(50,25)	(50,40)	(50,40)
<b>(r- <math>\theta</math>) Position of Ship # 7 (m,deg)</b>	(50,340)	(50,340)	(50,340)	(50,355)	(50,320)
<b>(r- <math>\theta</math>) Position of Ship # 8 (m,deg)</b>	(50,305)	(50,305)	(50,305)	(50,280)	(50,305)
<b><math>\Delta\tau_{max}</math> (N)</b>	71	82	100	107	112

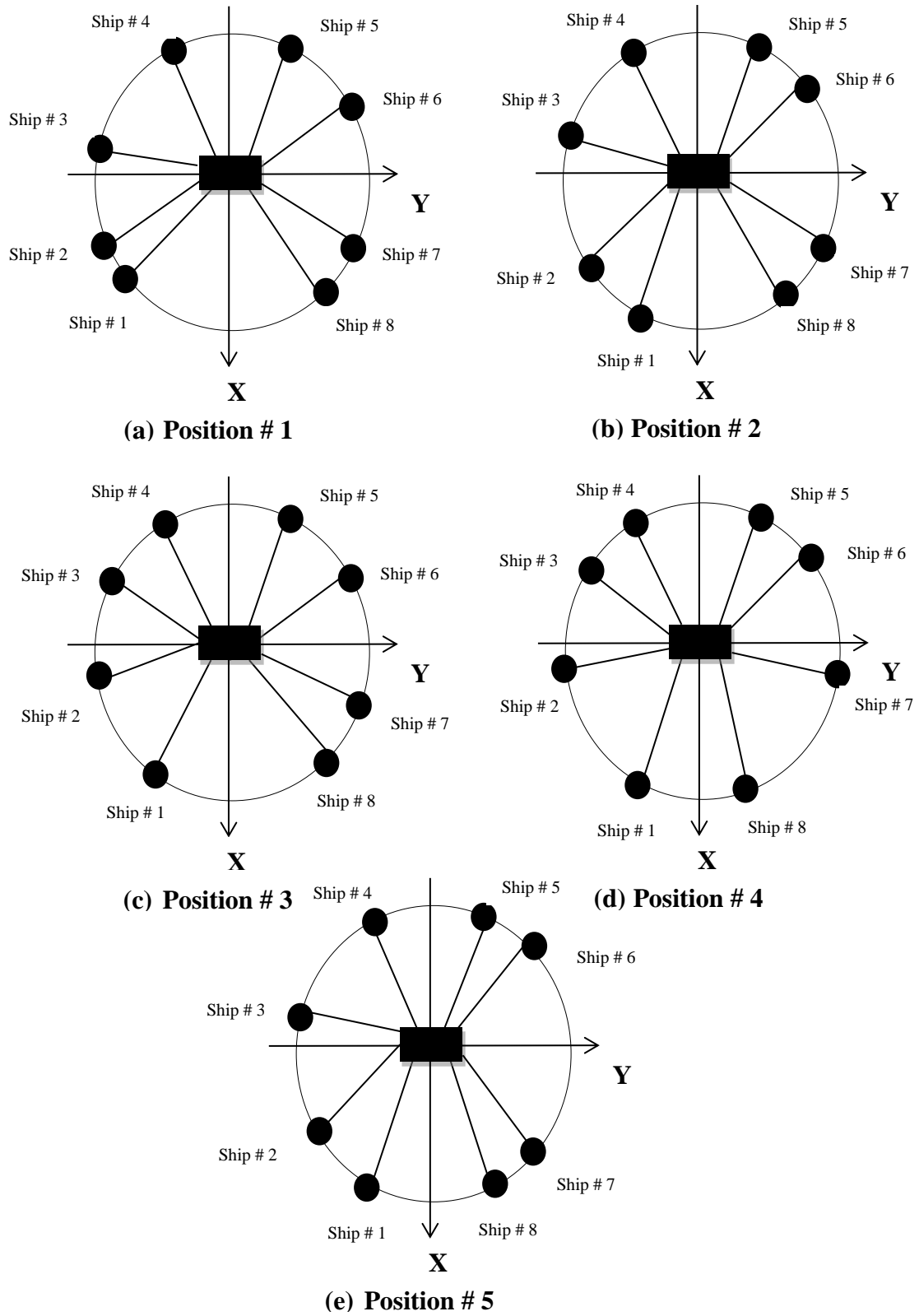


**Figure 5.8 Top five best positions of the ships based on minimizing post failure tensions in the CPM having eight cables.**

Table 5.4 summarizes the results obtained from algorithm and figure 5.8 is showing the schematic representation of table 5.4. The optimum position is shown in figure 5.8(a) having the maximum tension value equal to 71N. It shows the top view of the CPM in figure 4.1. By moving the ships to position no 2, the change in maximum tension is slightly increased to 82N. The pictorial representation for this ship position is shown in figure 5.8(b). Similarly, the tension value is further increased when ship positions are moved to position 3, 4 and 5 shown pictorially in figure 5.8(c), (d) and (e) respectively. With these ship positions, CPM having eight cables is optimized based on minimizing the maximum value of tension variation in the cables.

#### ***5.4.1.3 Ship position optimization for CPM having ten cables***

The algorithm described in figure 5.6 is now used to calculate the optimum positions of the ships for CPM for the case of ten cables. The schematic of the CPM having ten cables is shown in figure 4.2. The manipulator is capable of moving in 6 directions and therefore possesses 6DOF. The optimized ships positions are summarized in table 5.5 and shown pictorially in figure 5.9.



**Table 5.5 Computed  $\Delta\tau_{max}$  for CPM with ten cables by using the proposed algorithm in figure 5.6.**

<b>Optimized Ship Position No.</b>	<b>1</b>	<b>2</b>	<b>3</b>	<b>4</b>	<b>5</b>
<b>(r- <math>\theta</math>) Position of Ship # 1 (m,deg)</b>	(50,260)	(50,245)	(50,245)	(50,260)	(50,245)
<b>(r- <math>\theta</math>) Position of Ship # 2 (m,deg)</b>	(50,225)	(50,225)	(50,225)	(50,225)	(50,225)
<b>(r- <math>\theta</math>) Position of Ship # 3 (m,deg)</b>	(50,165)	(50,195)	(50,180)	(50,165)	(50,195)
<b>(r- <math>\theta</math>) Position of Ship # 4 (m,deg)</b>	(50,135)	(50,135)	(50,135)	(50,135)	(50,150)
<b>(r- <math>\theta</math>) Position of Ship # 5 (m,deg)</b>	(50,115)	(50,100)	(50,115)	(50,115)	(50,115)
<b>(r- <math>\theta</math>) Position of Ship # 6 (m,deg)</b>	(50,80)	(50,65)	(50,65)	(50,65)	(50,65)
<b>(r- <math>\theta</math>) Position of Ship # 7 (m,deg)</b>	(50,45)	(50,45)	(50,45)	(50,30)	(50,45)
<b>(r- <math>\theta</math>) Position of Ship # 8 (m,deg)</b>	(50,345)	(50,15)	(50,0)	(50,345)	(50,15)
<b>(r- <math>\theta</math>) Position of Ship # 9 (m,deg)</b>	(50,315)	(50,315)	(50,315)	(50,315)	(50,315)
<b>(r- <math>\theta</math>) Position of Ship # 10 (m,deg)</b>	(50,295)	(50,280)	(50,295)	(50,295)	(50,280)
<b><math>\Delta\tau_{max}</math> (N)</b>	65	67	70.7	82.5	82.3

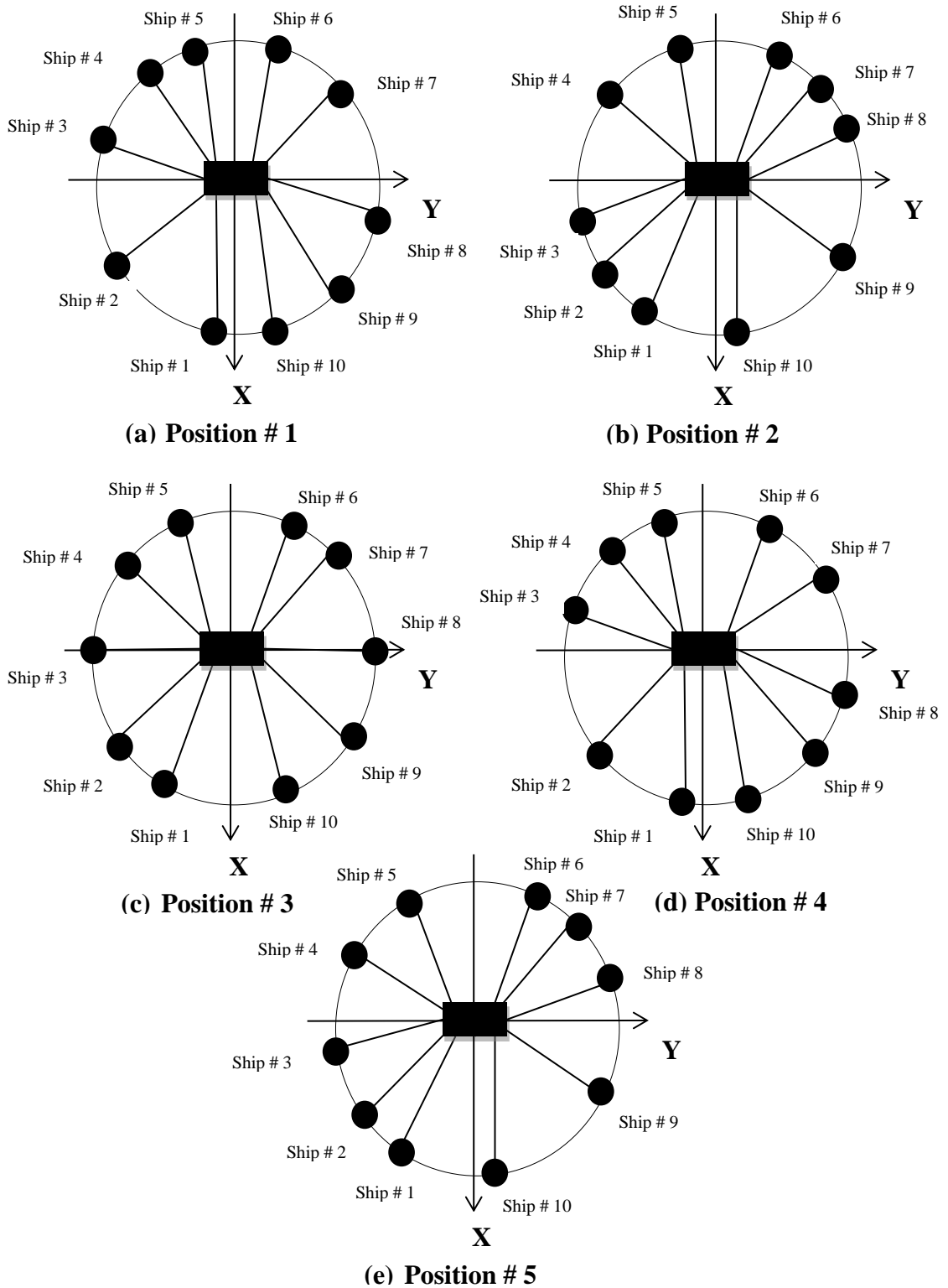


**Figure 5.9 Top five optimum ship positions based on minimizing post failure tensions in the CPM having ten cables.**

Table 5.5 shows the top five optimum positions of ships for the CPM having ten cables. These positions are illustrated in figure 5.9. The maximum change in tension for ship position set one is calculated as 65N, which is the minimum value of tension found among all other ship position sets. Therefore, it is the optimum position of the ships shown schematically in figure 5.9(a). With these positions of the ships, CPM will have the minimum value for the change in tension in the cables after failure. Change in tension will slightly increase after failure if ship positions are at position set two. The position is illustrated in figure 5.9(b). Similarly,  $\Delta\tau_{max}$  is further increased if ship positions are moved to position set three, four and five. These ship positions can be seen in figure 5.9(c), (d) and (e) respectively.

#### **5.4.2 Optimized fault tolerance ship positions**

Fault tolerance is a property that enables a system to continue operating properly in the event of a failure. As discussed in the previous sections, post failure tensions in some of the cable become negative. In order to avoid this situation, ship position optimization will be performed such that it will include only those position sets where the motion is controllable. The change in cable tensions is obtained from Eq. (5.13) and the maximum value of tension  $\Delta\tau_{max}$  is calculated at all poses of the manipulator from Eq. (5.14) such that the post failure tensions in all cables should be positive. This will ensure that there is no slack in the remaining cables in the event when one of the cables breaks. The algorithm to determine the optimized fault tolerance ship positions is reported in figure 5.10.

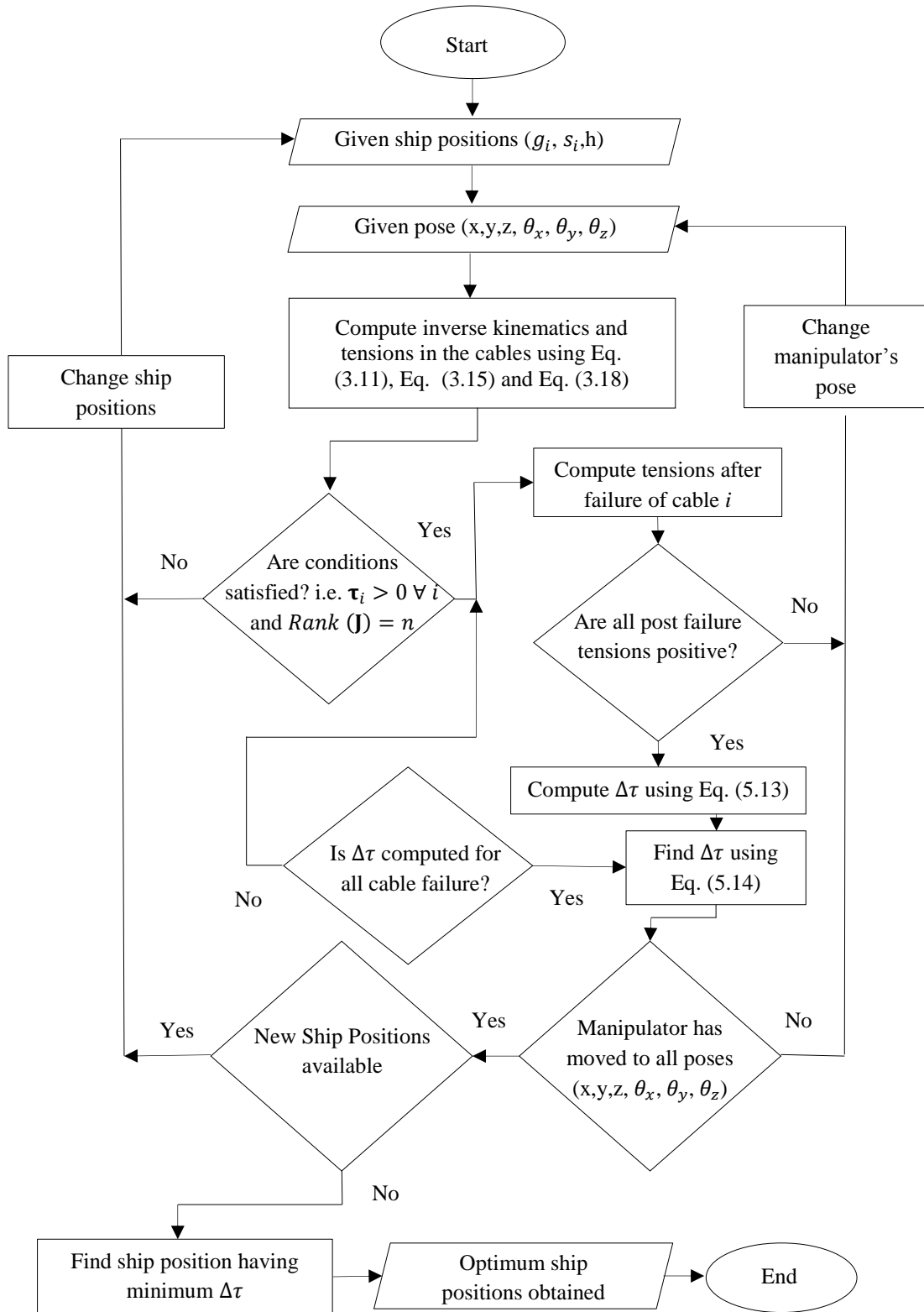


**Figure 5.10 A flow chart of the algorithm for computing the optimum ship positions based on minimizing the post failure tensions for fault tolerance design.**

The algorithm in figure 5.10 allows determining the optimum position set of the ships based on fault tolerance design criteria. For a given ship and manipulator's position, it calculates the cable tensions using Eq. (3.18). If the required conditions are satisfied i.e.  $\tau_i > 0 \forall i$  and  $Rank(\mathbf{J}) = n$ , it computes post failure tension in the cables using Eq. (5.4). If the post failure tensions are positive for every cable breakage case, the algorithm computes the maximum value of  $\Delta\tau$  at that pose of the manipulator otherwise if post failure tensions are negative at any cable breakage case, it changes the manipulator's pose and repeats the same procedure till the maximum change in value of tension is calculated at every pose of the manipulator satisfying the given conditions. The algorithm repeats itself for each combination of the ship position till it computes the maximum change in tension value for all ship positions. By determining the minimum value of the maximum change in tension value, optimized fault tolerance ship positions will be determined. The optimization is illustrated for CPM's with eight and ten cables.

#### ***5.4.2.1 Ship position optimization for CPM having eight cables***

The optimized ship positions for the layout design having eight cables will be determined in this section. The layout of the CPM is same as shown in figure 4.1 i.e. a rectangular moving platform that possesses 6DOF connected to eight ships via cables. The algorithm used to find the optimum ship positions is shown in figure 5.9. Results are reported table 5.6 and top five optimum ship positions are shown schematically in figure 5.11(a) to (e).

**Table 5.6 Computed  $\Delta\tau_{max}$  for CPM with eight cables by using the proposed algorithm in figure 5.10**

<b>Optimized Ship Position No.</b>	<b>1</b>	<b>2</b>	<b>3</b>	<b>4</b>	<b>5</b>
<b>(r- <math>\theta</math>) Position of Ship # 1 (m,deg)</b>	(50,260)	(50,260)	(50,260)	(50,260)	(50,260)
<b>(r- <math>\theta</math>) Position of Ship # 2 (m,deg)</b>	(50,215)	(50,215)	(50,200)	(50,215)	(50,200)
<b>(r- <math>\theta</math>) Position of Ship # 3 (m,deg)</b>	(50,175)	(50,175)	(50,145)	(50,160)	(50,145)
<b>(r- <math>\theta</math>) Position of Ship # 4 (m,deg)</b>	(50,100)	(50,125)	(50,100)	(50,100)	(50,100)
<b>(r- <math>\theta</math>) Position of Ship # 5 (m,deg)</b>	(50,80)	(50,55)	(50,80)	(50,55)	(50,80)
<b>(r- <math>\theta</math>) Position of Ship # 6 (m,deg)</b>	(50,25)	(50,25)	(50,40)	(50,25)	(50,25)
<b>(r- <math>\theta</math>) Position of Ship # 7 (m,deg)</b>	(50,355)	(50,340)	(50,355)	(50,340)	(50,355)
<b>(r- <math>\theta</math>) Position of Ship # 8 (m,deg)</b>	(50,305)	(50,305)	(50,305)	(50,305)	(50,305)
<b><math>\Delta\tau_{max}</math> (N)</b>	46.6	47.3	48.1	48.7	49.2

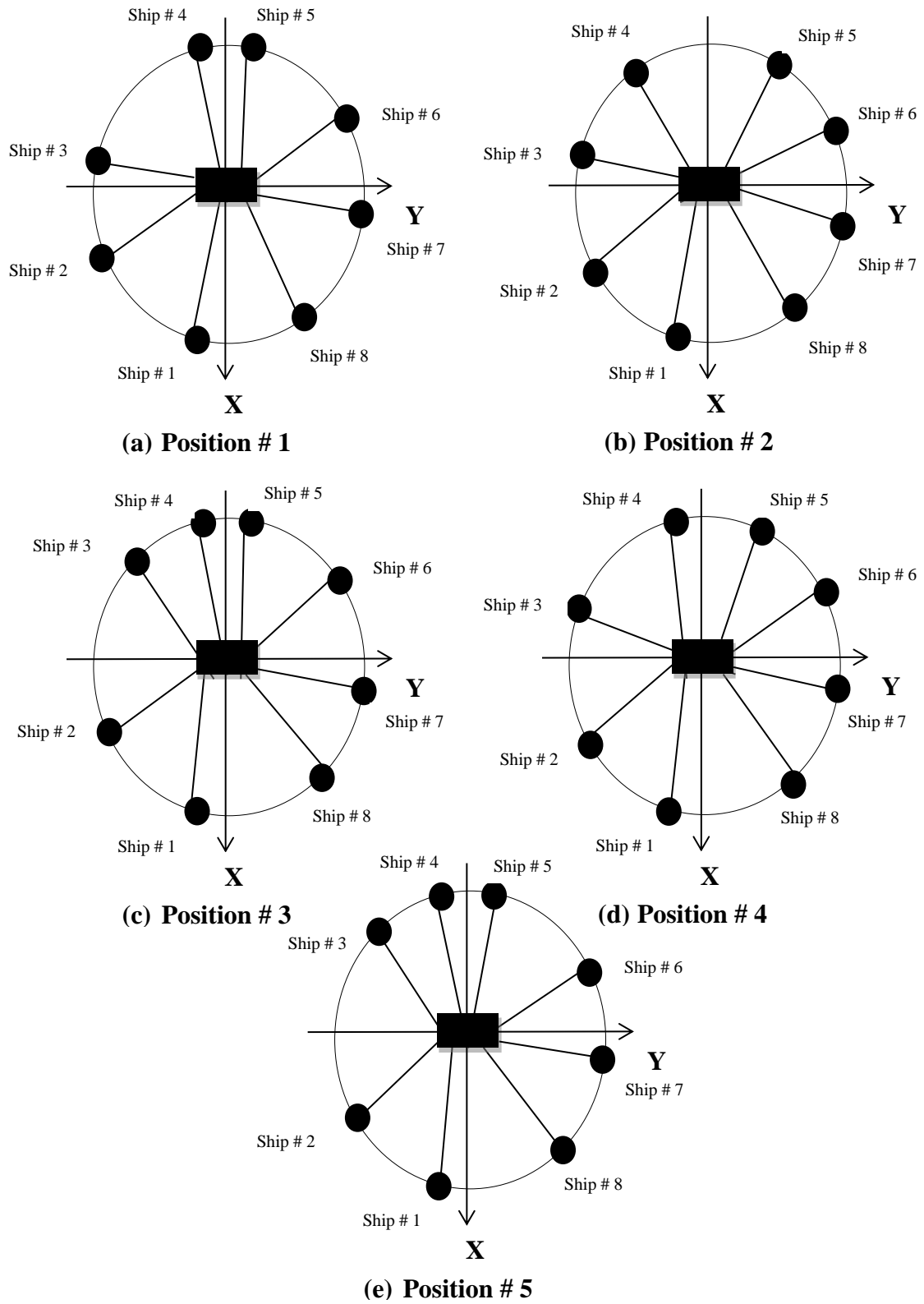


**Figure 5.11 Top five optimized fault tolerance positions of the ships based on minimizing post failure tensions in the CPM having eight cables.**

The results obtained from the algorithm shown in figure 5.10 are reported in table 5.6. Ship position set one is obtained as the most optimum position since the maximum change in cable tensions is found to be 46.6N. This value of cable tension is lower than the value in the previous case of ship optimization in figure 5.8(a) because the manipulator is not including the poses where tensions are negative. Similarly, for ship position set two in table 5.6,  $\Delta\tau_{max}$  is slightly increased to 47.3N. The position is shown in figure 5.11(b). The other three positions reported in table 5.6 are shown in figure 5.11(c), (d) and (e).

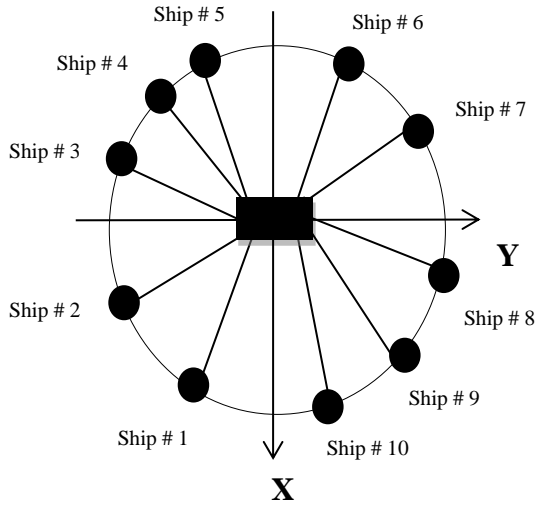
#### ***5.4.2.2 Ship position optimization for CPM having ten cables***

In this part, ship position optimization will be performed for CPM with ten cables using the algorithm reported in figure 5.10. With these sets of ship positions, post failure tensions will always remain positive. The CPM is shown in figure 4.2 and the results obtained are summarized in table 5.7 below.

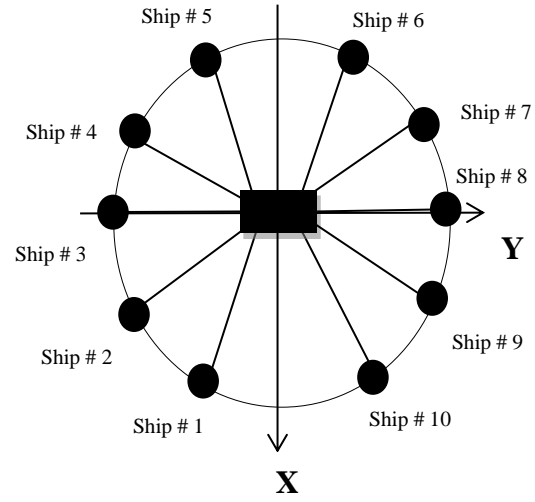


**Table 5.7 Computed  $\Delta\tau_{max}$  for CPM with ten cables by using the proposed algorithm in figure 5.10**

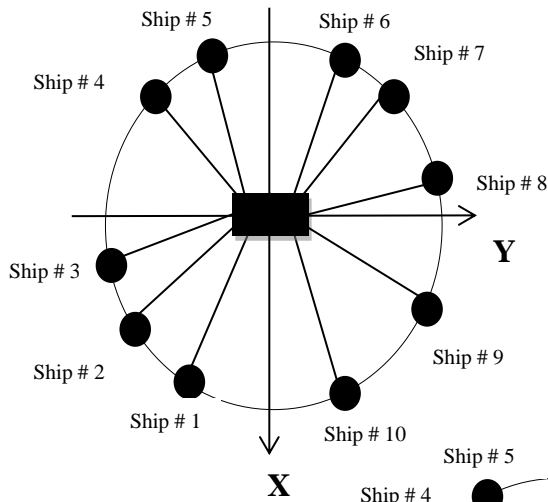
<b>Ship Position</b>	<b>1</b>	<b>2</b>	<b>3</b>	<b>4</b>	<b>5</b>
<b>(r- <math>\theta</math>) Position of Ship # 1 (m,deg)</b>	(50,245)	(50,245)	(50,245)	(50,245)	(50,260)
<b>(r- <math>\theta</math>) Position of Ship # 2 (m,deg)</b>	(50,210)	(50,210)	(50,225)	(50,225)	(50,225)
<b>(r- <math>\theta</math>) Position of Ship # 3 (m,deg)</b>	(50,165)	(50,180)	(50,195)	(50,180)	(50,180)
<b>(r- <math>\theta</math>) Position of Ship # 4 (m,deg)</b>	(50,135)	(50,150)	(50,135)	(50,135)	(50,135)
<b>(r- <math>\theta</math>) Position of Ship # 5 (m,deg)</b>	(50,115)	(50,115)	(50,115)	(50,100)	(50,115)
<b>(r- <math>\theta</math>) Position of Ship # 6 (m,deg)</b>	(50,65)	(50,65)	(50,65)	(50,65)	(50,65)
<b>(r- <math>\theta</math>) Position of Ship # 7 (m,deg)</b>	(50,30)	(50,30)	(50,45)	(50,45)	(50,30)
<b>(r- <math>\theta</math>) Position of Ship # 8 (m,deg)</b>	(50,345)	(50,0)	(50,15)	(50,0)	(50,0)
<b>(r- <math>\theta</math>) Position of Ship # 9 (m,deg)</b>	(50,315)	(50,330)	(50,315)	(50,330)	(50,315)
<b>(r- <math>\theta</math>) Position of Ship # 10 (m,deg)</b>	(50,295)	(50,295)	(50,295)	(50,295)	(50,295)
<b><math>\Delta\tau_{max}</math> (N)</b>	34.3	35.6	36.2	36.6	36.8



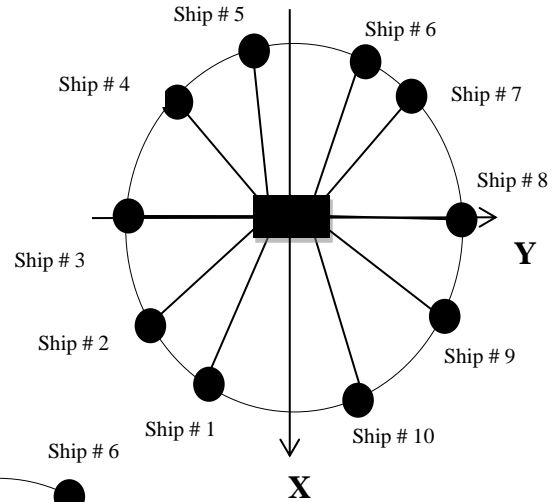
**(a) Position # 1**



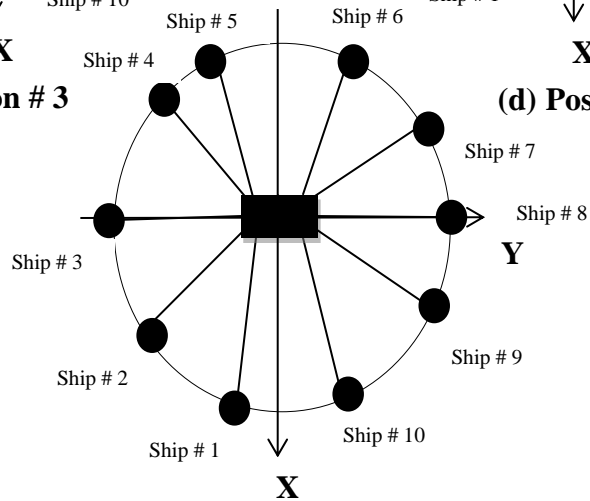
**(b) Position # 2**



**(c) Position # 3**



**(d) Position # 4**



**(e) Position # 5**

**Figure 5.12 Top five optimized fault tolerance positions of the ships based on minimizing post failure tensions in the CPM having ten cables.**

The ship positions reported in table 5.7 are shown schematically in figure 5.12. The maximum change in tension for ship position set one is calculated as 34.3N, which is the minimum value of tension found among all other ship position sets and thus the most optimum ship position. The top view with these positions is shown in figure 5.12(a). With these ship positions, the tension is lower than the previous case discussed in section 5.4.1. Moreover, the post failure tensions are always positive in each cable. The other positions reported in table 5.7 are shown pictorially in figure 5.12(b) to (e).

## **5.5 Comparison of optimized ship positions**

Ship position optimization of CPM is conducted based on the following criteria's

- Case1: Maximizing workspace of the manipulator
- Case 2: Maximizing stiffness and natural frequency of the manipulator
- Case 3: Minimizing post failure tensions in the cables

In the first case, ship position optimization is formulated based on maximizing the workspace of the manipulator. The ship positions having the maximum volume of the workspace was considered as the optimum one. The optimization was not just limited to the workspace volume but also incorporates stiffness of the manipulator in the workspace (case 2). The ship positions were determined such that the manipulator can have maximum stiffness and natural frequency in the workspace. Third case incorporates failure analysis in the optimization such that when one of the cables fails, the post failure tensions in the remaining cables are minimized. Results of the ship position optimization for the above three cases are summarized in table 5.8, 5.9 and 5.10 for CPM with six, eight and ten cables respectively.

**Table 5.8 Comparison of optimized ship positions of CPM with six cables.**

<b>Optimized ship positions</b>	<b>Number of Discrete points of workspace</b>	<b>Maximum summation of natural frequency of the manipulator (Hz)</b>	<b>Minimum post failure tension in the cable (N)</b>
<b>For maximum workspace</b>	1704	1175	1164
<b>For maximum stiffness</b>	1245	2038	1287
<b>For minimum post failure tensions</b>	65	689	81

Table 5.8 shows the results for all three cases for each optimum ship position for the case of CPM having six cables. It lists the workspace, stiffness and post failure tensions for each parameter's optimum ship positions. The results of these parameters can be observed in table 5.8. For the optimum ship positions for maximum workspace, the workspace of the manipulator is found maximum but other parameters such as stiffness and post failure tensions are not having optimum value. Similarly, for the case of optimum ship positions for maximum stiffness, the natural frequency and stiffness of the manipulator is observed to be maximum, but the workspace and post failure tensions are not optimum. When optimized ship positions for minimum post failure tensions are compared for the above mentioned parameters, the workspace and stiffness of the manipulator is reported very small which indicates the design will perform well in the event of a failure but is not suitable for normal operations since the workspace and stiffness of the manipulator is very small at that particular ship positions. These results for the CPM with eight and ten cables are shown in table 5.9 and 5.10 respectively.

**Table 5.9 Comparison of optimized ship positions of CPM with eight cables.**

<b>Optimized ship positions</b>	<b>Number of Discrete points of workspace</b>	<b>Maximum summation of natural frequency of the manipulator (Hz)</b>	<b>Minimum post failure tension in the cable (N)</b>
<b>For maximum workspace</b>	2428	3574	1139
<b>For maximum stiffness</b>	2428	3574	1139
<b>For minimum post failure tensions</b>	98	1125	71

**Table 5.10 Comparison of optimized ship positions of CPM with ten cables.**

<b>Optimized ship positions</b>	<b>Number of Discrete points of workspace</b>	<b>Maximum summation of natural frequency of the manipulator (Hz)</b>	<b>Minimum post failure tension in the cable (N)</b>
<b>For maximum workspace</b>	3823	2147	1045
<b>For maximum stiffness</b>	2500	3823	1186
<b>For minimum post failure tensions</b>	148	583	65

Similar analysis can be performed for the optimum positions of the ships shown in table 5.9 and 5.10 as was observed for the CPM with six cables. Workspace and stiffness values are low when optimized positions for minimum post failure tensions are used. By comparing table 5.8, 5.9 and 5.10, the workspace tends to be higher for the CPM with more number of cables. Similarly, the stiffness of the manipulator also

becomes high for CPM with ten cables as compared with six or eight cables. The minimum post failure tension decreases with increasing number of cables.

Since the results differ for each parameter's optimum ship positions especially the post failure tensions were very large when the ship positions were used for the case of maximum workspace or stiffness of the manipulator. Similarly, when those ship positions were used that give minimum post failure tensions, the workspace and stiffness of the manipulator was very small. Therefore, an optimization combining all criteria is to be determined and is formulated in the next section.

## **5.6 Layout Optimization using a combined criterion**

It was observed in the previous section that the performance of the manipulator varies at different optimum positions of the ships. The optimum positions, where the manipulator will have maximum workspace and stiffness but post failure tensions in the cables will not be minimum and vice versa. In this section, ship position optimization is conducted using a combined criterion. The criteria will include the following parameters.

- Workspace
- Stiffness and natural frequency
- Post failure tensions variation

Ship position optimization will be conducted based on a criterion that includes all of the above mentioned parameters. The algorithm will report the optimum ship positions that will give the optimum value for all the parameters. The criteria will be based on the following equation.

$$Val_{opt} = \frac{W_{present}}{W_{max}} + \frac{\sum_{j=1}^n \min_j(f_j^k)}{\max(\sum_{j=1}^n \min_j(f_j^k))} + \frac{\min(\max_j(\Delta\tau_j^k))}{\max_j(\Delta\tau_j^k)} \quad (5.15)$$

Where  $Val_{opt}$  gives the value obtained taking into account the three parameters;  $W_{present}$  represents the workspace discrete points at present positions of the ships and  $W_{max}$  represents the maximum workspace points that can be achieved;  $\sum_{j=1}^n \min_j(f_j^k)$  represents the summation of the minimum natural frequency calculated at all poses of the manipulator at the given positions of the ships;  $\max(\sum_{j=1}^n \min_j(f_j^k))$  represents the maximum summation of natural frequency that can be possibly achieved;  $\max_j(\Delta\tau_j^k)$  represents the maximum post failure tensions in the cables while  $\min(\max_j(\Delta\tau_j^k))$  gives the minimum value possible for the post failure tensions in the cables.

The Eq. (5.15) gives the optimum value taking into account the three parameters, i.e. workspace, stiffness and natural frequency of the manipulator and the post failure tension in the cables. The value closest to the value three will be considered as the most optimum value and those positions of the ships will be regarded as optimum ship positions. Therefore, using this criterion, the combined ship position optimization can be determined.

The flow chart of the algorithm that is used to find ship position optimization using this criterion is shown in figure 5.13. It calculates the tension in the cables at a given manipulator's pose and ship positions using Eq. (3.18). If the required conditions are satisfied i.e.  $\tau_i > 0 \forall i$  and  $Rank(\mathbf{J}) = n$ , it adds that manipulator's pose to the workspace, computes the minimum stiffness and natural frequency of the manipulator at that pose and adds the value with the previous result of natural frequency, if there is any.

With the above given conditions satisfied, it also calculates the post failure tensions for every cable breakage case and then finds the maximum value of  $\Delta\tau$  at a given pose of the manipulator. The manipulator then goes to another pose and the same procedure of calculating the workspace, natural frequency and post failure tension in the cables is repeated till the manipulator is moved to all possible positions. The algorithm then uses the values of workspace, natural frequency and post failure tensions in Eq. (5.15) to calculate  $Val_{opt}$ . This value of  $Val_{opt}$  is stored with the respective ship positions. The ship positions are then moved to another position and the same process is repeated. The ship positions having the maximum value of  $Val_{opt}$  are the optimum positions of the ships. The algorithm is explained for CPM having six, eight and ten cables.



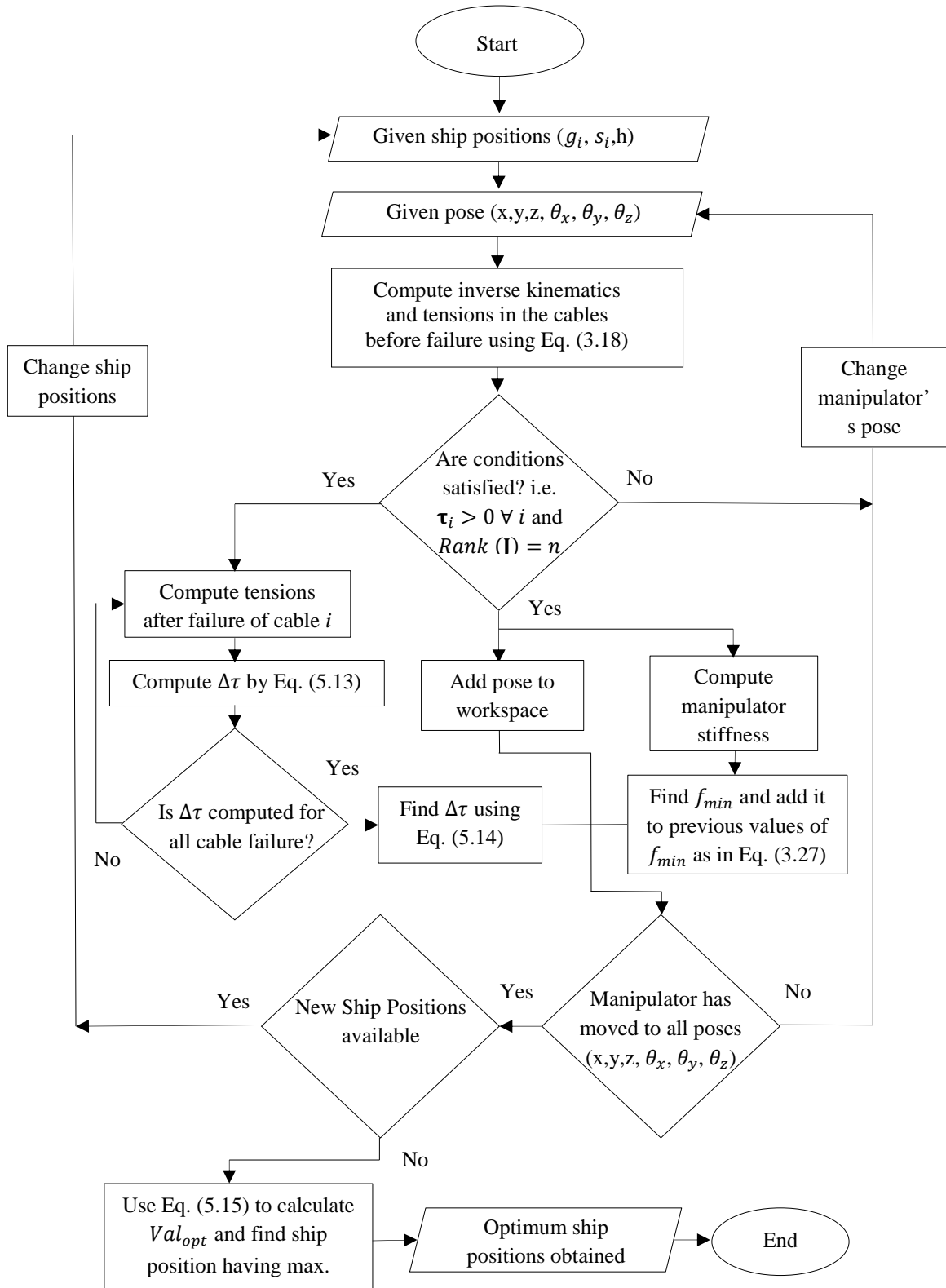


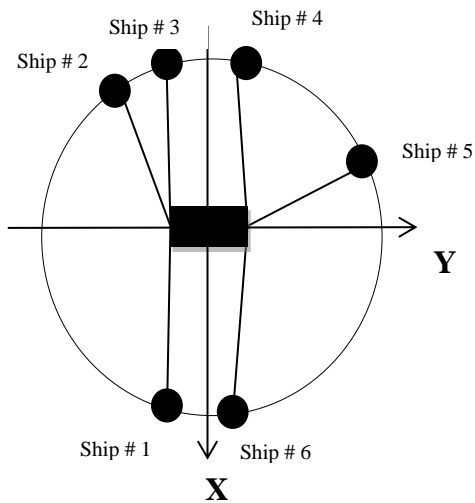
**Figure 5.13 A flow chart of the algorithm for computing the ship position optimization using a criterion expressed in Eq. (5.15).**

### 5.6.1 Ship position optimization for CPM having six cables

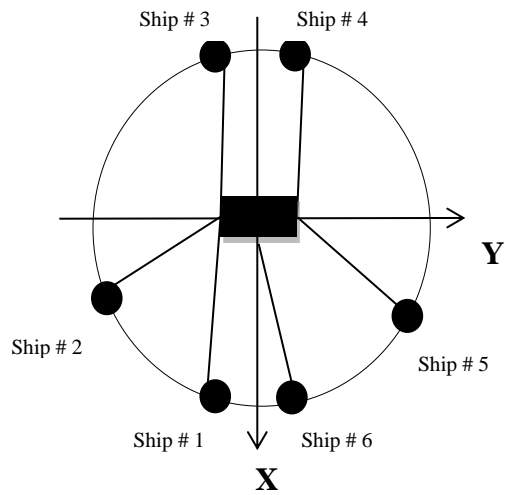
In this section, the algorithm in figure 5.13 is implemented in CPM having six cables. The schematic of CPM is shown in chapter 3 in figure 3.1. The algorithm is used to determine the optimum positions of the six ships connected to a rectangular platform through cables. The moving platform will work undersea. By implementing the algorithm shown in figure 5.13, ship position optimization is achieved using a combined criterion. These positions will give the optimum values for all the parameters of CPM. Results obtained are shown in table 5.11 and the ship positions are shown graphically in figure 5.14.

**Table 5.11 Optimized ship positions for CPM with six cables using the proposed algorithm in figure 5.13.**

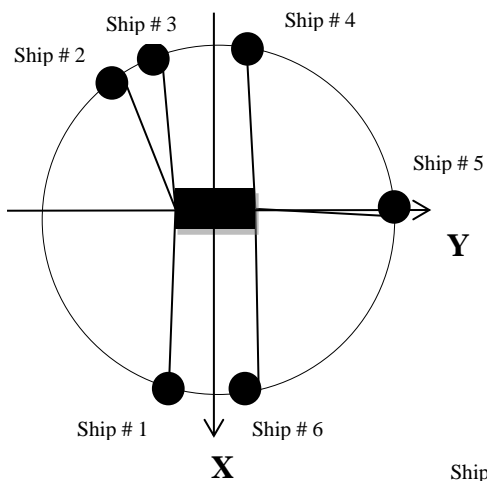
Ship Position	(r- $\theta$ ) Position of Ship # 1 (m,deg)	(r- $\theta$ ) Position of Ship # 2 (m,deg)	(r- $\theta$ ) Position of Ship # 3 (m,deg)	(r- $\theta$ ) Position of Ship # 4 (m,deg)	(r- $\theta$ ) Position of Ship # 5 (m,deg)	(r- $\theta$ ) Position of Ship # 6 (m,deg)	$Val_{opt}$
1	(50,265)	(50,120)	(50,95)	(50,85)	(50,20)	(50,275)	2.1144
2	(50,265)	(50,200)	(50,95)	(50,85)	(50,300)	(50,275)	2.0895
3	(50,265)	(50,120)	(50,115)	(50,85)	(50,0)	(50,275)	2.0805
4	(50,265)	(50,180)	(50,95)	(50,85)	(50,300)	(50,295)	2.0805
5	(50,265)	(50,120)	(50,95)	(50,85)	(50,0)	(50,275)	2.0089



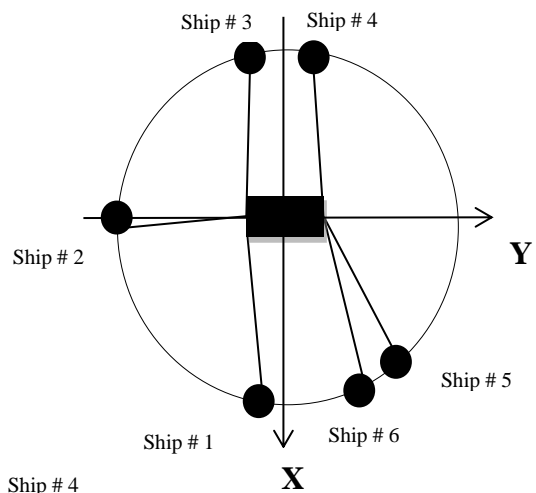
**(a) Position # 1**



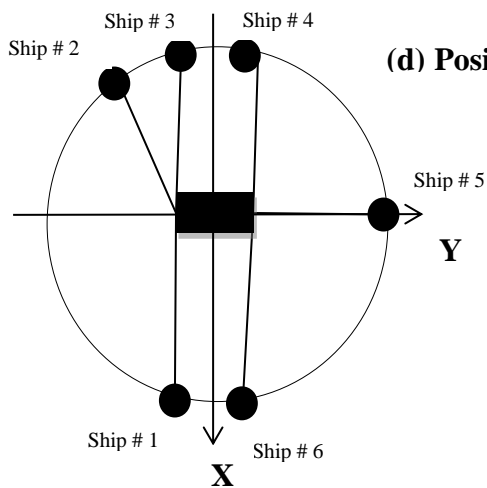
**(b) Position # 2**



**(c) Position # 3**



**(d) Position # 4**



**(e) Position # 5**

**Figure 5.14 Top five optimum ship positions for CPM with six cables based on the algorithm in figure 5.13.**

As can be observed in table 5.11, ship positions set #1 are the optimum positions since the value obtained from the combined criterion is 2.11, which is the largest among all. These ship positions are shown pictorially in figure 5.14(a). The value is slightly reduced for other ship positions depicted in table 5.8. These positions are shown schematically in figure 5.14(b) to (e).

### **5.6.2 Ship position optimization for CPM having eight cables**

In this section, ship position optimization will be conducted for CPM with eight cables. The CPM shown in figure 4.1 is used to illustrate the algorithm in figure 5.12 for eight cables. The platform is rectangular in shape and possesses 6DOF. Results obtained are shown in table 5.12 in which the optimum value for the combined criterion is shown against the respective ship positions.

**Table 5.12 Optimized ship positions for CPM with eight cables using the proposed algorithm in figure 5.13.**

<b>Optimized Ship Position No.</b>	<b>1</b>	<b>2</b>	<b>3</b>	<b>4</b>	<b>5</b>
<b>(r- <math>\theta</math>) Position of Ship # 1 (m,deg)</b>	(50,235)	(50,260)	(50,260)	(50,235)	(50,235)
<b>(r- <math>\theta</math>) Position of Ship # 2 (m,deg)</b>	(50,200)	(50,185)	(50,215)	(50,185)	(50,200)
<b>(r- <math>\theta</math>) Position of Ship # 3 (m,deg)</b>	(50,175)	(50,175)	(50,175)	(50,145)	(50,175)
<b>(r- <math>\theta</math>) Position of Ship # 4 (m,deg)</b>	(50,100)	(50,125)	(50,100)	(50,100)	(50,125)
<b>(r- <math>\theta</math>) Position of Ship # 5 (m,deg)</b>	(50,80)	(50,80)	(50,80)	(50,80)	(50,80)
<b>(r- <math>\theta</math>) Position of Ship # 6 (m,deg)</b>	(50,25)	(50,5)	(50,40)	(50,40)	(50,25)
<b>(r- <math>\theta</math>) Position of Ship # 7 (m,deg)</b>	(50,355)	(50,340)	(50,340)	(50,355)	(50,355)
<b>(r- <math>\theta</math>) Position of Ship # 8 (m,deg)</b>	(50,280)	(50,280)	(50,305)	(50,305)	(50,280)
<b><math>Val_{opt}</math></b>	2.2139	2.1984	2.1559	2.1128	2.1054

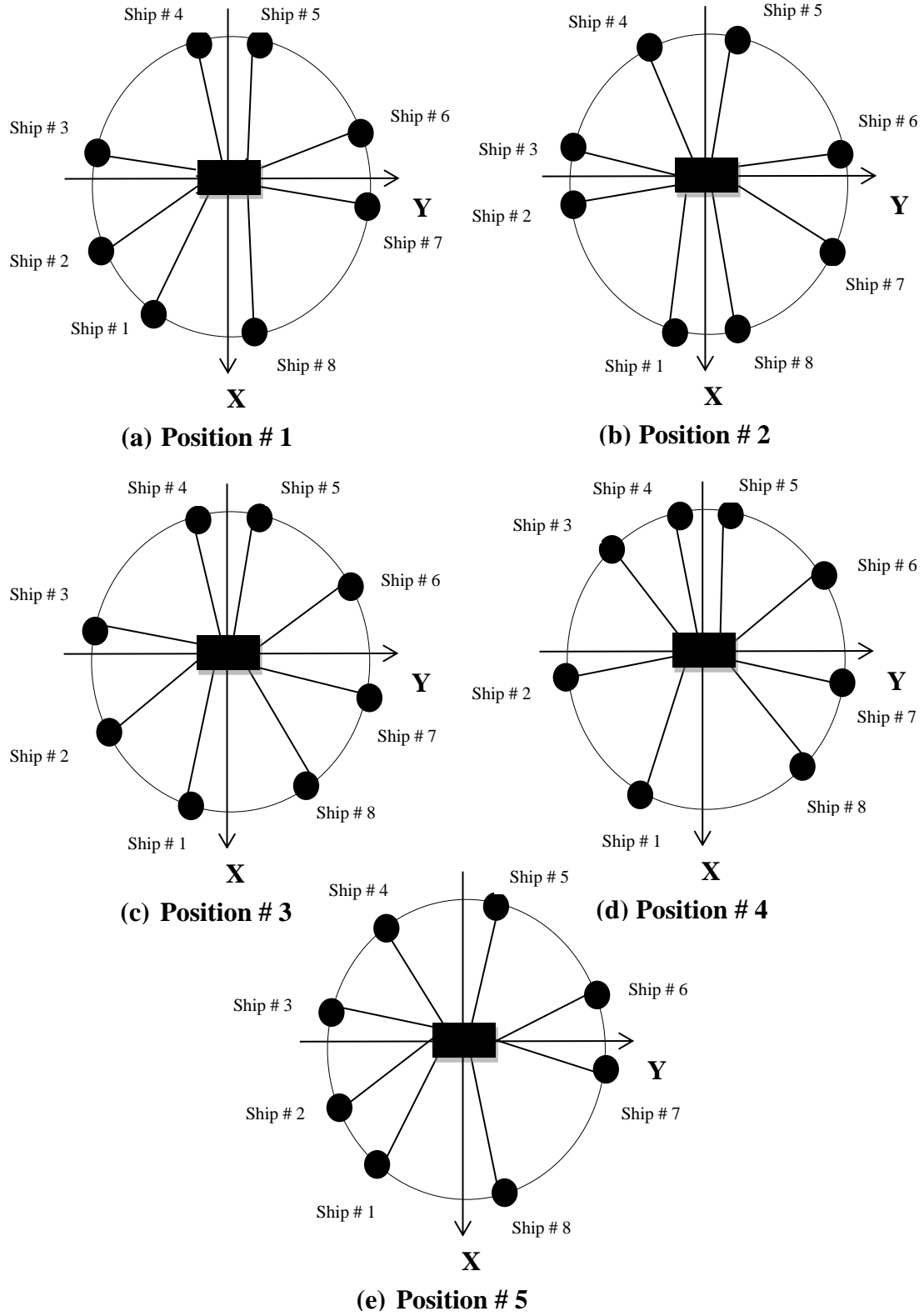


**Figure 5.15 Top five optimum ship positions for CPM with eight cables based on the algorithm in figure 5.13.**

The results tabulated in table 5.12 are shown in pictorial form in figure 5.15. The maximum value for  $Val_{opt}$  obtained is 2.21 corresponds to ship position 1 and shown in figure 5.15(a). The value slightly decreases for ship position set 2 which is shown pictorially in figure 5.15(b). For ship position 3, 4 and 5, the value further decreases. These positions are shown schematically in figure 5.15(c), (d) and (e) respectively.

### **5.6.3 Ship position optimization for CPM having ten cables**

The algorithm described in figure 5.13 is now used to calculate the optimum positions of the ships for CPM for the case of ten cables. The schematic of the CPM having ten cables is shown in figure 4.2. The rectangular platform is capable of moving in 6 directions and therefore possesses 6DOF. The optimized ships positions are summarized in table 5.13 and shown pictorially in figure 5.16.

**Table 5.13 Optimized ship positions for CPM with ten cables using the proposed algorithm in figure 5.13.**

<b>Optimized Ship Position No.</b>	<b>1</b>	<b>2</b>	<b>3</b>	<b>4</b>	<b>5</b>
<b>(r- <math>\theta</math>) Position of Ship # 1 (m,deg)</b>	(50,260)	(50,260)	(50,260)	(50,260)	(50,245)
<b>(r- <math>\theta</math>) Position of Ship # 2 (m,deg)</b>	(50,210)	(50,210)	(50,210)	(50,210)	(50,210)
<b>(r- <math>\theta</math>) Position of Ship # 3 (m,deg)</b>	(50,195)	(50,165)	(50,195)	(50,165)	(50,165)
<b>(r- <math>\theta</math>) Position of Ship # 4 (m,deg)</b>	(50,150)	(50,150)	(50,150)	(50,150)	(50,150)
<b>(r- <math>\theta</math>) Position of Ship # 5 (m,deg)</b>	(50,100)	(50,100)	(50,100)	(50,100)	(50,100)
<b>(r- <math>\theta</math>) Position of Ship # 6 (m,deg)</b>	(50,80)	(50,80)	(50,80)	(50,80)	(50,65)
<b>(r- <math>\theta</math>) Position of Ship # 7 (m,deg)</b>	(50,30)	(50,30)	(50,30)	(50,30)	(50,30)
<b>(r- <math>\theta</math>) Position of Ship # 8 (m,deg)</b>	(50,15)	(50,345)	(50,345)	(50,15)	(50,345)
<b>(r- <math>\theta</math>) Position of Ship # 9 (m,deg)</b>	(50,330)	(50,330)	(50,330)	(50,330)	(50,330)
<b>(r- <math>\theta</math>) Position of Ship # 10 (m,deg)</b>	(50,280)	(50,280)	(50,295)	(50,280)	(50,280)
<b><math>Val_{opt}</math></b>	2.4298	2.3174	2.2943	2.2517	2.2415



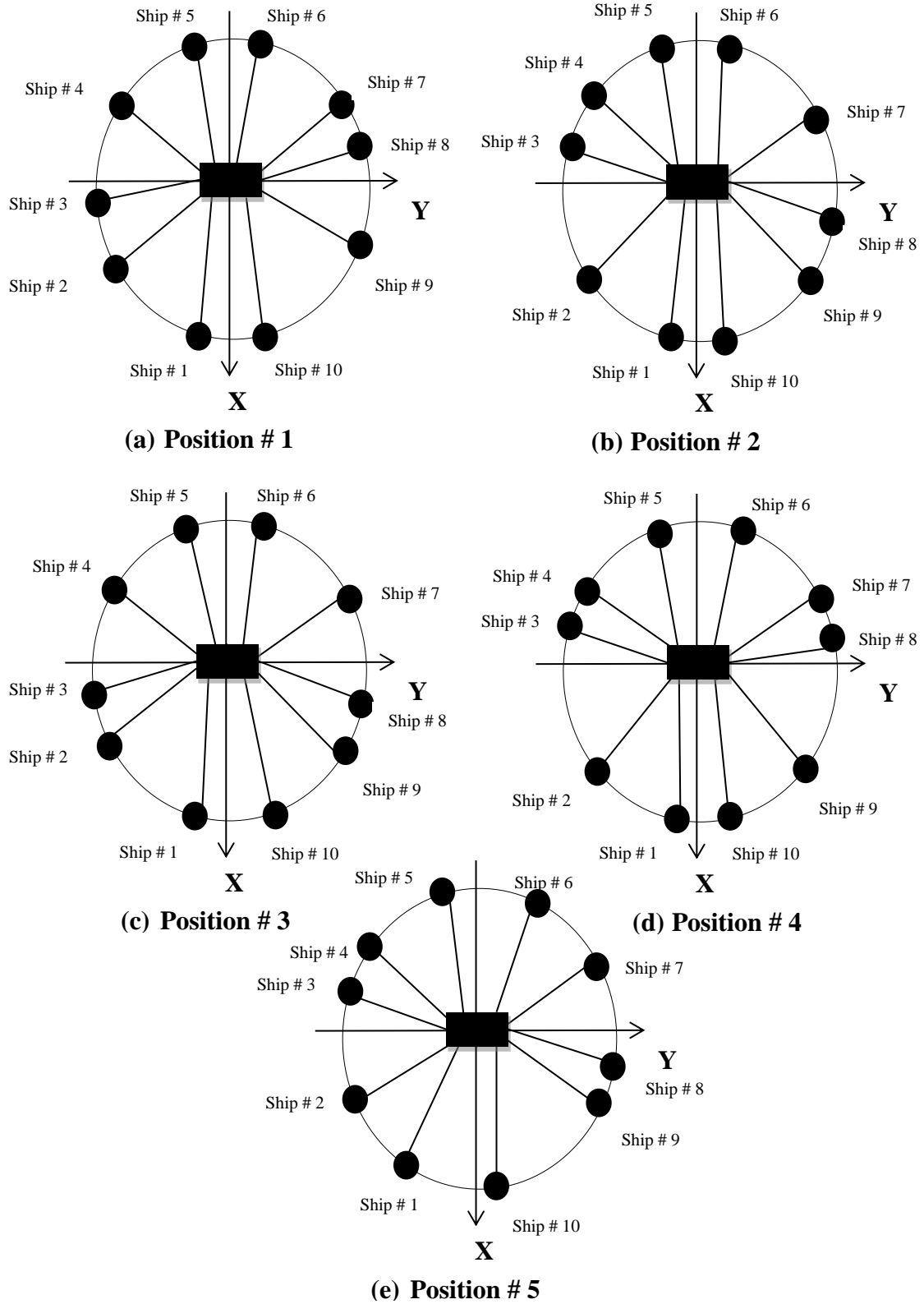


**Figure 5.16 Top five optimum ship positions for CPM with ten cables based on the algorithm in figure 5.13.**

Table 5.13 shows the position sets for top five optimum ship positions in the case for CPM having ten cables. These positions are illustrated in figure 5.16. The maximum value for  $Val_{opt}$  for ship position set one is calculated as 2.4298N, which is the maximum value among all other values of  $Val_{opt}$ , which indicates ship position set one as the most optimum position set. There is a slightly decrease in the value of  $Val_{opt}$  for other ship position set tabulated in table 5.13. These ship positions can be observed schematically in figure 5.16(a) to (e).

## 5.7 Results and discussions

In this chapter, the effect of failure on the operation of cable based parallel manipulators was conducted. Different layout designs have been proposed and ship position optimization was performed so that the system will have a minimum effect of failure on the cable tensions.

In section 5.2, post failure trajectory was reported for the manipulator that was connected to six ships via cables. The post failure trajectory was determined by eliminating the corresponding row of the Jacobian matrix  $J$ , and found by moving infinitesimal displacements onto the null space of the Jacobian matrix  $J$ . Examples were demonstrated for CPM with second and sixth cable failure. The post failure tension in the cables was investigated in section 5.3. It was observed that there was an immediate change in the remaining cable tensions in the event when one of the cables fails. In section 5.4, ship position optimization was performed such that the cables were have minimum post failure tension in the event of a failure of one of the cables. Optimized fault tolerance ship positions were also determined such that none of the cables were

having negative tensions after failure. The optimization was studied in six, eight and ten ships CPMs. It was observed that the post cable tensions were minimum for the case of ten ships as compared with eight and six ships CPM. Thus the effect of failure is minimized with higher number of cables. This is depicted in figure 5.17.

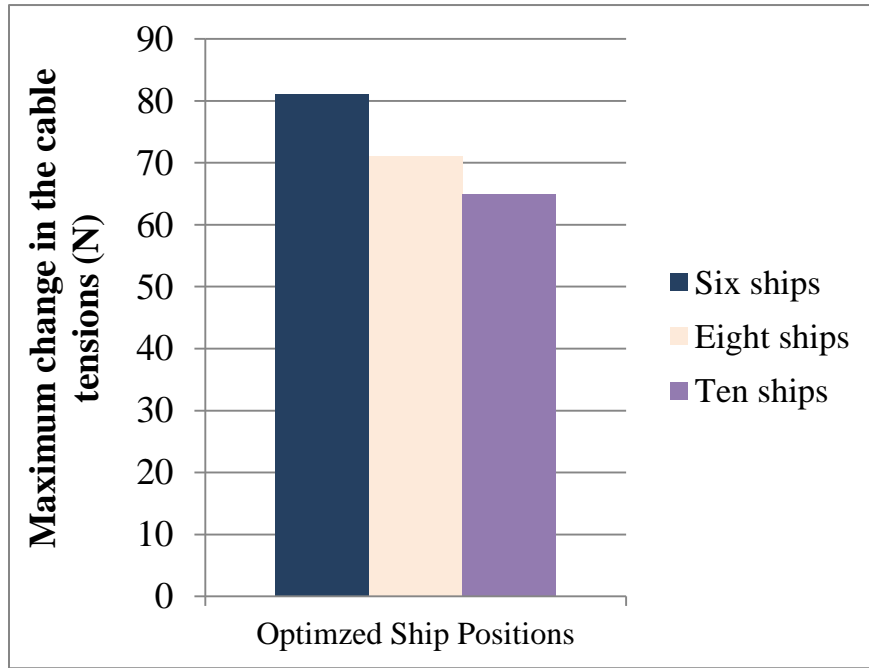


**Figure 5.17: Comparison of optimized ship positions for CPM with six, eight and ten ships in case of a failure**

In section 5.6, based on the work presented in chapter 3, 4 & 5, a combined criterion was determined in order to conduct the ship position optimization so that the system will have maximum workspace, maximum stiffness and minimum post failure tensions in the cables. The optimized positions were calculated for CPM having six, eight and ten cables. The combined criterion value was reported to be increased with higher number of cables. This is depicted in figure 5.18.

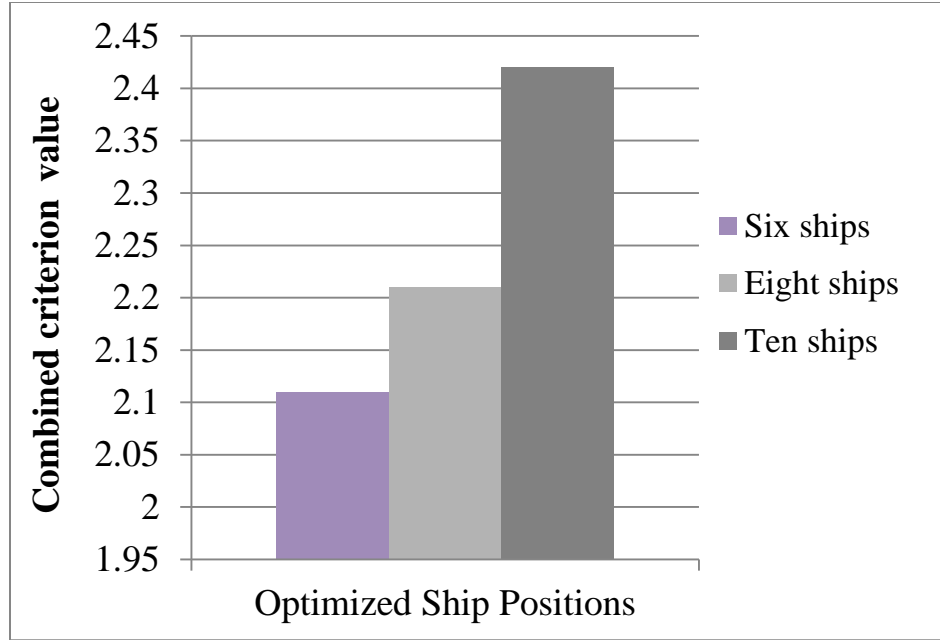


**Figure 5.18: Comparison of optimized ship positions for CPM with six, eight and ten ships using a combined criterion value.**

The ship position optimization using a combined criterion maximized the workspace and stiffness of the manipulator and simultaneously minimized the cable tensions in the event of a failure. As reported in figure 5.18, the combined performance of CPM was improved with ten ships as compared with six and eight ships CPM.

## **CHAPTER 6**

### **CONCLUSIONS**

In this work of Master thesis, layout optimization and failure analysis of a cable based parallel manipulator (CPM) for subsea applications has been performed. Layout optimization included determining the optimum ship positions such that the manipulator can have maximum workspace volume to work inside deep sea. Ship position optimization was also performed in order to maximize the stiffness of the manipulator. Failure analysis of the CPM was conducted in order to analyze the effect of cable failure on the performance of the manipulator and to obtain the optimum ship positions to minimize the post failure tension in the cables. A combined criterion was also determined for ship position optimization.

Since the CPM is designed for subsea applications, forces acting on the submerged bodies were analyzed and the forces equations were determined. They were useful in order to figure out the wrench acting on the manipulator. The position and velocity analysis of the CPM was conducted through inverse kinematics. Geometrical constraints for the problem solution have been formulated. The force analysis has been considered by looking at the static problem. The problem of the workspace analysis has been discussed and formulated. The singularity detection for CPM has been illustrated. The stiffness and natural frequency evaluation has also been discussed. Ship position optimization has been performed based on maximizing the workspace and stiffness of the manipulator. The optimization was illustrated for redundant as well as non-redundant CPM. In case of redundant cables, Dykstra's algorithm was utilized to calculate the

minimum-2-norm solution to the cable tensions. It was observed that the manipulator workspace as well as stiffness was increased as the number of cables was increased.

Failure analysis of the CPM was conducted in order to examine the effect of cable failure on the performance of the manipulator. For the case of non-redundant cables, the post failure trajectory of the manipulator was studied. The trajectory of the CPM after failure was investigated by examining the change in the Jacobian matrix, its inverse and transposes. The post failure tensions were calculated and discussed. It was observed that the tensions after failure instantly changes when one of the cables fails. Also the post failure tensions in some of the cables went negative which indicates a failure in those cables as well. In order to minimize the post failure tensions, ship position optimization was performed. The optimization was also conducted such that post failure tensions are minimized and none of the cables can have negative tensions after failure. A combined criterion for ship position optimization was also established. With those ship positions, the manipulator can have maximum workspace and stiffness with minimum post failure tensions in case of a cable failure.

The effect of having different number of cables on the workspace, stiffness and fault tolerance of the manipulator was studied on CPM with six, eight and ten cables. It was observed that the workspace was greater in CPM with ten cables than with six or eight cables. Similar trend was observed for the natural frequency and stiffness of the manipulator. Post failure tensions were reported minimum in CPM with ten cables and it increases with eight and six cables CPM. Therefore, it can be concluded that the performance of the CPM improves by using higher number of cables. The ship positions were also optimized to maximize the workspace and stiffness of the manipulator and

simultaneously minimize the effect of a cable failure. It was concluded that the combined performance of CPM was also improved with higher number of cables in a CPM.

## References

- [1] J. Albus, R. Bostelman and N. Dagalakis, “The Nist Robocrane”, *J. Robotic Systems*, vol. 10, no.5, pp. 709-724, 1993.
- [2] S. Kawamura, W. Choe, S. Tanak, “Development of an Ultrahigh Speed Robot Falcon Using Wire Driven Systems”, in *Proc. 1995 IEEE Int. Conf. on Robot. Autom.*, pp. 215-220.
- [3] K. Maeda, S. Tadokoro, T. Takamori, M. Hiller, R. Verhoeven, “On Design of a Redundant Wire-driven Parallel Robot WARP Manipulator” in *Proc. IEEE Int. Conf. on Robot. Autom.*, vol. 2, pp. 895-900.
- [4] C. Ferraresi, M. Paoloni, F. Pescarmona, “A new 6-dof Parallel Robotic Structure Actuated by Wires: The Wiro-6.3”, *J. of Robotic Systems*, vol. 21, no. 11, pp. 581-595, 2004.
- [5] S. Behzadipour, A. Khajepour, “A New Cable-based Parallel Robot with Three Degrees of Freedom”, *Multibody System Dynamics*, vol. 13, pp. 371-383, 2005.
- [6] G. Mroz, L. Notash, “Wire-actuated Robots with a Constraining Linkage”, *J. Robotic Systems*, vol. 21, no. 12, pp. 677-678, 2004.
- [7] Mahir Hassan, Amir Khajepour, “Analysis of a Large-Workspace Cable-Actuated Manipulator for Warehousing Applications”, ASME IDETC/CIE Conference, 2009, San Diego, California, USA.
- [8] Verhofen R, “ Analysis of the Workspace of Tendon-Based Stewart Platforms”, Ph. D. thesis, University of Duisburg-Essen, 2004



- [9] J. J. Gorman, K. W. Jablokow, and D. J. Cannon, "The cable array robot: Theory and experiment," in *Proc. IEEE ICRA*, Seoul, Korea, May 2001, pp. 2804–2810.
- [10] S. Fang, D. Franitza, M. Torlo, F. Bekes, and M. Hiller, "Motion Control of a Tendon-Based Parallel Manipulator Using Optimal Tension Distribution", *IEEE/ASME Transactions on Mechatronics*, 9(3), (2004) 561-568.
- [11] M. Hassan and Khajepour, A., "Analysis of Bounded Cable Tensions in Cable-actuated Manipulators", *IEEE Transactions on Robotics*, vol. 27, no. 5, pp. 891-900, 2011.
- [12] R. G. Roberts, T. Graham, and T. Lippitt, "On the inverse kinematics, statics, and fault tolerance of cable-suspended robots," *J. Robot. Syst.*, vol. 15, no. 10, pp. 581–597, 1998.
- [13] L. Mikelsons, T. Bruchmann, M. Hiller, and D. Schramm, "A real-time capable force calculation algorithm for redundant tendon-based parallel manipulators," in *Proc. IEEE Int. Conf. Robot. Autom.*, 2008, pp. 3869–3874.
- [14] S.R.Oh and S. K. Agrawal, "Cable suspended planar robots with redundant cables: Controllers with positive tensions," *IEEE Trans. Robot.*, vol. 21, no. 3, pp. 457–465, Jun. 2005.
- [15] Alp A. B. and Agrawal S. K., "Cable Suspended Robots: Design, Planning and Control". Proceedings of the 2002 IEEE International Conference on Robotics and Automation (ICRA), Washington D.C., 2002, pp. 4275-4280.

- [16] Bosscher P., Ebert-Uphoff I., “Wrench Based Analysis of Cable Driven Robots”, Proceedings of the 2004 IEEE International Conference on Robotics and Automation (ICRA), New Orleans, 2004, pp.834-841.
- [17] Gouttefarde M., Gosselin C., “Analysis of the Wrench Closure Workspace of Planar Parallel Cable Driven Mechanisms”, IEEE Transaction on Robotics, Vol. 22, n. 3, 2006, pp. 434-445.
- [18] Merlet J.-P. and Daney D., “Dimensional Synthesis of Parallel Robots with Guaranteed Given Accuracy Over a Specific Workspace”, Proceedings of the 2005 IEEE International Conference on Robotics and Automation (ICRA), Barcelona, 2005, pp.942-947.
- [19] Pham C.B., Yeo S.H., Yang G., Kurbanhusen M. S., and Chen I-M., “Force-closure Workspace Analysis of Cable driven Parallel Mechanisms”, Mechanism and Machine Theory, n. 41, 2006, pp. 53-69.
- [20] Merlet J.P., “Parallel Robots, second edition”, Springer, Dordrecht, 2006 a.
- [21] Tsai L. W., “Robot Analysis-The Mechanics of Serial and Parallel Manipulators”, Wiley-interscience, 1999.
- [22] Ceccarelli M., “Fundamentals of Mechanics of Robotic Manipulation”, Kluwer Academic Publisher, Dordrecht, 2004.
- [23] Nathan M., “Cooperative Manipulation and Transportation with Aerial Robots” Auton Robot (2011) 30: 73–86

- [24] Cheng, P., Fink, J., Kim, S., & Kumar, V. (2008). Cooperative towing with multiple robots. In *Proc. of the int. workshop on the algorithmic foundations of robotics*, Guanajuato, Mexico.
- [25] R. Verhoeven and M. Hiller, "Estimating the controllable workspace of tendon-based Stewart platforms," in *Proc. ARK 7th Int. Symp. Adv. Robot Kinematics*, Protoroz, Slovenia, 2000, pp. 277–284.
- [26] Ting Y., Tosunoglu, S. and Freeman, R. Torque Redistribution and Time Regulation Methods for Actuator Saturation Avoidance of Fault Tolerant Parallel Robots, *J. Robot. System*, 12(12): 807820, 1995.
- [27] Notash, L., and Huang, L., On the Design of Fault Tolerant Parallel Manipulators, *Mech. And Machine Theory*, 38(1):85101, 2003.
- [28] Notash, L., and Podhorodeski, R. P., Complete Forward Displacement Solution for a Class of Three Branch Parallel Manipulators, *J. Robotic Systems*, 11(6):471485, 1994.
- [29] Notash, L., and Podhorodeski, R.P., On the Forward Displacement Problem of Three Branch Parallel Manipulators, *Mechanism and Machine Theory*, 30(3):391404, 1995.
- [30] Notash, L., and Podhorodeski, R. P., Fixtureless Calibration of Parallel Manipulators, *Transactions of the Canadian Society for Mechanical Engineering*, 21(3):273294, 1997.

- [31] Notash, L., Joint Sensor Fault Detection for Fault Tolerant Parallel Manipulators, J. Robotic Systems, 17(3):149157, 2000.
- [32] Notash, L., Uncertainty Configurations of Parallel Manipulators, Mechanism and Machine Theory, 33(1/2):123138, 1998.
- [33] Notash, L., and Podhorodeski, R.P., Forward Displacement Analysis and Uncertainty Configurations of Parallel Manipulators with a Redundant Branch, J. Robotic Systems, 13(9):587601, 1996.
- [34] Chen, Y., McInroy, J.E., and Yi, Y., Optimal, Fault Tolerant Mappings to Achieve Secondary Goals Without Compromising Primary Performance, IEEE Trans. Robotics and Automation, 19(4): 680691, 2003.
- [35] Hassan, M., and Notash, L., Reduced Motion of Parallel Manipulators due to Active Joint Jam, special edition of CSME Transactions, 28(2A):165184, 2004.
- [36] Hassan, M., and Notash, L., Optimizing Fault Tolerance to Joint Jam in the Design of Parallel Robot Manipulators, Mech. And Machine Theory, 42(10):14011417, 2007.
- [37] Roberts, R.G., Graham, T., and Lippitt, T., On the Inverse Kinematics, Statics, and Fault Tolerance of Cable Suspended Robots, Journal of Robotic Systems, 15(10):581597, 1998.
- [38] Notash, L., Failure Recovery for Wrench Capability of Wire-Actuated Parallel Manipulators, Robotica, 30(6):941-950, 2012
- [39] Anthony, E., Fluid Mechanics with Applications, Prentice Hall, 1998

- [40] Tsai, L.W., Robot Analysis, The Mechanics of Serial and Parallel Manipulators, John Wiley & Sons, New York, 1999
- [41] R. L. Dykstra, "An Algorithm for Restricted Least Squares Regression," J. Amer. Statistical Assoc., vol. 78, pp. 837-842, 1983.
- [42] J. C. M. Carvalho, A. M. Barbosa, R. S. Goncalves, "New Advances in Mechanisms, Transmissions and Applications," Mechanisms and Machine Science vol. 17, pp 165-172, 2014.
- [43] Mohammad M. Aref, Hamid D. Taghirad, "Geometric Workspace Analysis of a Cable-Driven Redundant Parallel Manipulator," International Conference on Intelligent Robots and Systems, Nice, France. Sep, 22-26, 2008.
- [44] A. Pashkevich, D. Chablat, P. Wenger, "Stiffness Analysis of Overconstrained Parallel Manipulators," Mechanism and Machine Theory, 44(5):966-982, 2009.
- [45] Ahmad, Aftab, Kjell Anderson, and Ulf Sellgren. "An approach to stiffness analysis methodology for haptic devices." Ultra Modern Telecommunications and Control Systems and Workshops (ICUMT), 2011 3rd International Congress on. IEEE, 2011.
- [46] Zarif, Azadeh, Mohamad M. Aref, and Hamid D. Taghirad. "Force feasible workspace analysis of cable-driven parallel manipulators using lmi approach." Submitted to IEEE Int. Conf. on Robotics and Automation. 2009.

## **Vitae**

Name : Asim Ghaffar

Nationality : Pakistani

Date of Birth : 5/10/1987

Email : asimghaffar@hotmail.com

Address : Park View DHA Phase VIII, Lahore Pakistan

### **Academic Background:**

2012-2014 M.Sc Mechanical Engineering from King Fahd University of Petroleum and Minerals (KFUPM), Dhahran, Saudi Arabia.

2005-2009 B.Sc Mechatronics and Control Engineering from University of Engineering and Technology Lahore, Pakistan.